UNIVERSITY OF ZAGREB
FACULTY OF MECHANICAL ENGINEERING
AND NAVAL ARCHITECTURE

NUMERICAL MODELLING OF MULTIPHASE FLOW IN COMBUSTION OF LIQUID FUEL

DOCTORAL THESIS

Mentor:

Prof.dr.sc. NEVEN DUIĆ   MILAN VUJANOVIĆ

ZAGREB, 2010

BIBLIOGRAPHY DATA:

Acknowledgments

If you're not living on the edge, you're taking up too much space.

Anonymous

Contents

Preface

Fossil fuels currently supply the major part of the world's energy needs and will continue to do so in the foreseeable future. World fossil fuel consumption is rising, particularly in the developing world, where population and economic growth are greater than in developed countries and where the rate of migration from rural and urban areas is significantly higher.

The combustion of fossil fuels used, in order to meet the demands of society for energy, releases large quantities of pollutants into the environment. Allowable pollutant emission from combustion sources have been regulated for over two decades in industrialized countries, and new and more stringent regulations are expected within the next years. More stringent mitigation goals and sustainable energy planning will no doubt focus on the high combustion efficiency of fossil fuels because of its contribution to the pollution of the environment. These new policies and measures will shape the way fossil fuels are used, ensuring that the use of fossils fuels is more efficient and environmentally accepted. Improvements in energy efficiency of practical combustion systems will create environmental benefits through reduced emissions of greenhouse gases and air pollutants, reducing fuel costs and increasing competition for businesses and welfare for consumers. In response to these legislative restrictions and higher demand for energy produced by combustion, understanding the complex physical and chemical processes in technical combustion systems continues to be a major challenge for R&D due to the development of effective technologies in automotive and non-automotive applications.

The current energy crisis highlights the need for the design of more powerful, fuel-efficient, and environmentally friendly combustion systems. With the development of increasingly affordable and powerful computers, advanced computer simulation modelling, using Computational Fluid Dynamics (CFD), has become a valuable tool that can be used to improve efficiency of combustion systems and to reduce high cost and time-consuming experimental investigations in modern engineering development processes. The combustion efficiency and the formation of pollutants are dependant upon the fuel-air mixture process, which is strongly influenced by spray dynamics. The understanding of the complex nature of the spray process and pollutant formation in

experimental investigations is limited and this understanding can be significantly improved by numerical modelling and simulations.

Abstract

The focus of this work is on an integrated simulation approach, which can be applied in numerical simulations of turbulent multiphase droplet flow in practical combustion systems, adopting methods for simulation of dense and dispersed spray in conjunction with combustion and nitrogen emission formation.

The first objective was to establish the validated Eulerian multiphase spray modelling approach, which can be applied with confidence in high pressure diesel spray simulations, particularly in dense spray regions. The Eulerian multiphase spray modelling concept, using an approach with fixed droplet size classes, was applied in liquid spray simulations. Several simulations of high pressure diesel injections, combined with different chamber pressures, were carried out and compared with the experimental data. The suitable validated Eulerian multiphase spray method was then coupled with the classic the Lagrangian Discrete Droplet Model (DDM), in conjunction with the classic combustion model and the validated nitrogen oxides (NO_x) chemical reaction mechanisms. The NO_x reaction mechanisms were investigated and implemented into the CFD code FIRE. The nitrogen scheme was limited to sufficiently few homogeneous reactions to allow effective coupling with the turbulent mixing process. The effects of the turbulent fluctuations on the reaction rates when predicting NO_x concentrations were modelled by using the presumed Probability Density Function (PDF) approach. The model was applied to the turbulent non-premixed jet diffusion flame (Sandia flame D) and the nitrogen predictions were compared to the results obtained by the Steady Laminar Flamelet Model (SLFM) and to the experimental data. Furthermore, to demonstrate the capability of the coupling concept, an integrated simulation approach was applied for calculation of the real internal combustion engine, which is particularly challenging for such modelling. Two different CFD simulations, the Eulerian multiphase spray simulation and the single-phase engine simulation (DDM spray in conjunction with the combustion and nitrogen emission models), were coupled and performed simultaneously to take advantage of the capabilities inherent in both simulations.

Sažetak

U ovome radu prikazane su integrirane simulacijske metode koje objedinjuju opis ponašanja gustog i razrijeđenog spreja tekućeg goriva u sprezi s izgaranjem i stvaranjem emisija dušičnih polutanata, te se kao takve mogu koristiti za numeričke simulacije turbulentnih višefaznih strujanja u sustavima izgaranja u praksi.

Primarni cilj rada je bio uspostaviti validiran Eulerov pristup za modeliranje višefaznog strujanja tekućeg goriva koji se može pouzdano primijeniti u simulacijama visokotlačnog ubrizgavanja i raspršivanja tekućeg goriva, posebice u područjima gustog spreja. Eulerov višefazni model spreja s unaprijed određenim klasama veličina kapljica primijenjen je za simulacije spreja goriva. Provedene su numeričke simulacije visokotlačnog ubrizgavanja dizela za različite tlakove ubrizgavanja u kombinaciji s različitim tlakovima komore. Rezultati simulacija su uspoređeni su s eksperimentalnim podacima. Odgovarajuća validirana Eulerova metoda višefaznog spreja povezana je i s klasičnim Lagrange modelom diskretnih kapljica (MDK), te spregnuta s klasičnim modelom izgaranja i validiranim reakcijskim mehanizmima stvaranja dušičnih oksida (NO_x). Kemijski kinetički mehanizmi nastajanja NO_x-a istraživani su i implementirani u FIRE kod. Pritom su korišteni reducirani kemijski mehanizmi nastajanja dušičnih polutanata da bi se omogućilo efikasno povezivanje s procesima turbulentnog miješanja u numeričkim simulacijama. Utjecaj turbulentnih fluktuacija kod nastajanja NO_x modeliran je primjenom funkcije gustoće vjerojatnosti. Razvijeni model je primijenjen u proračunu izgaranja na pilotiranom metanovom slobodnom plamenu (Sandia plamen D). Rezultati simulacije uspoređeni su s rezultatima mjerenja te s rezultatima simulacije koja koristi standardni laminarni *flamelet* model. Nadalje, da bi se demonstrirale mogućnosti istovremenog izvođenja povezanih simulacija, primijenjen je integrirani simulacijski pristup u proračunima stvarne konfiguracije motora s unutrašnjim izgaranjem. Dvije različite simulacije, višefazna Eulerova simulacija spreja i jedno-fazna simulacija motora (Lagrangeovo računanje spreja u sprezi s procesom izgaranja i procesom stvaranja dušičnih polutanata), povezane su i računate istovremeno. Primjenom ovakvog integriranog pristupa omogućeno je da se ove dvije simulacije međusobno nadopunjavaju, odnosno da se iskoriste prednosti inherentne svakoj od simulacija.

Prošireni sažetak

Fosilna goriva trenutno zadovoljavaju najveći dio potreba za energijom u svijetu. Potrošnja fosilnih goriva je u porastu u cijelom svijetu, a osobito u zemljama u razvoju gdje su prirast stanovništva i ekonomski razvoj veći nego u razvijenim zemljama.

Izgaranje fosilnih goriva u cilju zadovoljavanja potreba za energijom ima kao posljedicu oslobađanje velikih količina polutanata u okoliš. U industrijskim zemljama dopuštene emisije polutanata nastale izgaranjem reguliraju se već dva desetljeća, a nove, oštrije odredbe se očekuju u godinama koje dolaze. Ciljevi za smanjenje zagađivanja okoliša i potreba za planiranjem održivog razvoja energetike bez sumnje će usmjeriti istraživanja u smjeru poboljšanja učinkovitosti sustava izgaranja fosilnih goriva. Nove strategije i mjere odredit će nove načine korištenja fosilnih goriva, osiguravajući da izgaranje fosilnih goriva bude učinkovitije i prihvatljivije za okoliš. Poboljšanja učinkovitosti sustava za izgaranje rezultat će dobrobiti za okoliš kroz smanjene emisije stakleničkih plinova i ostalih polutanata, istovremeno smanjujući potrošnju goriva i povećavajući konkurentnost poslovanja, ali i dobrobit za potrošače. Stoga, detaljno razumijevanje složenih fizikalnih i kemijskih procesa koji se odvijaju u tehničkim sustavima za izgaranje može poslužiti da bi se postigle sve strože zakonski dopuštene emisije polutanata i efikasno zadovoljila sve veća potražnja za energijom. Sveobuhvatno razumijevanje tih procesa i dalje je veliki izazov za istraživače i znanstvenike uslijed razvoja novih, učinkovitih tehnologija u praktičnoj inženjerskoj primjeni.

Napredno računalno simulacijsko modeliranje uz pomoć Računalne Dinamike Fluida (RDF) postalo je vrijednim alatom koji se koristi za bolji uvid u procese izgaranja fosilnih goriva. Računalna Dinamika Fluida postala je ključna metoda za provođenje temeljnih istraživanja strujanja fluida, višefaznog strujanja kod izgaranja i drugih povezanih pojava u sustavima izgaranja u praksi, tako da se numerički rješavaju diferencijalne jednadžbe koje opisuju fizikalne probleme. Korisnost RDF-a dodatno je podržana činjenicom da intenzivna eksperimentalna istraživanja u inženjerskim sustavima rezultiraju visokim troškovima i dugotrajnim istraživanjima. U posljednje vrijeme se pri razvoju modernih inženjerskih sustava sve više prelazi iz čisto eksperimentalnih istraživanja u mješavinu eksperimentalnih i numeričkih istraživanja.

Na taj način numeričke simulacije doprinose skraćivanju vremena i smanjenju troškova projektiranja modernih učinkovitih sustava za izgaranje, ali se pritom mogu koristiti i kao metoda za istraživanje koja pruža bolji uvid u turbulentna višefazna strujanja pri izgaranju, te za razvoj poboljšanih fizikalnih i kemijskih pod-modela. U posljednjih nekoliko desetljeća uloženi su veliki napori mnogih istraživača u razvoj višedimenzionalnih matematičkih modela kako bi se omogućio detaljan uvid u složene interaktivne fizikalne i kemijske procese potrebne za konstruiranje i optimizaciju različitih sustava za izgaranje. Usprkos stalnim naporima koji se ulažu u razvoj fizikalnog i kemijskog modeliranja, numeričke simulacije složenih višefaznih strujanja u stvarnim sustavima za izgaranje još se uvijek ne mogu smatrati dostatnom metodom za točna predviđanja na kvantitativnoj razini.

U raznim modernim industrijskim primjenama, istraživanje višefaznog strujanja je usmjereno prema razumijevanju pojava koje se javljaju u spreju (raspršenom mlazu) tekućeg goriva, kao što su raspored veličina kapljica u spreju i proces miješanja goriva i zraka. Izgaranje tekućih goriva često se susreće u praksi, kao na primjer u kotlovima na loživo ulje, industrijskim pećima, plinskim turbinama, motorima s unutarnjim izgaranjem, raketama na tekuće gorivo, kemijskim procesima, itd. Tekuća goriva ubrizgavaju se u komoru za izgaranje pomoću sustava za ubrizgavanje i raspršivanje te izgaraju nošena plinovitom strujom kao raspršena tekućina. Sustav za ubrizgavanje i raspršivanje pritom stvara velik broj malih kapljica kako bi ubrzao isparavanje i izgaranje povećanjem slobodne površine goriva. U procesu stvaranja spreja uključene su različite pojave kao što su primarno i sekundarno razbijanje kapljica, širenje kapljica i njihovo isparavanje, sudari kapljica itd. Kao rezultat, višefazna strujanja predstavljaju vrlo složene procese koji su međusobno povezani uključujući turbulenciju, prijenos mase i topline, dinamiku kapljica i promjenu faza. Stoga, duboko razumijevanje ponašanja spreja tekućeg goriva predstavlja veliki izazov i ključ za poboljšanje učinkovitosti modernih uređaja za izgaranje kako bi se udovoljilo sve strožim zakonskim ograničenjima štetnih emisija.

Trenutno postoji nekoliko različitih pristupa modeliranju višefaznih strujanja, kao što su Euler-Lagrangeov model, Eulerov višefazni model, Volumen Fluida (VF), itd. Metoda koja se najviše koristi je Euler-Lagrangeova metoda koja je također poznata pod imenom Diskretni Model Kapljica (DMK). Ova metoda posebno je pogodna za

modeliranje razrijeđenih sprejeva, ali ima neke nedostatke u području blizu mlaznice s obzirom na nedostatnost opisa fizikalnih procesa u gustom spreju. Nadalje, ova metoda je vrlo osjetljiva na rezoluciju mreže kontrolnih volumena u području oko mlaznice, te njena primjena rezultira problemima statističke konvergencije. Ovi nedostaci se mogu poboljšati jačom fizikalnom spregom plinovite i tekuće faze u području oko mlaznice korištenjem Euler-Eulerove metode. Ova metoda daje točniji opis fizikalnih procesa u području gustog spreja tako što tretira svaku grupu veličina kapljica kao potpuno odvojenu fazu i riješava jednadžbe konzervacije za svaku od njih. Zbog toga se kao glavni nedostatak većine Eulerovih modela za opisivanje nameće duže vrijeme potrebno za izračun prilikom provođenja simulacija za više od jedne grupe veličina kapljica.

Postoji niz različitih modela koji mogu opisati proces spreja. Većina tih modela funkcionira dobro za neka područja višefaznih strujanja spreja, ali potpun i učinkovit integrirani pristup koji bi se mogao nositi s praktičnim problemima u industriji još se istražuje. U ovom kontekstu, ovaj doktorski rad je usmjeren na numeričke simulacijske metode koje opisuju višefazno strujanje kapljica u stvarnim sustavima za izgaranje. Ovim radom prikazane su validirane simulacije koje se mogu koristiti s punim povjerenjem kao važan dio modernog inženjerskog razvojnog procesa sa svrhom smanjenju troškova, ali i vremena potrebnog za razvoj proizvoda.

Hipoteza rada i opis istraživanja

U ovom radu integrirane su metode koje se mogu koristiti za numeričku simulaciju turbulentnog višefaznog strujanja u praktičnim sustavima izgaranja. S takvim integriranim simulacijskim tehnikama moguće je numerički izračunati strujanje gustog i razrijeđenog spreja u sprezi s izgaranjem i stvaranjem dušičnih emisija. U tu svrhu je potrebno izvesti pogodan i validiran Eulerov višefazni model spreja, koji bi se mogao koristiti s povjerenjem za točne proračune gustog kapljičastog spreja blizu mlaznice, te da bi se mogao povezati s klasičnim Lagrangeovim modelom spreja (metoda diskretnih kapljica), koji se koristi za opisivanje razrijeđenog spreja u preostalom prostoru komore izgaranja. S druge strane, za učinkovito i točno računanje stvaranja dušičnih oksida, shema stvaranja dušičnih polutanata mora biti ograničena na nekoliko važnih

homogenih reakcija koje dopuštaju povezivanje s turbulentnim procesom miješanja u komori izgaranja s naglaskom postizanja kompromisa između točnosti i računalnih mogućnosti. Takav integrirani pristup može poslužiti kao vrijedan alat za istraživanje i bolje razumijevanje složenih procesa višefaznog strujanja pri procesima izgaranja kao što su ponašanje gustog, ali i razrijeđenog spreja, kao i stvaranja dušičnih polutanata u praktičnim sustavima izgaranja.

Euler-Lagrangeova metoda (model diskretnih kapljica) je posebno prikladna za modeliranje razrijeđenih sprejeva, ali ima nekih nedostataka u blizini izlaza mlaznice u području gustog spreja. Ovi nedostatci mogu se poboljšati jačim fizikalnim povezivanjem plinovite i tekuće faze u području oko mlaznice korištenjem Eulerove višefazne metode. U ovoj metodi oblak kapljica se smatra kontinuumom, a jednadžbe konzervacije se rješavaju za plinovitu i sve tekuće faze. U usporedbi s Lagrangeovom shemom Eulerova shema računanja je učinkovitija za strujanja s velikom koncentracijom kapljica budući da Lagrangeova shema, osobito za nestacionarna izračune, zahtijeva velik broj skupina kapljica u svakom kontrolnom volumenu računalne domene. Kako bi se Eulerovom metodom bolje opisalo ponašanje spreja i karakteristike kapljica u gustom području spreja distribucija veličina kapljica je podijeljena na određeni broj odvojenih klasa (n tekućih faza) u kojima svaka faza zahtjeva svoj vlastiti set jednadžbi konzervacije, što znatno povećava vrijeme računanja. Oba pristupa, Euler-Lagrangeov i Euler-Eulerov, mogu rezultirati dugim vremenom računanja. Međutim, do neke mjere ta su dva pristupa komplementarna u smislu da jedan pristup može pomoći odvijanju drugog.

Glavni fokus ovog rada je primjena, optimizacija i validacija Euler-Eulerovog koncepta modeliranja gustog spreja u području blizu mlaznice. Osnovni cilj je bio uspostaviti validiran Eulerov pristup za modeliranje višefaznog strujanja koji se može s povjerenjem primijeniti u simulacijama visokotlačnog ubrizgavanja i raspršivanja goriva, naročito u području gustog spreja, pa se kao takav može primijeniti za spregnutu simulaciju s postojećim klasičnim Lagrangeovim pristupom modeliranja spreja pomoću modela diskretnih kapljica. S druge strane, rad je istovremeno usmjeren prema istraživanju i primjeni NO_x reakcijskih mehanizama, koji su važan dio ovog integriranog simulacijskog pristupa, kako bi se poboljšalo razumijevanje procesa stvaranja dušičnih polutanata u praktičnim inženjerskim primjenama.

<u>Eulerova višefazna simulacija spreja</u>

Korištenjem Eulerove višefazne metode provedena je opsežna računalna analiza visokotlačnog ubrizgavanja tekućih goriva (dizela) za različite tlakove ubrizgavanja u kombinaciji s različitim tlakovima komore.

Tekuće gorivo se ubrizgava u komoru za izgaranje u plinovitu fazu pomoću sustava za ubrizgavanje i raspršivanje tzv. mlaznice goriva. Struja tekućine raspršuje se u gusti oblak kapljica koje prodiru u komoru za izgaranje. Ovaj proces, poznat kao proces raspršivanja, uključuje primarno razbijanje mlaza u kapljice i naknadno sekundarno razbijanje kapljica. Primarno razbijanje mlaza odvija se u području oko mlaznice, dok se sekundarno razbijanje javlja u nizvodnoj zoni spreja i ono ne ovisi o mlaznici. U ovim procesima tekućina se raspada na male diskretne kapljice pod utjecajem jake turbulencije i aerodinamične interakcije s plinovitom fazom. Pritom se javljaju površinski valovi mlaza tekućine koji se razbijaju u kapljice zbog dominantnog utjecaja sila napetosti površine. Jake aerodinamične sile uzrokuju valove s kraćom duljinom i rezultiraju manjim kapljicama.

Pretpostavka Eulerove višefazne metode je da su plinovita i tekuće faza u međusobnoj interakciji i prožimanju. To znači da se Eulerov opis primjenjuje na raspršenu tekuću fazu, koja se tretira istom diskretizacijom, sličnim numeričkim metodama i osnovnim jednadžbama toka fluid kao i plinovita faza. Kapljice spreja su klasificirane u različite klase veličina kapljica prema volumnim udjelima i promjerima, te su tretirane kao odvojene tekuće faze.

Transportne jednadžbe mase, količine gibanja i energije riješavaju se za svaku fazu. Interakcije između faza izračunava se pomoću dodatnih članova jednadžbi koji opisuju izmjenu mase, količine gibanja i entalpije na granici između faza. Izmjena mase na granici između faza uključuje:

- primarno razbijanje mlaza;
- sekundarno razbijanje kapljica.
- isparavanje kapljica;

Kod visokotlačnog ubrizgavanja goriva izmjena mase u spreju počinje na samom izlazu goriva iz mlaznice gdje se mlaz goriva raspršuje prvo u ligamente, a onda u veće kapljice. Detaljni matematički model ovog procesa prikazan je u poglavlju 4.4.1.

U navedenom modelu izračunava se karakteristična duljina i karakteristično vrijeme razbijanja mlaza pomoću karakteristične turbulentne duljine, te karakterističnog turbulentnog i aerodinamičnog vremena. Kapljice proizvedene primarnim razbijanjem mlaza dalje se razbijaju u manje kapljice zbog djelovanja aerodinamičnih sila induciranom relativnom brzinom između kapljica i plinovite faze. Matematički model sekundarnog razbijanja kapljica prikazan je u poglavlju 4.4.2.

Izmjena količine gibanja na granici između faza opisana je silama otpora kapljica i turbulentne disperzije. Matematički modeli koji su korišteni za opisivanje ovih pojava opisani su u poglavlju 4.4.4.

Izmjena mase i entalpije uslijed isparavanja kapljica određena je Abramzon/Sirignano modelom koji je opisan u poglavlju 4.4.3.

Numerička simulacija visokotlačnog ubrizgavanja dizela provedena je uzimajući u obzir ukupno 6 faza. Prva faza je definirana kao plinovita faza, a ostale faze su definirane kao tekuće faze sa sljedećim klasama veličina kapljica: 5, 10, 20, 40 μm, i 205 μm što ujedno predstavlja i promjer mlaznice.

Provedena je varijacija koeficijenata pod-modela i ispitivan je njihov utjecaj na rezultate simulacija kako bi se optimizirao Eulerov višefazni model spreja i njegova stabilnost. Rezultati numeričke simulacije, penetracija gorivih para i tekuće faze, uspoređeni su s eksperimentalnim podacima za različite tlakove ubrizgavanja goriva u kombinaciji s različitim tlakovima u komori. Rezultati su u dobrom slaganju s mjerenjima za sve provedene simulacije za različite tlakove ubrizgavanja u kombinaciji s različitim tlakovima komore. Pokazalo se da je Eulerovom višefaznom metodom moguće predvidjeti utjecaj različitih tlakova ubrizgavanja na penetraciju gorivih para i tekuće faze.

Modeliranje dušičnih oksida

Učinkovito izgaranje tekućih goriva i emisije štetnih dimnih plinova ovise o procesu miješanja goriva i zraka, a na taj proces jako utječe dinamika spreja. U tom kontekstu, uz točno predviđanje ponašanja spreja, potrebno je predvidjeti i emisije polutanata kako bi se zadovoljile sve strože svjetske regulative o dopuštenim graničnim vrijednostima

emisija štetnih dimnih plinova. Dušični oksidi (NO_x), kao glavni polutanti proizvedeni izgaranjem, mogu nastati od molekula dušika (N_2) koje se nalaze u zraku i dušika koji je organski vezan u gorivu. Nastajanje dušičnih oksida opisano je detaljnim kemijskim kinetičkim mehanizmima. Stotine elementarnih reakcija uključeno je u stvaranje dušičnih oksida koji mogu nastati ili nestati preko 4 osnovna mehanizma tvorbe:

- termički NO;
- promptni NO:
- NO iz goriva
- dušični suboksid (N_2O).

Budući da se NO_x u pravilu ne emitira u ravnotežnim koncentracijama, kemijska kinetika pojedinih reakcija ima glavnu ulogu u određivanju razine emisija.

Numeričko modeliranje nastajanja dušičnih oksida ograničeno je s obzirom na modeliranje izgaranja, s obzirom da su reakcije koje proizvode NO i NO_2 mnogo sporije od cjelokupnog procesa oksidacije goriva. Da bi se razvio učinkoviti NO_x model potrebno je pojednostaviti opće reakcijske mehanizme, ali je s druge strane potrebno uzeti i u obzir dovoljno detalja kako bi se primjereno opisalo stvaranje NO_x-a. Takav pristup omogućuje povezivanje s procesima turbulentnog miješanja u RDF simulacijama stvarnih sustava za izgaranje kao što su kotlovi, peći, plinske turbine, motori s unutarnjim izgaranjem, itd. Stoga, za opisivanje stvaranja dušičnih oksida korišteni su reducirani kemijski kinetički mehanizmi. Ovakvim načinom znatno je skraćeno potrebno vrijeme računanja što čini ovu vremenski zahtjevnu metodu mnogo privlačnijom za industrijsku primjenu.

Prema tome pored modeliranja spreja, ovaj rad je usmjeren na istraživanje i implementaciju NO_x modela kao dijela integriranog simulacijskog pristupa, koji može modelirati stvaranje dušičnih polutanata u stvarnim sustavima za izgaranje, te se kao takav može koristiti za ispitivanje, projektiranje i optimiziranje različitih metoda izgaranja u svrhu smanjenja emisija dušičnih polutanata. Osnovna strategija u razvoju modela bila je prikupiti dostupne termo-kemijske parametre te važne kinetičke mehanizme nastale kao rezultat teoretske analize i pregleda literature, kako bi se što bolje aproksimirala osnovna obilježja stvaranja dušičnih polutanata u stvarnim sustavima za izgaranje. Kinetički mehanizmi korišteni u ovome radu bazirani su na dovoljno detalja da primjereno opišu stvaranje NO_x-a u turbulentnim sustavima

izgaranja, ali isto tako oni su bazirani i na dovoljno malo reakcija kako bi se omogućilo efikasno povezivanje s turbulentnim procesom miješanja. Kemijski kinetički mehanizmi korišteni u ovom radu za opisivanje stvaranja NO_x-a opisani su u poglavlju 5.2.2.

Proces izgaranja obično se odvija u turbulentnoj okolini, što zahtijeva posebnu pažnju kad se računaju koncentracije dušičnih oksida. Naime, uključivanje učinaka turbulentnih fluktuacija na reakcijske procese dušičnih polutanata vrlo je važan korak. Upravo zato, funkcija gustoće vjerojatnosti korištena je da bi se uzele u obzir turbulentne fluktuacije na brzinu nastajanja NO_x. Validacija NO_x modela izvedena je s pilotiranim slobodnim mlaznim plamenom metana i zraka, Sandia D plamenom, za koji postoje ekstenzivni eksperimentalni podaci. Rezultati simulacija pokazali su dobro slaganje s eksperimentalnim podacima, te su na taj način pokazane mogućnosti modela u proračunu dušičnih polutanata.

Validirani NO model primjenjen je kao dio integriranog simulacijskog pristupa i za računanje emisija dušičnih polutanata u stvarnoj konfiguraciji motora s unutarnjim izgaranjem.

Povezivanje Eulerove višefazne metode s Euler-Lagrangeovom metodom

Optimiziran i validiran Eulerov višefazni model gustog spreja korišten je zajedno s Lagrangeovim pristupom, modelom diskretnih kapljica, kao spregnuti model koji pokriva istovremeno i gusto područje spreja i razrijeđeno područje spreja, pružajući tako bolji opis oba režima strujanja. Takav spregnuti model primijenjen je u simulaciji stvarne konfiguracije motora s unutrašnjim izgaranjem. Ovime su spregnute dvije različite simulacije odnosno dva različita načina računanja spreja tekućeg goriva u motoru, višefazno Eulerovo računanje spreja i Lagrangeovo računanje spreja.

Kao što je već rečeno, Euler-Lagrangeova metoda posebno je prikladna za modeliranje razrijeđenih sprejeva, ali ima neke nedostatke u području gustog spreja. Naime, ograničenje ovog modela očituje se u tome da sprej mora biti dovoljno razrijeđen odnosno volumni udio diskretne faze mora biti manji od 10%. Daljnji nedostatak Euler-Lagrangeva pristupa je njegova računalna zahtjevnost za praktične

primjene budući da je za njegovo korištenje potrebna simulacija velikog broja skupina kapljica za zadovoljavajuće opisivanje ponašanja spreja. S druge strane, glavna prednost Euler-Lagrangeove formulacije je mogućnost dobivanja detaljnog fizikalnog opisa pojedinačnih raspršenih skupina kapljica u polju plinovitog strujanja.

U ovome radu, model diskretnih kapljica je korišten kao Euler-Lagrangeova metoda za računanje razrijeđenog spreja. U tom modelu sprej je opisan konačnim brojem grupa kapljica koje još nazivamo i skupinama kapljica. Pretpostavljeno je da su sve kapljice unutar jedne skupine približno jednako velike i da imaju ista fizikalna svojstva. Gibanje i prijenos skupina kapljica pratili su se kroz polje strujanja pomoću Lagrangeove formulacije, dok je plinovita faza opisana Eulerovom formulacijom. Putanja svake skupine kapljica unutar polja strujanja proračunata je uz pomoć niza jednadžbi koje opisuju njihovo dinamičko ponašanje tijekom gibanja kroz izračunato polje strujanja. Povezivanje između tekuće i plinovite faze postignuto je uvođenjem odgovarajućeg izvornog člana za masu, količinu gibanja i izmjenu energije na granici između faza.

Dvije simulacije, Eulerova višefazna simulacija spreja i Euler-Lagrangeovo računanje spreja, izvedene su istovremeno tako da se tijekom računanja izvorni članovi i rubni uvjeti međusobno preslikavaju i izmjenjuju između dva koda odnosno dvije simulacije. Eulerov višefazni model spreja simuliran je na mreži s finom rezolucijom koja pokriva samo mali dio motora neposredno blizu izlaza mlaznice. Cjelokupni proces izgaranja, nastajanja dušičnih polutanata i razrijeđenog spreja (Euler-Lagrangeov model) simuliran je na grubljoj pokretnoj mreži (*eng. moving mesh*) koja se preklapa s finijom mrežom i obuhvaća cijelu geometriju motora. To znači da postoje dvije različite simulacije koje se provode s dva različita koda kao što je prikazano na slici I. Prva simulacija se sastoji od računanja spreja s Eulerovim višefaznim modelom, a druga simulacija se sastoji od računanja razrijeđenog spreja s modelom diskretnih kapljica, ali i od računanja cjelokupnog procesa izgaranja i stvaranja dušičnih polutanata.

Rubni uvjeti potrebni za računanje Eulerova spreja preslikavani su od drugog koda odnosno druge simulacije koja pokriva cjelokupnu domenu računanja. S druge strane, izvorni članovi za masu, količinu gibanja i energije izračunati su s višefaznom Eulerovom metodom te mapirani su za računanje plinovite faze kod simulacije cijelog motora pomoću ACCI servera koji povezuje ta dva koda.
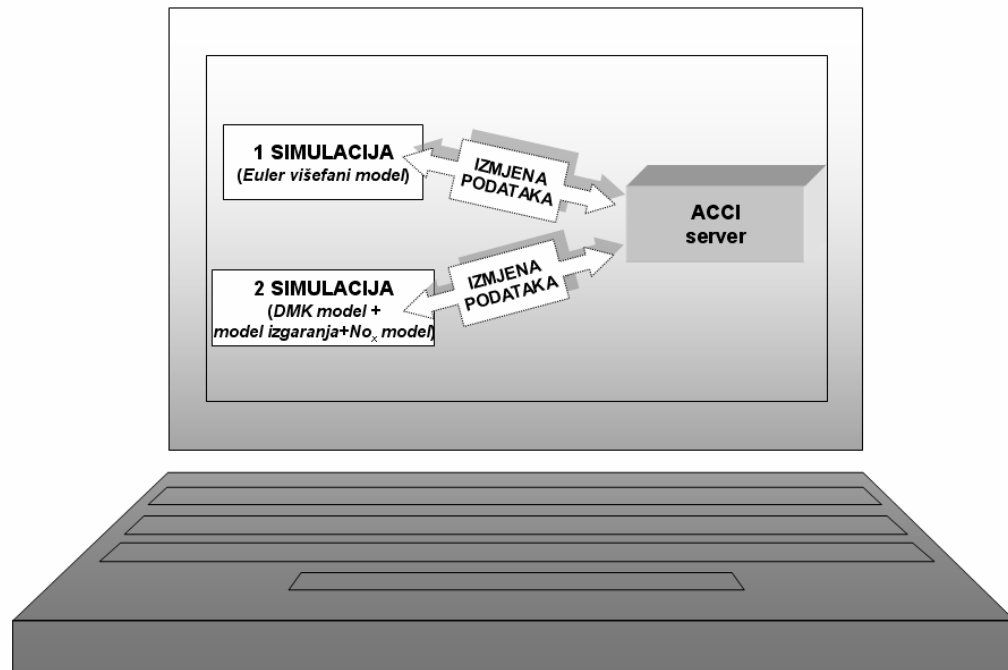
Slika I: Povezivanje dvije simulacije - Eulerove višefazne metode s Euler-Lagrangeovom metodom

Nadalje, tekuće višefazno strujanje odnosno udijeli kapljičastih faza, izračunati Eulerovim sprejom na finoj mreži, mapirani su na Lagrangeov sprej na način da se tekuće faze pretvaraju u određene grupe diskretnih kapljica.

Ova integrirana metoda nastala spajanjem validiranog Eulerovog modela spreja i postojećeg Lagrangeovog modela spreja predstavlja koristan koncept za računanje dinamike spreja koji se može koristiti za simulaciju različitih fizikalnih režima strujanja. Rezultati proračuna pokazali su da ovakav pristup povezivanja i istovremenog računanja dviju simulacija radi dobro i daje zadovoljavajuće rezultate.

Doprinos rada

Ovaj rad je unaprijedio i objedinio validirane simulacijske metode pomoću kojih je moguće dovoljno točno opisati gusti i razrijeđeni sprej tekućeg goriva u sprezi s

procesima izgaranja i stvaranja dušičnih polutanata. Ovakav integrirani pristup može se koristiti kao napredan alat za numeričke simulacije turbulentnih višefaznih strujanja u sustavima izgaranja u praksi. Prema tome, ove objedinjene metode omogućavaju detaljnu analizu i razumijevanje složenih procesa ponašanja spreja pri ubrizgavanju tekućih goriva i stvaranja dušičnih polutanata pri izgaranju. Pored toga, ovakav predloženi integrirani pristup doprinosi smanjenju visokih troškova i dugotrajnih eksperimentalnih istraživanja u modernim inženjerskim razvojnim procesima.

U ovome radu predložene su metode koje objedinjuju opisivanje ponašanja gustog i razrijeđenog spreja tekućeg goriva s ciljem boljeg opisivanja stvaranja polutanata. Na taj način unaprijeđeno je opisivanje procesa miješanja goriva i zraka, a samim time i stvaranje polutanata u cijeloj komori izgaranja. S takvim pristupom moguće je postići veću učinkovitost potrošnje goriva s minimalnom produkcijom emisije polutanata u modernim sustavima izgaranja u praksi. Nadalje, RDF alati razvijeni u ovom radu moći će poslužiti kao osnova za daljnji znanstveno istraživački rad u modeliranju složenih fizikalnih i kemijskih procesa kao što su raspršivanje i izgaranje tekućeg goriva u sustavima za izgaranje.

Keywords

Computational fluid dynamics, multiphase flow, nitrogen oxides, Eulerian multiphase model, discrete droplet model, diesel spray

Ključne riječi

Računalna dinamika fluida, višefazno strujanje, dušični oksidi, Eulerov višefazni model, model diskretnih kapljica, dizel sprej

Nomenclature

Roman	Description	Unit
A	Surface area;	m^2
	Coefficient in the Arrhenius expression;	
	Eddy break-up model constant	
A_1	NO_x model constant	
b	Oxygen reaction order	
B	Eddy break-up model constant	
B_0, B_1	Secondary break-up constants	
B_2, B_3, B_4	NO_x model constant	
B_M	Mass transfer number	
B_T	Heat transfer number	
c	Concentration	mol/ m³
c_p	Specific heat capacity	J/(kgK)
c_D	Drag coefficient	
c_T	Turbulent dispersion coefficient	
C	Constant	
$C_1, C_2...C_7$	Primary break-up constants	
C_μ	Constant in turbulence model	
$C_{\varepsilon 1}, C_{\varepsilon 2}, C_{\varepsilon 3}$	Constants in turbulence model	
D	Turbulent dissipation inter-phase exchange;	W/(m³s)
	Diffusion coefficient of the species;	m^2/s
	Diameter	m
D_k	Diffusion coefficient of the species k	m^2/s
D_{ij}	Strain rate tensor component	1/s
e	Specific energy	J/kg
E	Activation energy	J/kmol
f	Correction factor	

f_i	Cartesian component of the force vector	m/s^2
F_D	Drag force	N
F_M, F_T	Diffusional film correction factors	
h	Specific enthalpy	J/kg
H	Interfacial heat exchange term	W/m³
i	Specific Internal energy	J/kg
k	Turbulent kinetic energy;	m^2/s^2
	Thermal conductivity;	W/(mK)
	Reaction rate coefficient	
$k_{f,j}$	Forward rate coefficient of the reaction j	
$k_{b,j}$	Backward rate coefficient of the reaction j	
K_j	Equilibrium constant of the reaction j	
K	Turbulent kinetic energy inter-phase exchange term	W/m³
L	Length	m
Le	Lewis number	
L_T	Turbulent length scale	m
L_W	Aerodynamic length scale	m
m	Mass	kg
$m(\Gamma)$	Probability of occurrence	
M	Momentum inter-phase exchange term;	N/m³
	Mass inter-phase exchange;	$kg/(m^2 s)$
	Molecular weight of the species	kg/kmol
M_i	Species i	
n	Number of carbon	
n_j	Cartesian component of the unit normal vector	
n_{ph}	Number of phases	
N	Number of experiments;	
	Droplet number density;	$1/m^3$
	Number	
Nu	Nusselt number	

Oh	Ohnesorge number	
p	Pressure	Pa
P	Production term in equation for the turbulent kinetic energy;	kg/(ms^3)
	Probability density function	
q_j	Cartesian component of the heat flux vector	W/m^2
Q	Heat transfer	J
r	Radius	m
Re	Reynolds number	
R	Universal gas constant ($R = 8314.4$)	J/(kmolK)
S	Distance;	m
	Surface;	m^2
	Source term	
Sc	Schmidt number	
Sh	Sherwood number	
t	Time	s
T	Temperature;	K
	Taylor number	
u	Velocity;	m/s
	Normal velocity	m/s
u_j	Cartesian velocity component	m/s
v	Velocity	m/s
V	Volume	m^3
w	Reaction rate	1/s
wf	Weighting factor	
W_i	Molecular weight of the species *i*	kg/kmol
We	Weber number	
x	Co-ordinate direction	
x_j	Cartesian co-ordinate	m
X_i	Species mole fraction	kmol/kmol
X_k	Phase indicator	

$[X_i]$	Species mole concentration	kmol/m^3
Y	Species mass fraction	
Z	Mixture fraction	

Greek	**Description**	**Unit**
α	Argument in beta function	
α_k	Volume fraction;	
β	Argument in beta function;	
	Binary diffusion coefficient;	
	Coefficient in Arrhenius expression	
Γ	Diffusion coefficient;	
	Realisation in event space;	
	Mass inter-phase exchange term	kg/(m^{3}s)
ε	Dissipation rate of the turbulent kinetic energy	m^2/s^3
θ	Specific energy source	W/kg
κ_k	Thermal conductivity	W/(mK)
λ	Thermal conductivity;	W/(mK)
	First viscosity coefficient	Pas
Λ	Wave length	m
μ	Dynamic viscosity (molecular);	Pas
	First viscosity coefficient	Pas
μ_t	Turbulent viscosity	kg/(ms)
ν	Kinematic viscosity (molecular)	m^2/s
ν'_{ij}	Reactant species stoichiometric coefficient	kmol
ν''_{ij}	Product species stoichiometric coefficient	kmol
ρ	Density	kg/m^3
σ	Surface tension	
$\sigma_k, \sigma_\varepsilon$	Constants in turbulence model	
σ_{ji}	Stress tensor component	N/m^2
σ_T	Turbulent Prandtl number	

τ	Time	s
τ_a	Secondary break-up time scale	s
τ_A	Break-up time scale	s
τ_T	Turbulent mean time scale	s
τ_W	Aerodynamic time scale	s
τ_{ij}	Tangential stress tensor component	N/m^2
φ	Intensive (scalar) property	
Φ	Equivalence ratio	
χ	Scalar dissipation rate	1/s
$\dot{\omega}_i$	Production rate of the species i	kg/(m^{3}s)
Ω	Growth rate	1/s

Subscripts	Description
avg	Average
e	Engine
eq	Equilibrium
E	Evaporation
D	Droplet;
	Drag
F	Fuel
g	Gas
i	Species index
j	Reaction index
k,l	Phase indices
N	Bulk liquid phase
noz	Nozzle
O	Oxidiser
P	Primary break-up
primbr	Primary break-up
s	Spray

sec *br*	Secondary break-up
spec	Species
st	Stoichiometric
stable	Stable
S	Secondary break-up;
	Surface
reac	Reactions
t	Turbulent
T	Turbulent dispersion force
Y	Species
ε	Dissipation rate of the turbulent kinetic energy
φ	Intensive (scalar) property
∞	Ambient conditions

Superscripts	**Description**
'	Reynolds fluctuation
"	Favre fluctuation
*	Modified
$^{-}$	Reynolds average
$\sim$	Favre average
Eq	Equilibrium
Ext	Extinction
old	Value from previous time step
t	Turbulent

Mathematical symbols	**Description**
$e = 2.718281828\ldots$
erfc^{-1}	Inverse complementary error function
$\exp$	Exponential function ($\exp(x) \equiv e^{x}$)
B	Beta function
Γ	Gamma function

$\prod$	Product
$\sum$	Summation
δ_{ij}	Kronecker tensor component
$\pi = 3.141592654\ldots$	

Abbreviations	**Description**
2D, 3D	Two-, three-dimensional
CFD	Computational fluid dynamics
CSC	Chemistry pre-processor (abbr. conserved scalar chemistry)
DDM	Discrete droplet model
DNS	Direct numerical simulation
DTRM	Discrete transfer radiation method
LES	Large-eddy simulation
PDF	Probability density function
RANS	Reynolds averaged Navier-Stokes
SLFM	Stationary laminar flamelet model
VOF	Volume of fluid method

List of Figures

List of Tables

1 Introduction

1.1 Motivation and General Overview

With the development of increasingly affordable and powerful computers, advanced computer simulation modelling using Computational Fluid Dynamics (CFD), also referred as virtual engineering, has become a valuable tool that can be used to provide insight and understanding of the fossil fuel combustion processes. CFD has become one of the key technologies used for performing basic research of fluid flow, multiphase and reacting flow, and related phenomena in practical combustion systems by numerically solving physics-based differential equations. The usefulness of CFD has also been supported by the fact that intensive experimental investigations of the practical engineering applications result with a high cost and are time-consuming investigations. Recently, modern engineering development process has been making the transition from purely experimental investigations to a mixture of experimental and numerical simulation investigations. Besides the significant reduction of time and costs involved in designing modern efficient combustion systems CFD simulations can be used as a research tool to provide insights in turbulent, reacting multiphase flows and for the development of improved physical and chemical sub-models. Researchers have invested significant effort over the last few decades in the development of multidimensional, mathematical models in order to provide detailed insight into the complex interacting physical and chemical processes required for design and optimization of the various combustion systems. Despite ongoing efforts in the development of both physical and chemical modelling, CFD simulation of the complex multiphase processes in practical combustion systems cannot yet be considered fully predictive on a quantitative level.

In many modern industrial applications, multiphase flow research has been directed toward the understanding of the phenomena occurring within the spray, such as droplet size distribution and mixing process of fuel and air. Combustion of liquid fuel flows are frequently encountered in practical circumstances, e.g., oil-fired boilers, industrial furnaces, gas turbines, internal combustion engines, liquid rockets, chemical processes etc. The liquid fuels are injected into the combustion chamber by an injector

atomizer system and burned as a dispersed liquid phase carried by a gaseous flow. The injector atomizer system forms a large number of droplets in order to accelerate evaporation and combustion by increasing the free fuel surface area. Different phenomena are involved in the spray process such as primary and secondary atomization, droplet propagation and evaporation, droplet collisions etc. The resulting multi-phase flows are very complex processes, including turbulence, mass and heat transfer, droplet dynamics, and phase changes that are strongly coupled. Thus, in-depth understanding of spray behaviour is very challenging yet critical regarding the improvement of efficiency of modern combustion devices in order to meet future limitations on pollutant emissions.

Different modelling approach currently exists for multiphase flows such as Eulerian-Lagrangian, Eulerian Multiphase, Volume of Fluid (VOF) etc. The most commonly used is the Eulerian-Lagrangian methode, also known as the Discrete Droplet Model (DDM). This method is especially suitable for modelling dilute sprays, but has some disadvantages in the near nozzle region with respect to insufficiency of the physics in a dense spray, where particle interaction is strongly influenced by collision. Furthermore, this method is very sensitive to the grid resolution in the near nozzle region and also shows statistical convergence problems. This can be improved by stronger physical coupling of the gas and the liquid phase in the near nozzle region using an Eulerian-Eulerian method. This method provides a more accurate description of the physics in the dense spray region by treating each size group as a completely separate phase and solving conservation equations for each of them. However, the main disadvantage of most Eulerian spray models is the higher computational effort if more than one droplet size group is to be simulated.

In that context, this doctoral thesis will focus on adopted methods for numerical simulation of multiphase droplet flow phenomena in practical combustion systems. This work will tend to provide validated simulation strategies that can be used with confidence as an important part of the modern engineering development process in order to contribute to the reduction of product development time and costs.

1.2 Literature Review

Numerous studies of spray processes have helped engineers establish criteria to design and develop a more efficient use of liquid fuels with a minimal amount of pollutant emissions in practical engineering and related fuel technology [1][2][3][4][5][6]. It is known that formation of nitrogen pollutants is highly dependent on temperature [7], and that soot can occur in fuel rich zones [8]. Common methods to reduce pollutants are therefore to reduce maximum flame temperature and to reduce the size of fuel-rich zones where fuel rich concentration and high temperature gradients can arise. In order to achieve these goals, a deep knowledge of multiphase flow processes, spray dynamics and the interaction between the liquid and gas phase is required. Therefore, various modelling approaches have been developed that involve consideration of various multiphase gas-liquid flows and spray phenomena such as primary and secondary atomization, droplet propagation and evaporation, droplet collisions etc. Reviews by Kuo [5], Chiu [11], Faeth [9][10], Crowe [14][15] and Sirignano [13] cover in detail discussion of current research results and directions of spray and droplet modelling.

Numerical simulation of spray dynamics in complex turbulent multiphase flow is a particularly challenging problem. Researchers who investigate the droplet and spray modelling concepts and methodologies have contributed to major accomplishments of basic and practical significance. During the last few decades, the droplet and spray research has been focused in two main directions:

- Modelling of fundamental physical and chemical phenomena that occur in spray processes, isolating and studying the details of a single droplet as a detailed description of evaporation, mass and energy molecular transport in the gas phase, in the droplet and at the inter-phase. This modelling approach has been and is still appreciated by researchers because of its simplicity compared with the much complex nature of dense spray.

- Modelling of modern industrial applications, where spray involves a number of complicated physical and chemical phenomena and therefore the sub-models, including models for spray injection, atomization, primary and secondary break-up, drop drag, droplet distortion, coalescence, spray-wall impingement,

droplet evaporation, heat transfer etc. for all of the physical process need to be employed.

The liquid fuels are usually injected into the combustion chamber by an injector atomizer system. The emerging liquid stream breaks-up into a dense cloud of droplets that penetrate into the combustion chamber. This process, known as atomization, involves primary break-up at the liquid surface followed by secondary break-up [14][15]. The primary break-up takes place in the region close to the injector atomizer, while the secondary break-up occurs in the downstream spray zone and is independent of the injector atomizer. In these processes the liquid is disintegrated into small discrete droplets by the influence of strong turbulence and aerodynamic interaction with the gas phase environment. Surface waves of the liquid jet arise and break-up into droplets due to the dominance of the surface tension force. Higher aerodynamic forces cause shorter wave lengths and result in smaller droplets.

In the analysis of dilute sprays and related dilute, dispersed flows, a locally homogenous flow model, referred by Faeth [9][16] can be used. Locally homogenous flow analysis only accurately represents dilute, dispersed flows because it assumes that the phases are in dynamic and thermodynamic equilibrium, having the same velocity and temperature at each point in the fluid, whereas inter-phase exchanging rates are assumed to be infinitely fast. According to Faeth [16] this model is most appropriate when the droplet size is small enough and the densities of the phases are similar. In order to take into consideration the effects of finite rates of exchange of mass, momentum, and energy between the liquid and gas phase, the other analytical method, the separated flow method, can be used [5]. In recent years, the development of separated flow models has proven to be of great importance, since the former method is limited to the condition when the droplets in the spray are infinitely small. The separated flow method has three different approaches: Eulerian-Lagrangian, Eulerian-Eulerian and probabilistic [5][13]. The most commonly used is the Eulerian-Lagrangian method, also known as the Discrete Droplet Model (DDM) [17][18]. In this approach, the spray is represented by finite numbers of droplet groups, called droplet parcels. It is assumed that all the droplets within one parcel are similar in size and that they have the same physical properties. The motion and transport of the droplet parcels are tracked through the flow field using a Lagrangian formulation, while the gas phase is described

by solving conservation equations using a Eulerian formulation. The trajectory of each droplet parcel within the flow field is calculated using the Lagrangian scheme, which means that representative parcels are tracked by using a set of equations that describe their dynamic behaviour as they move through the calculated flow field. The coupling between the liquid and the gaseous phases is taken into account by introducing appropriate source terms for interfacial mass, momentum and energy exchange [18][19].

In the last few decades, various Lagrangian-Eulerian approaches have been developed and used, but all of them have difficulty determining the fluid instantaneous velocity field at the discrete partical location, all along the trajectory of the traced discrete parcel [17]. The Lagrangian-Eulerian approach has been used by many researchers and various improvements to the basic scheme have been proposed [17][20][22]. In recent years this approach has been dominate in predicting the behaviour of spray. Although various researchers and engineers have used the Lagrangian-Eulerian formulation as a numerical simulation tool for prediction of characteristics of complex multiphase flows to guide their engineering devices design, the concept and application have severe limitations. This formulation is very sensitive to the grid resolution in the near nozzle region [23][24] and is limited for adequate representation of dense spray. This assumes that spray is sufficiently diluted; usually discrete phase volume fractions must be less than 10 %. An even greater disadvantage of the Lagrangian-Eulerian approach is that it is computationally expensive for practical applications, since a huge number of parcels is required to describe spray behaviour. It also entails   statistical convergence problems [25]. On the other hand, the main advantage of the Lagrangian-Eulerian formulation is obtaining a detailed physical description of individual parcels of dispersed phase in the gaseous flow field.

In the Eulerian-Eulerian separated flow model, both the gas-phase and liquid phase are considered as though they were interacting and interpenetrating continua. That means that the Eulerian description is applied to the dispersed liquid phase, which can be treated with the same discretization, similar numerical techniques and governing equations as are used for the gaseous phase. This approach was first addressed by Harlow and Amsden [26][27]. They developed this numerical technique for the multiphase flow dynamics in which several fields interpenetrate and interact with each

other. The Eulerian-Eulerian approach has been adopted by a number of researches and applied for numerical simulation, e.g. [28][29][30][31][32][33]. Recently an alternative approach to the modelling of spray has been developed by Beck and Watkins [34][35] In this approach the size information regarding the spray is obtained by solving transport equation for two moments of the drop number distribution, and their respective mean velocities, and by obtaining two other moments from an assumed size distribution function [36]. This approach has been applied by Edelbauer [37] in simulations of the oil droplet flow in the crankcase of an IC engine.

Currently, the most commonly used models based on the Eulerian formulation in numerical simulation are the Volume of Fluid (VOF) model and the Eulerian multiphase model. The VOF technique, first reported in [38], is designed as an interface tracking method where sharp changes in physical properties occur across interfaces. A detailed review of VOF methods is given by Scardovelli and Zaleski [39]. In the VOF model, a single momentum equation is calculated for all phases that interact and the volume fraction of each of the phases is tracked throughout the calculation domain. In this way calculation of volume fraction equations are more accurate by allowing sharp resolution between the interfaces. The VOF method is a useful tool for investigating interfacial behaviour in multiphase flows and is of great interest in applications that explain the fundamental microphysics of multiphase flows. However, its application in practical industrial systems is limited because of the complexity and vast computational effort involved. In order to reduce computational effort, instead of tracking the interface between the phases and determining the exact location of the surface, it is possible to calculate the average values of interest by using a multiphase Eulerian interpenetration continua formulation [40]. Basically, all phases are treated as inter-penetrating media and conservation equations are written for each phase, with closure laws (often empirically based) written to describe their interaction. The behaviour of the dispersed phase is represented only in terms of its phase fraction and velocity, while the behaviour of individual droplets is lost in the modelling.

As discussed in the first section, an efficient use of liquid fuel and generated pollutant emissions depend on the fuel-air mixture process, which is strongly influenced by the spray dynamics. In that context, in addition to accurate prediction of spray behaviour, it is necessary to have an advanced numerical tool for the prediction of

pollutants in order to meet increasingly stringent regulation worldwide. As one of the top pollutants produced by combustion, nitrogen oxides (NO_x) can be formed from the molecular nitrogen (N_2) carried with the air and the organic nitrogen bound in fuels (fuel-N) via different paths, which are included in detailed chemical kinetic mechanisms and account for the reactions leading to NO_x. Hundreds of elementary gas-phase reactions are involved in the formation of NO_x, which can be formed or destroyed by at least four separate reaction processes in the gas phase: thermal NO; prompt NO; fuel NO; and nitrous-oxide (N_2O). Since NO_x pollutants are typically not emitted in equilibrium concentrations, finite-rate kinetics plays a role in determining the levels of emissions. Emissions of oxides of nitrogen are limited because the reactions that produce NO and NO2 are much slower than the overall process of fuel oxidation. Available detailed NOx chemical kinetic mechanisms come from Miller and Bowman [41], Glarborg [42] and GRI [43], Baulch [44] , Dagaut [45], Glassman [46] and Kilpinen [47]. However, the development of an effective NO_x model requires simplification of such generalized reaction mechanisms, taking into account sufficient details to adequately describe the NO_x reaction process, and to allow coupling with the turbulent mixing process in CFD simulation of practical combustion systems such as boilers, furnaces, internal combustion engines etc. [48][49][50][51]. Consequently, reduced kinetic mechanisms have to be used in comprehensive combustion codes to describe the NO_x reaction processes, allowing the reduction of calculation time and making this time-consuming method more attractive for industrial application. NO_x pollutant modelling, by means of CFD, has been reviewed by Hill and Smoot [48], providing an overview of NO_x mechanisms and modelling for the prediction of NO_x in practical combustion systems. One of the recent approaches for prediction of NO_x in practical combustion systems by means of CFD, presented by Faticelli [52] and Frassoldati [53], are based on a 3D CFD simulation coupled to a postprocessor which yields reactor networks, extracted from 3D fields, as equivalent simplified flow models for which it is possible to use a detailed reaction kinetics for the calculation of the NO_x formation and destruction.

To summarize, the Eulerian-Lagrangian method (Discrete Droplet Model) is especially suitable for modelling dilute sprays, but has some disadvantages in the near nozzle region with respect to insufficiency of the physics in a dense spray. It is very

sensitive to the grid resolution and shows statistical convergence problems. This can be improved by stronger physical coupling of the gas and the liquid phase in the near nozzle region using the Eulerian multiphase method, where a cloud of droplets is regarded as a continuum, and conservation equations are solved for gas and liquid phase. Compared to the Lagrangian scheme, the Eulerian scheme calculation is fairly efficient for flows with a high concentration of droplets, while the Lagrangian scheme, particularly for unsteady calculations, generally requires a large number of parcels in each control volume of the calculation domain. However, in order to better capture the behaviour of spray and the characteristics of droplets in the dense region using the Eulerian framework, the droplet-size distribution has to be divided into a number of separate size classes (n liquid phases), where each phase requires its own set of conservation equations, which considerably increases computational effort. Both of these approaches can result in very long calculation times and to some extent, these approaches are complementary in many respects- the use of one approach can lead to progress to the other. For instance, the Euler Lagrange Spray Atomization model for two phase flows [54][56] was proposed recently, where the Eulerian method is applied for calculation of the dense region of spray and is then completed in the diluted region of spray by the Lagrangian method. A further concept for simulation of different flow regimes, both dense and dilute spray, by using the Eulerian multiphase approach coupled by Lagrangian DDM approach is proposed in [57]. It is clear that such an approach may successfully capture the behaviour of spray in complex flow regimes, both for dense and dilute flow regimes, which is very important for many industrial problems.

The preceding review clearly illustrates that there exists a variety of spray models that can predict a variety of spray phenomena. Most of these models work well for some regions of multiphase spray flows, but a complete efficient integrated approach to deal with real practical industrial problems is still being investigated. Moreover, the required integrated approach, besides the suitable validated spray modelling process, needs to capture and other important aspects of reacting multiphase flows such as prediction nitrogen emission formation. in order to serve as a valuable tool to design and develop a more efficient use of liquid fuel with a minimal production of nitrogen pollutants.

1.3 Hypothesis and Work Outline

An integrated simulation approach can be applied in numerical simulation of turbulent multiphase droplet flow in practical engine configuration, adopting and optimizing methods for simulation of dense and dispersed spray in conjunction with combustion and nitrogen emission formation. Suitable validated Eulerian multiphase spray is required in order to be used with confidence for accurate calculation of the dense liquid spray near the nozzle region and to be coupled with the classic Lagrangian spray DDM method used in the remaining combustion chamber. For efficient and accurate calculation of NO_x formation, a nitrogen pollutants prediction scheme needs to be limited to sufficiently few homogeneous reactions to allow effective coupling with the turbulent mixing process in a selected practical combustion chamber, emphasising compromised solution between accuracy and affordability. This integrated simulation approach can be applied as a valuable tool used to investigate and improve understanding of these complex processes, including spray behaviour in the dense and dispersed region, respectively, on one side, and on the other side nitrogen pollutants formation processes in practical combustion chambers.

The main focus of this work, on one side, is on application, optimisation and validation of the Eulerian multiphase spray modelling concept for spray in a near nozzle dense spray region. The objective is to establish the validated Eulerian multiphase spray modelling approach that can be applied with confidence in high pressure spray simulations, particularly in dense regions of spray, and as such can be applied for a coupled simulation with the existing classic Lagrangian DDM spray modelling approach. On the other side, the work is aimed at research and implementation of NO_x reaction mechanisms, as an important part of this integrated simulation approach, to be used to improve understanding of formation of nitrogen pollutant processes in practical engineering applications.

In the first step of this work, the comprehensive calculation study is performed for high pressure liquid spray with the Eulerian multiphase method for variations of injection and chamber back-pressure. The spray droplets are classified into different size classes by volume fractions and diameters, and treated as separate liquid phases. Both gaseous and liquid phases are treated as interpenetrating, interacting continua.

Mass, momentum and energy conversation equations are solved for each phase as well as equations for turbulent kinetic energy, turbulent energy dissipation, and species transport. The interactions between the phases are calculated by mass, momentum and enthalpy interfacial exchange terms. The interfacial mass exchange between the gaseous phase and the liquid phase includes droplet evaporation, primary break-up and secondary break-up, while the interfacial momentum exchange includes drag forces and turbulent dispersion forces. In this part of research, droplet size classes are treated with fixed droplet size classes. The variation of sub-model coefficients is performed and its impact on predictions is investigated to optimize the Eulerian multiphase spray model and its stability. The results of numerical simulation for vapour and liquid penetration curves are compared with experimental data for different injection pressures combined with two different chamber pressures.

In the next step of the research, the optimized and validated Eulerian multiphase spray approach is used together with the Lagrangiane DDM spray approach and applied for coupled simulation of real engine configuration, covering at the same time the dense and dispersed spray region and providing better description in both flow regimes. The Eulerian multiphase spray calculation is only performed close to the nozzle, while the Lagrangian spray calculation is performed in the remaining combustion chamber. Two different calculations are coupled, multiphase Eulerian spray calculation with the Lagrangian spray single phase engine calculation, performed and simultaneously run by mapping and exchanging spray source terms and boundary conditions during simulations. The Eulerian multiphase spray is calculated in a finer mesh that covers only a small part of the engine downstream of the nozzle exit, while the single phase engine is calculated in the coarser moving mesh, which overlaps the finer mesh and covers the entire engine geometry. The boundary conditions for the Eulerian spray calculations are mapped from the engine calculation. On the other side, mass, momentum, and energy sources calculated in multiphase Eulerian spray are transferred to the gas phase calculation of the single-phase engine via the code-coupling server. The liquid flow calculated by Eulerian multiphase spray on a fine mesh is transferred to Lagrangian spray and converted to DDM parcels in the remaining combustion chamber. This integrated method, coupling between validated Eulerian spray with existing

Lagrangian DDM spray, provides a useful concept for the calculation of spray dynamics that can be used for the simulation of different physical flow regimes.

Besides spray modelling, this work is also aimed at research and implementation of the NO_x model, as part of an integrated simulation approach, which is capable of modelling nitrogen-containing pollutant formation in practical combustion systems, and which can be used to investigate, design, and optimize various combustion techniques used to reduce nitrogen pollutant emissions. The strategy in model development is to collect the best available thermo-chemical parameters and important kinetic mechanisms as a result of theoretical analysis and the literature review, using a "minimum" set of reactions to approximate the essential features of the NO_x reaction process in practical combustion systems. These kinetic mechanisms must contain sufficient details to adequately describe the NO_x reaction process in turbulent combustion systems, but on the other hand they must also consist of sufficiently few reactions to allow for coupling with the turbulent mixing process. The combustion process typically takes place in a turbulent environment, which requires special consideration when predicting NO concentrations. Therefore, incorporating the effects of the turbulent fluctuations on NO pollutant reaction processes is a very important step, and consequently the presumed probability density function (PDF) approach is used to account for the effects of turbulent fluctuations on the kinetic rates of NO, integrating the kinetic rates with respect to turbulent fluctuations. The validation of the model is performed for the piloted methane/air jet flame. The implemented NO model is also applied, as an integrated simulation approach, for the calculation of nitrogen pollutant emission in real engine configuration.

1.4 Thesis Contribution

It is expected that this work contributes to the enhancement and integration of different simulation methods that describe high pressure dense and dispersed liquid fuel spray behaviour in conjunction with combustion and nitrogen emission formation. This work establishes a validated integrated simulation approach used in numerical simulation of turbulent, reacting multiphase flow in practical combustion systems, which can serve as an advanced tool to analyze and improve understanding of these complex processes with an emphasis on spray behaviour and the nitrogen pollutant formation process. Furthermore, this integrated simulation approach can be applied to reduce high cost and time-consuming experimental investigations in modern engineering development processes.

The adopted integrated simulation methods describe very well high pressure dense and dispersed liquid fuel spray behaviour, resulting in a better description of the fuel-air mixing process and the pollutant formation process in the entire combustion chamber, which are crucial issues to ensure achieving today's highest fuel conversion efficiency and minimum production of pollutant emissions of modern combustion systems. Furthermore, CFD tools developed in this work can serve as a basis for further research in modelling of complex physical and chemical processes such as spray behaviour and combustion of liquid fuel in practical combustion systems.

2 Fundamentals of Spray

2.1 General Consideration

Liquid sprays are important and used in a widespread field of technical applications, including in process industries, the pharmaceutical industry, agriculture, industrial boilers, internal combustion engines, gas turbines, rockets, spray painting, spray cooling, fire extinction, and many other applications. A spray can be generated in diverse ways depending on the field of application. This thesis considers sprays produced by the pressure atomization technique from the fuel injection system. The liquid fuel is injected through the nozzle hole into the combustion chamber, where fuel is dispersed in order to increase surface area for fast evaporation, ensuring appropriate mixing between the liquid fuel and gas. The produced spray significantly influences the combustion efficiency and the formation of pollutants. Thus, in-depth understanding of spray processes is relevant for the design and development of effective modern combustion devices. Consequently, optimization of the spray process and production of spray with desired quality is very important for improving fuel consumption and reducing exhaust emission both of which are essential in meeting future emission restrictions.

In this study, the spray is formed by a high-pressure injection of liquid fuel trough a small nozzle hole into a gaseous environment. The liquid enters the combustion chamber at very high velocity in the form of a liquid jet, tends to become unstable and disintegrates into fragments, and then further dissolves into smaller droplets, as illustrated in Figure 2.1.
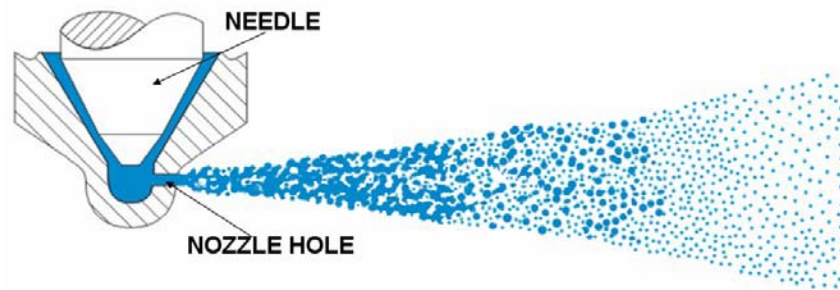
Figure 2.1: Schematic illustration of spray structure

In a case of high pressure injection the main break-up mechanisms are cavitation and turbulence generated inside the nozzle, and caused by a significant pressure difference and small nozzle dimensions. Once the fragments and droplets are formed, after primary atomization they may further break-up into smaller droplets. A full cone spray is formed where most of the liquid is located near the spray axis, while the edge of the spray region is compromised by less liquid mass. Downstream from the nozzle the spray is more and more diluted. Droplet velocities are maximal at the spray axis, while they decrease in the radial directions.

The break-up of the injected liquid and subsequent break-up of the droplets are distinguishable processes and they can generally be classified as:

- **primary break-up of the liquid jet**: This type describes the break-up of the liquid jet first into fragments and then disintegration into spherical droplets after further disintegration. It typically takes place in the region near the injector nozzle exit, as illustrated in Figure 2.2. In this region spray is usually termed as dense spray.

- **secondary break-up of the liquid droplets**: The initial spherical droplets can further break-up into smaller fragments and droplets by means of aerodynamic forces. This type of break-up typically takes place far from the nozzle, as illustrated in Figure 2.2, and is largely independent of the nozzle type. In this region spray is termed as thin and dilute spray.
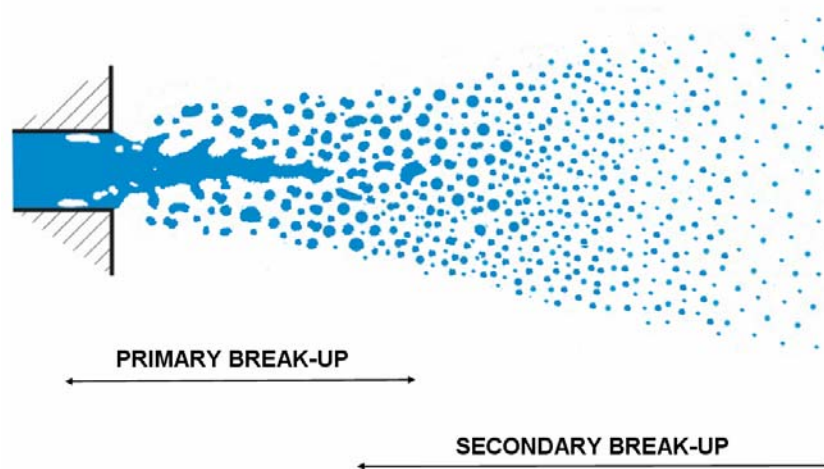
Figure 2.2: Schematic illustration of main break-up mechanisms

The primary break-up of the liquid jet and secondary break-up of the liquid droplets occur as a result of hydrodynamic instabilities on the liquid gas interface known as Kelvin-Helmholtz and Rayleigh-Taylor instabilities. Kelvin-Helmholtz instabilities are caused by the viscous forces due to relative motions between liquid and the ambient gas. These forces produce waves on the liquid surface, which grow and can break-up into droplets. The Rayleigh-Taylor instabilities happen on droplets due to inertia of the denser fluid opposing the system acceleration. The waves are formed on the backside of the droplet due to deceleration of the injected droplet and can further break-up into smaller droplets. The knowledge obtained from the instability analyses [58] in combination with experimental observation has resulted in the basis for liquid atomization and droplet break-up modelling of sprays.

The exact mechanisms behind the liquid and droplet break-up, despite extensive theoretical and experiential studies, are still poorly understood and not completely established due to spray complexity and its transient nature. Dramatic improvements in computer hardware performance and advances in numerical modelling and simulation ensure that the complex nature of spray processes can be better understood. In that context, this doctoral thesis is focused on methods for numerical simulation of spray processes that can be used to investigate and improve understanding of spray processes. The methods and models for numerical simulation of spray processes are addressed in section 4.

2.2 Spray Regimes

The spray dynamics are influenced by the different spray regime, which can be defined as: liquid core region or the dense spray; thin region, and very thin region or the dilute spray, as shown in Figure 2.3. The core region of the liquid occurs in the nozzle or very close to the nozzle exit. This region is still recognizable as a liquid jet which, when coming out of the nozzle, begins to disintegrate into fragments and bigger droplets. The break-up region is located at the edge of the core region, where perturbations are high enough to disintegrate the liquid core. The following region is intermediate thin spray, which is located further downstream from the liquid core region, where the spray is entirely atomized. In the intermediate thin spray regime, volume fraction of the liquid

phase is negligible compared to the gas phase, but mass fraction is still significant, due to the high density ratio between the gas and the liquid. Hence, there is influence of the liquid phase on the gas phase and there is mass momentum and energy exchange between the liquid and the gas phase. The dilute regime occurs far from the nozzle where the spray droplets are widely spaced and become isolated, making both the volume fraction and the mass fraction of the liquid phase negligible compared to the gas phase.
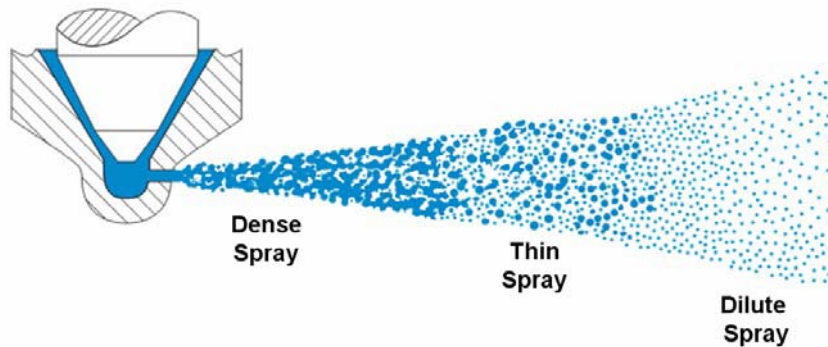
Figure 2.3: Schematic illustration of spray regimes

2.3 Spray Characteristics

The droplet size distribution, the spray cone angle, the nature of the spray pattern (full cone or hollow cone) and the spray penetration are the main liquid spray characteristics. These spray characteristics depend on nozzle design, liquid properties, and operating conditions. For example, small droplet size can be achieved with a combination of high injection pressure with low ambient pressure and small nozzle diameter. High liquid viscosity causes poor atomization, large droplet sizes and low evaporation rates. Furthermore, properties of the gas such as gas pressure, the density and temperature within the combustion chamber also influence the spray pattern. Thus, the spray characteristics play an important role in the improvement of spray process performance, e.g. in internal combustion engines they improve engine performance and reduce emissions.

Each spray provides a range of droplet sizes commonly known as droplet size distribution. The nozzle type, liquid properties, spraying pressure and spray angle affect

the droplet size distribution. The droplet size distribution is a very important liquid spray characteristic because the efficiency of any process involving a spray highly depends on the size of the liquid droplets.
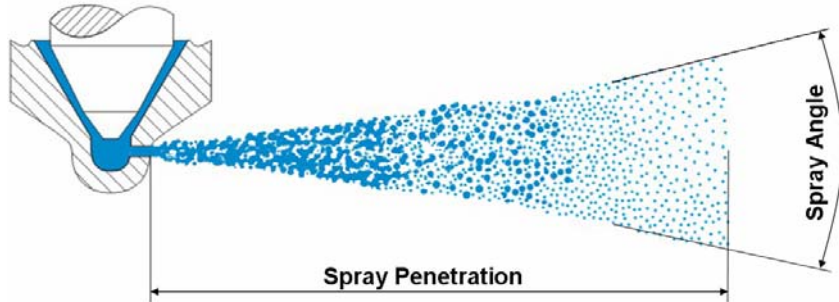
Figure 2.4: Schematic illustration of spray characteristics

There are two main parameters representing the quality of atomization involved in droplet size distribution: level of atomization and uniformity of atomization. The former refers to the mean diameter of droplets. For instance, if the spray is used in combustion processes then production of smaller droplets is desired, a so-called higher level of atomization, in order to increase evaporation and improve combustion. The latter refers to the scatter of droplet diameters. A smaller scatter of droplet diameters denotes higher uniformity of atomization.

The spray angle is the opening angle that the nozzle jet of droplets forms at the moment when it leaves the nozzle. Figure 2.4 shows a schematic illustration of the spray angle.

The spray penetration is defined as the maximum axis length of the spray injected in ambient gas as shown in Figure 2.4. The penetration is determined by the relative magnitude of the kinetic energy of the liquid jet to the aerodynamic resistance of the ambient gas. For instance, if the liquid is injected in a chamber whose ambient gas has higher density, then the spray penetration is reduced. This characteristic is very important for the injection of diesel in the combustion chamber because of its effect on the combustion process.

2.4 Atomization

Atomization is defined as a process of disintegration of bulk liquid into a large number of droplets by internal and external forces as a result of the interaction between liquid and ambient gas. Liquid atomization, produced by devices known as atomizer or nozzle, plays an important role in a wide variety of technical applications, ranging from fuel injection systems of the internal combustion engines, gas turbines, rockets, crop spraying in agriculture, spray drying of food and detergents, spray painting, spray cooling etc. Different types of atomizer have been developed and are in use. They are based of different principles and produce various types of spray shapes. Atomization of a liquid into fine droplets can be brought by the use of different energy sources used to produce instability on the liquid: pressure energy for pressure atomization; centrifugal energy for rotary atomization; vibratory energy for ultrasonic atomization; and so on. Pressure atomization and rotary atomization are commonly used for liquid atomization. In these atomization processes a liquid at high velocity under high pressure is injected into still or slow-moving gas and the resulting aerodynamic, viscous forces and centrifugal forces lead to the formation of fine droplets. The pressure atomization is the simplest method for atomization process and is typically used in engines in passenger cars and trucks, turbines, industrial furnaces and coating devices, while the rotary atomization is typically used in spray drying and spray painting applications. On the other hand, atomization of the liquid can also be aided by a flow of high velocity gas, which is called twin fluid atomization or air assisted atomization. This method of atomization is typically used in industrial applications for atomization of high viscous media. More specifically, this thesis considers sprays from high-pressure diesel nozzles.

The spray production results with the three basic processes associated with atomization: the internal flow in the nozzle; the break-up of the liquid jet; and the break-up of the liquid droplets.

2.4.1 Internal Nozzle Flow

The primary function of the injectors is to introduce the fuel to the combustion chamber. Several factors, such as engine performance, combustion process, reliability and hydraulics characteristics all contribute to an injector's success.

Fuel atomization is closely linked with internal nozzle flow characteristics and thus the control of the liquid fuel injection process plays a key role in the combustion and emissions performance of combustion systems. The liquid injection system need to be able to produce the appropriate spray structure and shape with a high degree of atomization in order to enable effective fuel-air mixing, evaporation and combustion. The most important part of the injection system is the nozzle. The nozzle design varies from application to application, but the basic concept is identical. The liquid fuel is injected through the nozzle hole into the combustion chamber. The flow within the nozzle is controlled through the rapid opening and closing of the needle valve and is shaped by the injector itself. The flow exits from the nozzle in the form of a high-speed jet and starts to break-up in conical spray. The flow inside the nozzle may be single phase or even two-phase as a consequence of turbulence and cavitation generated within the nozzle. A high level of turbulence can be originated under high pressure conditions when the liquid fuel is injected in the nozzle with the small diameter. This mechanism can destabilize the liquid jet and cause the primary break-up of the liquid jet once it exits the nozzle. The cavitation of the flow is a complex phenomenon that depends on the operating conditions and nozzle geometry, as characteristics of the holes and of the needle. In general, the cavitation is caused by significant pressure differences and small nozzle diameter size, leading to very high liquid velocities and low static pressures that can be below the vapour pressure.

Numerous studies have clearly demonstrated that an increase of pressure plays the dominant role on the spray behaviour, combustion and pollutant formation. For example, modern fuel injection systems in Diesel engines operate at very high pressures up to 1 500 bar. The demand for well-atomized sprays has also led to small nozzle diameters, approximately 200-250 microns. In combination with the high pressure, the liquid velocities are very high, approximately 500 meters per second or more.

2.4.2 Primary Break-up of Liquid Jets

The break-up of a liquid jet depends on the relative velocity and properties of the liquid jet and the ambient gas. It is initiated by the growth of small disturbances on the liquid surface promoted by the gas-liquid interaction that leads to the break-up of the jet into

fragments or droplets, the stripping of the liquid into fragments, and the generation of droplets from further break-up of fragments.

The dimensionless numbers, the Reynolds number, Weber number and Ohnesorage number, are used to characterize the liquid jet break-up process.

The Reynolds number, widely used to characterize the turbulence and energy of flow, relates the force on the droplet from the dynamic pressure of the ambient fluid, due to its velocity relative to the droplet, and in relation to the viscous drag forces. It is defined as:

$$Re = \frac{\rho d v}{\mu} \tag{1}$$

where characteristic length is the nozzle exit diameter d, v is liquid injection velocity, ρ is density of liquid, and μ is dynamic the viscosity of liquid.

The Weber number is a significant parameter used to describe the rate of break-up. It relates the external pressure distribution to droplet distortion. The Weber number represents the ratio of internal and surface tension forces and is defined as:

$$We = \frac{\rho d v^2}{\sigma} \tag{2}$$

where σ is surface tension at the liquid-gas interface.

The Ohnesorge number, representing liquid phase characteristics, is the ratio of the viscous and inertial and surface tension forces and is defined as:

$$Oh = \frac{\sqrt{We}}{Re} = \frac{\mu}{\sqrt{\rho d \sigma}} \quad . \tag{3}$$

Four different break-up regimes of a liquid jet have been identified that each correspond to various combinations of liquid inertia, aerodynamic forces and surface tension influencing the jet:

- **Rayleigh break-up regime:** If the liquid jet exits the nozzle with a very low injection velocity, the inertia forces and the surface tension of the liquid leads to oscillation of the surface jet that leads to the break-up of the liquid jet. Droplet

diameter is larger than the nozzle diameter and liquid break-up occurs many nozzle diameters downstream of the nozzle, see Figure 2.5 a.

▪ **First wind-induced regime:** Increasing the liquid jet velocity, the aerodynamic forces amplify the oscillation of the surface jet and produce the unstable growth of surface waves with a smaller break-up length than in the Rayleigh regime. Droplet diameter is in the order of nozzle diameter and liquid break-up occurs many nozzle diameters downstream of the nozzle, see Figure 2.5 b.

▪ **Second wind-induced regime:** In this regime the flow inside the nozzle is turbulent and aerodynamic forces have even greater influence on the surface jet. The liquid jet breaks up due to unstable growth of surface waves caused by turbulence and aerodynamic forces. Droplet diameter is even more reduced in this regime and smaller than the nozzle diameter and break-up starts a few nozzle diameters from the nozzle, see Figure 2.5 c.

▪ **The atomization regime:** The break-up of liquid jet starts directly at the nozzle exit for large injection velocities. A characteristic conical shape of the spray is generated, as depicted in Fig 2.5 d. Droplet diameter is much smaller than the nozzle diameter. This regime is still not well understood, but is relevant for pressure atomization, particularly for high-pressure injectors in engines, gas turbines and rockets.
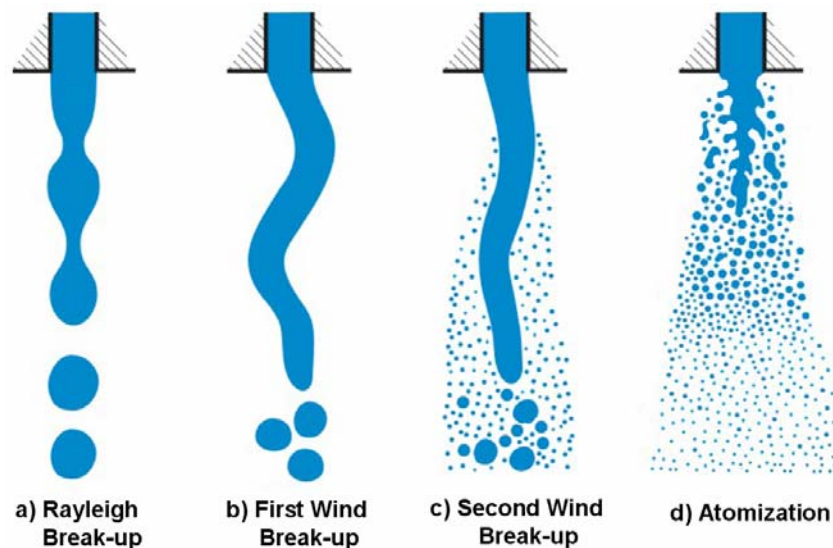
Figure 2.5: Schematic illustration of liquid jet disintegration regimes
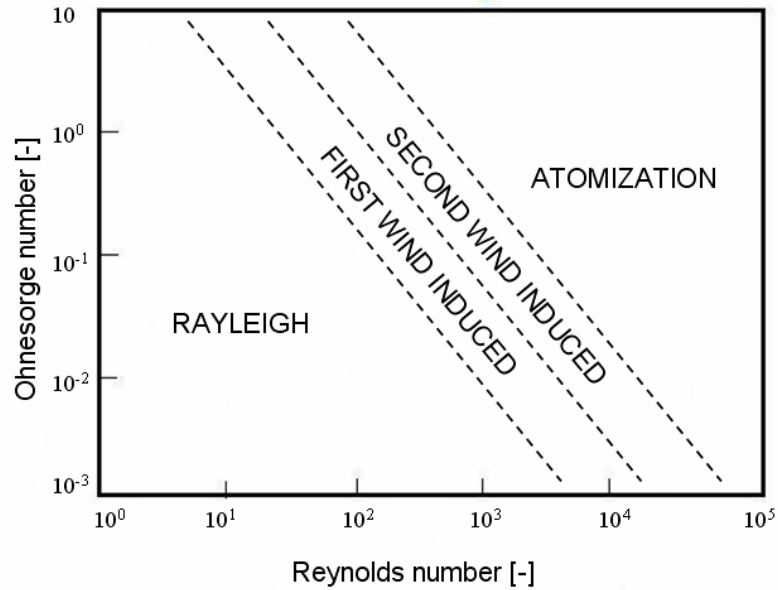
Figure 2.6: Liquid jet disintegration regimes

This thesis considers sprays generated by high-pressure injection of fuel liquid jet through a small hole into a gaseous environment. Thus, the atomization break-up regime is dominant where break-up of liquid jet starts directly at the nozzle exit. The liquid jet starts to disintegrate in fragments and large droplets, forming dense spray near the nozzle. In this case, the break-up mechanisms for the primary break-up of liquid jets are cavitation and turbulence, generated inside the nozzle and caused by a big pressure difference, small nozzle hole diameter, and aerodynamic forces that have an effect on the liquid jet.

The turbulence is produced inside the nozzle hole due to high injection pressure and small nozzle dimensions where liquid is very accelerated. The turbulence causes the oscillation phenomena of the jet. It generates the formation of initial perturbation on the liquid surface i.e. surface waves. The developed surface disturbances start to grow and at the critical amplitude the turbulent eddies overcome the surface tension, forming the fragments and larger droplets.

The cavitation is developed inside the nozzle hole when the static pressure is decreased to a value as low as the vapour pressure of the liquid due to strong acceleration of the liquid. The cavitation areas are generated along the wall inside the nozzle and separated from the walls into cavitation bubbles. In that case the flow inside the nozzle is a two phase flow. The cavitation bubbles may already begin to implode

inside the nozzle hole, but usually they are transported out of the nozzle where they implode because of high ambient pressure and contribute to the break-up of the liquid jet. For example, the cavitation formed in the nozzle of fuel injection equipment for modern automotive and power generation systems is a well known phenomenon occuring at sharp corners where the pressure may fall below the vapour pressure that then affects the instantaneous values of the flow rate, the injection velocity, spray structure and the atomization process. It has also been observed in many experiments that cavitation occurs in the nozzle with a short length diameter ratio and under high pressure operating conditions.

Due to turbulence within the liquid inside the nozzle hole, the jet surface is destabilized by small surface waves after leaving the nozzle. These waves can be additionally amplified by the aerodynamic forces, which are a result of the relative velocity between the liquid jet and the gas. The aerodynamic forces affect the liquid jet and cause surface disturbance that lead to disintegration of the jet in the form of primary fragments and droplets. The aerodynamic forces are not essentially an important break-up mechanism of the liquid jet, like turbulence and cavitation, since they can only influence at the edge of the jet and not the inner part of the liquid jet. The atomization regime has show that the break-up of the whole jet, not only the edge of the jet, occurs immediately after leaving the nozzle.

2.4.3 Secondary Droplet Break-up

Once the spherical droplets are formed, after primary break-up of the liquid jet, they may further break-up into smaller ligaments and droplets due to aerodynamic forces acting on the droplets in case that relative velocity of the droplets and the ambient gas is high enough. The aerodynamic forces (friction and pressure) cause an unstable growth of waves on the droplet surface that can lead to break-up into smaller ligaments and droplets. If the aerodynamic forces are equal to or higher than the surface tension, droplets are distorted from their initial spherical shape and become unstable and break-up. The critical Weber number, ratio of aerodynamic and surface tension forces, determines whether break-up of a droplet will occur and whether it is capable of characterizing the break-up type that the droplets can bring out. The droplet is stable if

the Weber number is below the critical Weber number. The dimensionless Weber number is defined as:

$$We = \frac{\rho_g d v_{rel}^2}{\sigma} \tag{4}$$

where ρ is the gas density, d is the droplet diameter before break-up, v is the relative velocity between the droplet and the gas and σ is the surface tension. From experimental studies was observed that depending on the Weber number, different droplet break-up mechanisms can be found [59][60][61]. Pilch and Erdman [59] conducted a comprehensive analysis of the published experimental data for various fluids and used the date to characterize droplet break-up into five distinct mechanisms based on an increasing size of Weber number. These mechanisms are listed below and illustrated schematically in Figure 2.7:

- **Vibrational Break-up** *We ≤ 12*: This mechanism is very slow compared with the other break-up mechanisms and it appears for very low Weber numbers near the critical value We ≈ 12 where under certain conditions oscillation can results in break-up into droplets of similar size. Vibrational break-up is not usually considered important in droplet break-up analysis.

- **Bag Break-up** *12 < We ≤ 50*: If the Weber number is increased *We > 50* the droplet is flattened by aerodynamic pressure and a bag shape with a liquid rim is formed. The bag eventually disintegrates into a large number of small droplets while the rim, a short time later, is disintegrated into a small number of large droplets, as illustrated in Figure 2.7 b.

- **Bag/Stamen Break-up** *50 < We ≤ 100*: This mechanism is similar to the bag break-up mechanism but with an additional stamen that appears in the middle of the bag, as displayed in Figure 2.7 c.

- **Sheet Stripping Break-up** *100 < We ≤ 350*: This mechanism is characterized by the stripping of the thin sheet of the flattened droplet as a consequence of K-H instabilities. During the entire break-up process the parent droplet exists while the sheet disintegrates, a short distance downstream from the parent droplet, into small droplets.

- **Wave Stripping Break-up** *We > 350;* followed by **catastrophic break-up**: This mechanism takes place in two stages. Waves with large amplitude and small wavelength, induced by K-H instabilities, are formed on the surface of the droplet where wave crests are eroded, forming small droplets. On the other side, waves with large amplitude and long wavelength, caused by droplet deceleration, induce R-T instabilities on the flattened droplet and create a few large droplets, while at the same time surface wave crests are eroded, forming small droplets. The latter mode is referred to as catastrophic break-up.

a) Vibrational Breakup   We ≥ 12

b) Bag Breakup   12 < We ≤ 50

c) Bag/Stamen Breakup   50 < We ≤ 100

d) Sheet Stripping Breakup 100 < We ≤ 350

e1) Wave Stripping Breakup   We > 350

e2) Catastrophic Breakup   We > 350
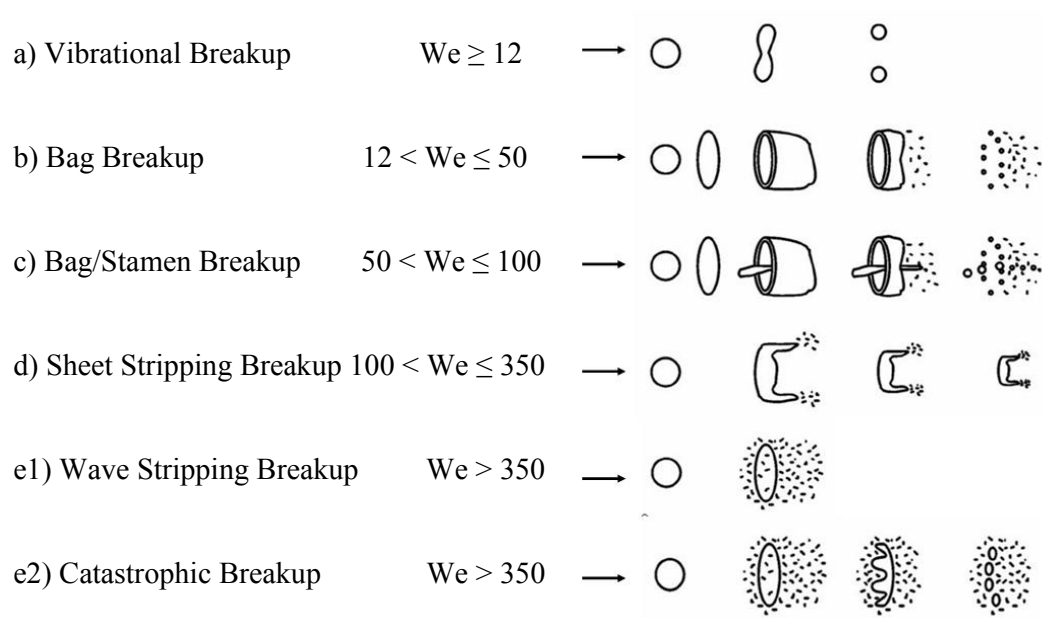
Figure 2.7: Droplet break-up mechanism by [59][60]

In high pressure fuel sprays all of the mechanisms may occur since the droplet velocities and hence Weber numbers, may vary widely.

3 Fundamental Equations of Fluid Flow and Heat Transfer

The fundamental equations of continuum mechanics are based on the conservation laws of:

- ❑   Mass
- ❑   Momentum
- ❑   Energy

The fundamental equations may be obtained by using the finite volume approach, where the fluid flow is divided into a number of control volumes and a mathematical description is developed for the finite control volume. This concept ensures an important framework for Computational Fluid Dynamics (CFD). The fluid is regarded as a continuum, where properties such as density, pressure, velocity etc., are defined as averages over fluid elements, neglecting the behaviour of individual molecules. In continuum mechanics conservation laws are fundamentally derived in integral form, taking into consideration the total amount of some property within the control volume. The rate of change of this total amount is equal to the net rate at which the property flows across the bounding surface of the control volume, known as "flux", plus the net rate of production or destruction within the control volume, known as "source or sink".

$$
\begin{pmatrix} RATE\,OF\,CHANGE \\ in\ V \end{pmatrix} + \begin{pmatrix} FLUX \\ out\ of\ boundary \end{pmatrix} = \begin{pmatrix} SOURCE\,/\,SINK \\ in\ V \end{pmatrix}
$$

In the following sub-sections conservation equations are first derived in integral form, since it is more fundamental and forms the base of the finite volume approach. In addition, the conservation equations are then given in differential forms, which are very often used due to easier manipulation, and in writing to show their physical meaning more clearly. Detailed discussion of the derivation of these equations can be found in standard textbooks, see for example[62][63][64]. The scalar transport equation is also shown, which represents that all equations have a common form that can be used as a starting point for numerical procedures in the finite volume approach. In order to close

26

the conservation equations, the relation between the stress tensor and deformation rate, ant the relation between the heat flux vector and the temperature, are also given.

This section introduces the fundamental laws of fluid mechanics that have been used in this work. In this section the detailed analysis of the conservation equations is based on single phase flow for the purpose of simplicity. Furthermore, in section 4 these derived differential equations for single phase flow are also applied to multiphase flow.

3.1 Mass Conservation Equation

One of the basic equations describing the behaviour of fluid is the conservation of mass. The equation of mass conservation can be derived for a finite volume element, V, fixed in space and passed by the flow without resistance. In case of single phase fluid flow, the fluid mass cannot be created or destroyed. The mass within the control volume will increase if the inflow is higher than the outflow, and in the opposite case it will decrease. If there are no volume or surface sources, the mass balance for the control volume can be written as

$$\int_S \rho u_j n_j dS = -\frac{d}{dt} \int_V \rho dV \tag{5}$$

representing the integral form of mass conservation. The term on the left hand side represents the rate of mass flux, i.e. the net mass flow through the bounding surface of the control volume. The term on the right hand side denotes the time rate of change of total mass in the control volume V. The fluid mass of this infinitesimal volume is defined as

$$\int_V \rho dV . \tag{6}$$

Using the Gauss divergence theorem we can transform the integral over the bounding surface into the volume integral, and then the Equation (6) can be rewritten as

$$\int_V \left[\frac{\partial \rho}{\partial t} + \frac{\partial}{\partial x_j}(\rho u_j) \right] dV = 0 . \tag{7}$$

For an arbitrary volume V, the only way the equation can be satisfied is for the integrand to be zero at each point within the volume, which can be written in differential form:

$$\frac{\partial \rho}{\partial t} + \frac{\partial}{\partial x_j}(\rho u_j) = 0 \tag{8}$$

or

$$\frac{\partial \rho}{\partial t} + \nabla \cdot (\rho \mathbf{u}) = 0 \tag{9}$$

which presents a very common form in literature.

3.2 Momentum Conservation Equations

The equation for conservation of momentum can be derived in a similar manner as the equation of mass conservation, as discussed previously. According to Newton's second law, the time rate of change of momentum of a fluid particle is equal to the sum of the volume and surface forces acting on the particle. This can be expressed in terms of a control volume fixed in space, through which the fluid moves as

$$\int_V \frac{\partial}{\partial t}(\rho u_i)dV + \int_S (\rho u_i)u_j n_j dS = \int_V \rho f_i dV + \int_S \sigma_{ji} n_j dS \; . \tag{10}$$

The conservation of momentum represents a vector equation that comprises three momentum equations for the x, y, and z components of the Cartesian coordinate system. The first term on the left hand side represents the rate of change of momentum in the control volume. The second term on the left hand side represents the net rate momentum flux across the control volume boundaries. The right hand side is the sum of volume and surface forces acting on fluid within the control volume.

Using the Gauss theorem we can transform the integral over the bounding surface into the volume integral, and then the Equation (10) can be rewritten as

$$\int_V \left[\frac{\partial}{\partial t}(\rho u_i) + \frac{\partial}{\partial x_j}\left(\rho u_i u_j\right) \right] dV = \int_V \left(\rho f_i + \frac{\partial \sigma_{ji}}{\partial x_j} \right) dV \; . \tag{11}$$

For an arbitrary volume, V, an above integral equation can be written in differential form as

$$\frac{\partial}{\partial t}(\rho u_i) + \frac{\partial}{\partial x_j}(\rho u_i u_j) = \rho f_i + \frac{\partial \sigma_{ji}}{\partial x_j}$$

(12)

or

$$\frac{\partial}{\partial t}(\rho u_i) + \nabla \cdot (\rho \mathbf{u}\mathbf{u}) = \rho f_i + \nabla \cdot \boldsymbol{\sigma} .$$

(13)

As previously mentioned, the right hand side is the sum of volume and surface forces acting on fluid within the control volume. The first term on the right hand side denotes the volume forces and the second term denotes the surface forces acting on the fluid. Volume forces (gravitational, centrifugal forces, etc.), act directly on the mass of the volume. Surface forces act directly on the surface of the control volume. They can be decomposed in two components: pressure forces and viscous stress forces. The surface force vector is usually defined by the stress tensor σ_{ji}. The total stress tensor, due to fluid pressure and viscous forces in the fluid, is

$$\sigma_{ij} = -p\delta_{ij} + \tau_{ij}$$

(14)

where δ_{ij} is the Kronecker delta equal to 1 if $i=j$ and 0 if $i{\neq}j$. In a Newtonian fluid the viscous stress tensor τ_{ij} is related to the rate of the strain tensor (the symmetric part of deformation tensor) [65] and is given as

$$\tau_{ij} = \mu\left(\frac{\partial u_i}{\partial x_j} + \frac{\partial u_j}{\partial x_i}\right) + \lambda \frac{\partial u_k}{\partial x_k}\delta_{ij}$$

(15)

where μ is the first viscosity coefficient and λ is the second viscosity coefficient. The Stokes hypothesis relates μ and λ for gases as

$$\lambda + \frac{2}{3}\mu = 0.$$

(16)

Accordingly, the viscous stress tensor can be expressed as

$$\tau_{ij} = \mu\left(\frac{\partial u_i}{\partial x_j} + \frac{\partial u_j}{\partial x_i}\right) - \frac{2}{3}\mu\frac{\partial u_k}{\partial x_k}\delta_{ij}. \tag{17}$$

Substitution of Newton's law of viscosity in the conservation of the momentum equation results in a set of equations known as Navier-Stokes equations.

$$\frac{\partial}{\partial t}(\rho u_i) + \frac{\partial}{\partial x_j}(\rho u_i u_j) = -\frac{\partial p}{\partial x_i} + \frac{\partial}{\partial x_j}\left[\mu\left(\frac{\partial u_i}{\partial x_j} + \frac{\partial u_j}{\partial x_i}\right) - \frac{2}{3}\mu\frac{\partial u_k}{\partial x_k}\delta_{ij}\right] + \rho f_i. \tag{18}$$

The first term on the right hand side represents the pressure gradient forces acting on the control volume. The second term on the right hand side represents the normal and shear stress actions on the control volume surface, and the last term represents the volume forces acting on the control volume.

3.3 Energy Conservation Equation

The energy equation is derived by following the physical principle that the amount of energy remains constant and energy is neither created nor destroyed. Energy can only be converted from one form to another and the total energy within the domain remains constant. The conservation of energy is derived from the first law of thermodynamics. The rate of energy change equals the sum of the rate of heat addition and the rate of work done on the fluid particle.

The conservation equation for energy or enthalpy results from consideration of the total energy of the fluid defined as the sum of kinetic and internal energy:

$$e = \frac{1}{2}u_i u_i + i \tag{19}$$

where e denotes the total specific energy and i marks the specific internal energy. Accordingly, the equation of energy for a control volume is given by

$$\int_V \frac{\partial}{\partial t}(\rho e)dV + \int_S (\rho e)u_j n_j dS = \int_V \rho f_i u_i dV + \int_V S dV + \int_S \sigma_{ji} n_j u_i dS - \int_S q_j n_j dS \tag{20}$$

30

where the first term on the left represents the rate of increase of total energy, while the second term on the left represents the total energy lost across the control volume boundaries. The first term on the right hand side is the specific power by the volume forces f_i, which have been introduced for the momentum equation. In the second term on the right hand side S denotes the distributed internal heat source due to radiation, or chemical reactions or any other volumetric heat sources. The third term denotes the surface sources, the time rate of work done by the pressure and viscous stresses on the fluid element:

$$\sigma_{ij} = -pu_i\delta_{ij} + u_i\tau_{ij} \ . \tag{21}$$

The q in the last term on the right hand side denotes the heat flux vector, which can be written in the form of Fourier's law of heat conduction

$$q_j = -k\frac{\partial T}{\partial x_j} \tag{22}$$

representing that the heat flux vector is linearly related to the temperature gradient where k is the thermal conductivity.

Using the Gauss theorem we can transform the integral over the bounding surface into the volume integral and then the Equation (20) can be rewritten as

$$\int_V \left(\frac{\partial}{\partial t}(\rho e) + \frac{\partial}{\partial x_j}(\rho e u_j) \right) dV = \int_V \left(\rho f_i u_i + S + \frac{\partial}{\partial x_j}(\sigma_{ji}u_i - q_j) \right) dV \ . \tag{23}$$

For an arbitrary volume V, the integrands will be equal 0, which can be written in differential form:

$$\frac{\partial}{\partial t}(\rho e) + \frac{\partial}{\partial x_j}(\rho e u_j) = \rho f_i u_i + S + \frac{\partial}{\partial x_j}(\sigma_{ji}u_i - q_j) \tag{24}$$

or

$$\frac{\partial}{\partial t}(\rho e) + \nabla \cdot (\rho e \mathbf{u}) = \rho \mathbf{f} \cdot \mathbf{u} + S + \nabla \cdot (\sigma \cdot \mathbf{u} - \mathbf{q}) \tag{25}$$

The equation above can be rewritten as a conservation equation for the specific enthalpy taking into account that $\rho h = \rho i + p$ as

$$\frac{\partial}{\partial t}(\rho h) + \frac{\partial}{\partial x_j}(\rho h u_j) = \frac{\partial p}{\partial t} + \frac{\partial}{\partial x_j}(p u_j) + S + \frac{\partial}{\partial x_j}(\sigma_{ji} u_i - q_j) \quad . \tag{26}$$

3.4 Species Mass Conservation

In case of fuel combustion, the conservation equations for each of the chemical species of interest have the following form:

$$\int_V \frac{\partial}{\partial t}(\rho Y_k)dV + \int_S (\rho Y_k)u_j n_j dS = \int_S (\rho D_k \frac{\partial Y_k}{\partial x_j})n_j dS + \int_V S_k dV \tag{27}$$

where Y_i is the mass fraction of the k-th chemical species defined as

$$Y_k = \frac{m_k}{m}. \tag{28}$$

The total mass is represented by m , while the mass of species k is m_k.

The diffusion term is usually modelled by Fick's law, which states that the mass flux of species is proportional to the product of the diffusion coefficient and the concentration gradient of the species. The first term on the right hand side represents Fiks's law of diffusion. The last term on the right hand side is the source term due to chemical reactions.

Using the Gauss divergence theorem we can transform the integral over the bounding surface into the volume integral, and then the Equation (27) can be rewritten as

$$\int_V \frac{\partial}{\partial t}(\rho Y_k)dV + \int_V \frac{\partial}{\partial x_j}(\rho Y_k u_j)dV = \int_V \frac{\partial}{\partial x_j}(\rho D_k \frac{\partial Y_k}{\partial x_j})dV + \int_V S_k dV . \tag{29}$$

The differential form can be written for an arbitrary volume V as

$$\frac{\partial}{\partial t}(\rho Y_k) + \frac{\partial}{\partial x_j}(\rho Y_k u_j) = \frac{\partial}{\partial x_j}(\rho D_k \frac{\partial Y_k}{\partial x_j}) + S_k . \tag{30}$$

3.5 General Transport Equations

A similar equation can be derived for any dependent variable, usually a specific scalar property denoted as φ, by obeying a generalized conversation principle. For example, this dependent variable φ can be the species mass fraction, the enthalpy, a velocity component etc. The conservation equation for the scalar property φ for a fixed control volume can be written as

$$\int_V \frac{\partial}{\partial t}(\rho\varphi)dV + \int_S (\rho\varphi)u_j n_j dS = \int_S (\Gamma_\varphi \frac{\partial\varphi}{\partial x_j})n_j dS + \int_V S_\varphi dV \tag{31}$$

where the first term is an unsteady term, the second term is convection, the third term is diffusion and the last term is source or sink. The first term on the left hand side represents the rate of change of the scalar property φ in the control volume. The second term on the left hand side is the net convective flux of this property across the control volume boundaries. The first term on the right hand side is the net diffusive flux across the control volume boundaries. The final term on the right hand side is the source or sink of the property φ. Two transport mechanisms can be distinguished across the control volume boundaries: convection – transport due to the motion of the fluid, and diffusion – transport due to the differences in concentration (concentration gradient).

Using the Gauss divergence theorem we can transform the integral over the bounding surface into the volume integral, and then the Equation (31) can be rewritten as

$$\int_V \frac{\partial}{\partial t}(\rho\varphi)dV + \int_V \frac{\partial}{\partial x_j}(\rho\varphi u_j)dV = \int_V \frac{\partial}{\partial x_j}(\Gamma_\varphi \frac{\partial\varphi}{\partial x_j})dV + \int_V S_\varphi dV \ . \tag{32}$$

For an arbitrary volume V, the integrand will be equal 0, which gives a corresponding differential form:

$$\frac{\partial}{\partial t}(\rho\varphi) + \frac{\partial}{\partial x_j}(\rho\varphi u_j) = \frac{\partial}{\partial x_j}(\Gamma_\varphi \frac{\partial\varphi}{\partial x_j}) + S_\varphi \tag{33}$$

where Γ_φ is the diffusion coefficient and S_φ is the source term.

In the case of time-dependent problems Equation (31) must be integrated with respect to time t over a small interval Δt and can be written as

$$\int\limits_{\Delta t}\frac{\partial}{\partial t}\left(\int\limits_{V}(\rho\varphi)dV\right)dt+\int\limits_{\Delta t}\int\limits_{S}(\rho\varphi)u_j n_j dSdt=\int\limits_{\Delta t}\int\limits_{S}(\Gamma_\varphi\frac{\partial\varphi}{\partial x_j})n_j dSdt+\int\limits_{\Delta t}\int\limits_{V}S_\varphi dVdt. \qquad (34)$$

It is necessary to emphasize that this equation is very important and it is used as a base and starting point for computational procedures in the finite volume CFD approach. It can be noted that by using this common form, the so-called transport equation, for all relevant equations of fluid flow, turbulence and heat transfer, allow us to formulate a general subroutine that can be used for the CFD calculation procedure for all relevant equations. This common form represents an important time saving step in the calculation procedure.

3.6 Turbulent Flows

The conservation equations described above represent laminar fluid flow, but these conservation equations can be applied with or in some cases without modification for turbulent flows as well. These conservation equations can be solved for turbulent flows directly only if the mesh is fine enough with spacing smaller than the length scale of the smallest turbulent eddies, and the time step is smaller than the time scale of turbulent fluctuations. This method, used for the modelling and simulation of turbulent flows by solving the equations directly on mesh that is fine enough to resolve the smallest eddies, is called Direct Numerical Simulation (DNS), see for example [66][67][68]. The size of the smallest eddies are proportional to the Kolmogorov length scale that becomes smaller with an increasing Reynolds number. The main advantage of this method is that no modelling needed to close the governing fluid flow equations. On the other hand, this method is not suitable for solving turbulence problems for realistic geometries because of its significant demand on computer memory and time. Application of DNS is limited to low Reynolds number flows and very simple geometric domains due to resolution requirements. Thus appropriate methods, taking into account a balance between accuracy and effectiveness, usually must be used for modelling and simulation of complex turbulent flows in engineering applications.

The most favoured method for modelling turbulent flows in industrial applications is Reynolds Averaged Navier-Stokes equations (RANS) with an appropriate turbulence

model. This approach is derived by averaging the equations defined in section 3.6.1, where the instantaneous variables of the turbulent flow quantities are substituted by an averaged (mean) value and a fluctuating value. With this approach the turbulent flow is described with the conservation equations in terms of time quantities. The RANS equations have a similar form to those of the original Navier-Stokes (conservation) equations derived in a previous section. Two additional terms, the Reynolds stresses and the turbulent heat flux appear due to the averaging process. They must be modelled by the turbulence model in order to close the system of equations.

Furthermore, the modelling and simulation of turbulent flows may be improved compared to the RANS approach by using more descriptive modelling methods such as Large Eddy Simulation (LES) [66]. It represents a compromise between the averaging type models and DNS. In this approach large scale eddies of the flow are solved directly, while small scale eddies are modelled with simpler turbulent models. The LES approach is still very expensive in terms of calculation time when compared with RANS, but requires less time and computational power than DNS, and it becomes more and more computationally feasible for engineering applications due to the rapid progress of computer technology. Although the LES approach has been successfully applied to a number of turbulent flow problems for both reacting and non-reacting flows, see for example [69][70][71][72][73], most of the current LES implementations are limited to single phase flows. However, only limited work has been done regarding the application of LES to model multi-phase flows [74]. LES can typically be used for simulation of turbulent flows in more complex geometry where the Reynolds numbers are too high for DNS, but whenever possible, the DNS method is a more desirable choice due to much greater accuracy. However, both methods are still too computationally expensive, and thus in practical engineering applications the Reynolds Avaraged Navier Stokes Equations are usually used for modelling and simulation of multiphase turbulent flows.

3.6.1 Averaging of Conservation Equations

Averaging the instantaneous quantities of the turbulent flow ensures a way of describing the mean flow field where the local fluctuating components are integrated into the mean quantities. As shown in Figure 3.1, the instantaneous quantity φ fluctuates around a mean quantity. A statistical method can be used to describe the random flow, and various types of averaging procedures are possible. For example, the mean quantity can be obtained by using the time averaging for flow property φ as

$$\overline{\varphi} = \frac{1}{\Delta t} \int\limits_{t}^{t+\Delta t} \varphi(\vec{x},t)dt \ . \tag{35}$$

The instantaneous quantity φ can be split into a mean and fluctuating component as:

$$\varphi = \overline{\varphi} + \varphi' \tag{36}$$

as illustrated in Figure 3.1. If φ is averaged, the mean of the fluctuation component is equal to zero.
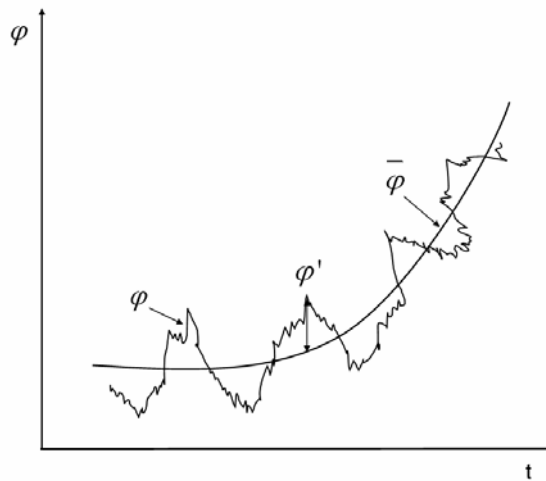
Figure 3.1: Illustration of turbulent fluctuations in unsteady flow

The RANS equations are obtained by substituting the instantaneous quantities with the mean and fluctuating components, and then averaging the equations over time. Information about the fluctuating variables is lost with respect to time averaging, and the RANS equations for incompressible flow have a similar form as original the conservation equations, with the addition of two terms. These two terms, the Reynolds

stress in the momentum equation and the turbulent heat flux in the energy equation, appear due to the averaging process. These terms need to be modelled in order to close the equations system.

In combustion processes, heat release causes large density variations and thus the RANS equations are much more complicated due to additional correlations that include density fluctuations such as the velocity-density correlation $\overline{\rho' u'}$. In order to avoid difficulty with respect to Reynolds averaging, a more appropriate density-weighted average $\tilde{\varphi}$, called Favre average is often used:

$$\tilde{\varphi} = \frac{\overline{\rho\varphi}}{\overline{\rho}}. \tag{37}$$

The instantaneous quantity φ can be again split into a mean and a fluctuating component as:

$$\varphi = \tilde{\varphi} + \varphi'' \tag{38}$$

where $\widetilde{\varphi''} = 0$. This is done for all quantities except density and static pressure, which are only time-averaged:

$$\begin{aligned} \rho &= \overline{\rho} + \rho' & u_i &= \tilde{u}_i + u_i'' \\ p &= \overline{p} + p' & h &= \tilde{h} + h''. \end{aligned} \tag{39}$$

The Favre averaged equations for incompressible flows have the same form as the RANS equations. In the case of compressible flow, the conservation equations, obtained by the density-weighted time averaging procedure, are similar to the original conservation equations with the addition of a few terms due to turbulence. After the application of the Favre averaging procedure, which consist of algebraic manipulation and simplifications, the averaged conservation equations can be written as:

$$\frac{\partial \overline{\rho}}{\partial t} + \frac{\partial \left(\overline{\rho} \tilde{u}_j \right)}{\partial x_j} = 0 \tag{40}$$

$$\frac{\partial \left(\overline{\rho} \tilde{u}_i \right)}{\partial t} + \frac{\partial \left(\overline{\rho} \tilde{u}_i \tilde{u}_j \right)}{\partial x_j} = \overline{\rho} \overline{f}_i - \frac{\partial \overline{p}}{\partial x_i} + \frac{\partial \overline{\tau}_{ij}}{\partial x_j} - \frac{\partial \left(\overline{\rho u_i'' u_j''} \right)}{\partial x_j} \tag{41}$$

$$\frac{\partial\left(\bar{\rho}\tilde{h}\right)}{\partial t}+\frac{\partial\left(\bar{\rho}\tilde{h}\tilde{u}_j\right)}{\partial x_j}=\frac{\partial\bar{p}}{\partial t}+\tilde{u}_j\frac{\partial\bar{p}}{\partial x_j}+\overline{S}-\frac{\partial\left(\overline{\bar{\rho}h''\widetilde{u_j}''}\right)}{\partial x_j}\;.$$
(42)

The new terms that arise from the Favre averaging process account for the effects of turbulence. The turbulent Reynolds stress tensor in the momentum equation represens the transport of the mean due to turbulent fluctuation:

$$-\overline{\bar{\rho}u_i''\widetilde{u_j}''}$$
(43)

and the turbulent heat flux vector in the energy equation:

$$\bar{\rho}\overline{h''\widetilde{u_j}''}.$$
(44)

These terms are unknown quantities and need to be approximated by the turbulence model in order to close the equations system. The main task of a turbulence model is to approximate these unknowns in terms of the mean quantities of flow. This problem is commonly refereed to as a turbulent closure problem. The turbulence models can be classified into first-ordered closures (eddy viscosity/diffusivity models) and second-ordered closures (Reynolds stress models).

3.6.2 Turbulence Modelling

Many turbulent models employ the concept of a turbulent viscosity or a turbulent diffusivity to approximate the turbulent Reynolds stresses and the turbulent heat fluxes. They are based on the Boussinesq assumption, which assumes that the turbulent Reynolds stress tensor can be modelled in the same way as the viscous stress tensor, except that the molecular viscosity is replaced with turbulent viscosity. The same principle can be applied to other constitutive equations, such as turbulent heat flux. A a result the time averaged conservation equations for turbulent flow have the same form as the equations for laminar flow, but the laminar exchange coefficients (viscosity, diffusivity and conductivity) are replaced by effective turbulent exchange values (sum of molecular and turbulent values). The first-ordered closures (eddy viscosity/diffusivity models) can be classified according the number of transport equations to be solved:

- ▪ Zero-equation models

  Which are also known as algebraic models where the turbulent exchange coefficients are calculated by empirical relations.

- ▪ One-equation models

  In this model only one additional transport equation for the turbulent kinetic energy k (representing turbulent exchange coefficients) is solved.

- ▪ Two-equation models

  In this model two additional transport equations for the turbulent kinetic energy k and turbulent energy dissipation ε are solved.

Reynolds stress models, also known as second-ordered closure models, solve partial differential equations for each component of the Reynolds stress tensor. This means that at least six additional partial differential conversation equations have to be solved. The details about this model can be found for example in [66]. The high number of additional equations that require solving is a disadvantage of this model. However, the solution of a separate transport equation for each component of the turbulent stress has greater potential to give an accurate prediction for complex flow and thus should capture turbulence physics better than two-equation models.

3.6.2.1 k - ε model

In this thesis the $k - \varepsilon$ model [76] is used as a turbulence model for simulation of practical turbulent flow problems, which were performed by FIRE CFD solver [77]. This is the most widely used turbulence model in CFD simulations in practical engineering applications. Like all other turbulence models it has its own serious disadvantages, such as limited applicability to flow of strong streamlines curvature or strong rotation. The k-ε model is based on the fact that the turbulent viscosity is isotropic and therefore must the same for all Reynolds stresses. However, the $k - \varepsilon$ model has a few important advantages - it is simple, numerically stable and has proved successful in many applications (including heat transfer, combustion, etc.). Despite the fact that the Reynolds stress models have a greater potential to fully describe three-dimensional anistropic turbulent flows than the $k - \varepsilon$ model, its application to practical problems has not always produced superior results. This is due to fact that errors

originated by the numerical solution of the comprehensive equations system can occasionally be greater than the improvement by the turbulence model. For this reasons the $k - \varepsilon$ model is used in this work. It is numerically robust, and it is generally accepted that the $k - \varepsilon$ model yields reasonably realistic predictions of major mean-flow features in most situations.

It is worth noting that there is no single turbulence model that is capable of realiably predicting turbulent flows for all practical configurations and problems in order to obtain satisfying results. Each of the turbulent models have strengths and weaknesses, and deciding on an appropriate models depends on the specific nature of the flow being investigated. It is also important to point out that computational effort versus the accuracy required by a particular application should be taken into account in order to choose an appropriate turbulence model.

The k-ε models are based on the Boussinesq eddy viscosity concept, assuming that the turbulent Reynolds stress tensor can be modelled in analogy with the viscous stress tensor. This means the turbulent stress tensor is related linearly to the mean rate of the strain tensor $\widetilde{D}_{ij}$ and in the case of compressible Favre and Reynolds averaged Navier-Stokes equations can be expressed as

$$-\overline{\rho \widetilde{u_i " u_j "}} = 2\mu_t \widetilde{D}_{ij} - \frac{2}{3}\left(\mu_t \frac{\partial \widetilde{u_k}}{\partial x_k} + \overline{\rho}\widetilde{k} \right)\delta_{ij} \tag{45}$$

which can be rewritten in the following form:

$$-\overline{\rho \widetilde{u_i " u_j "}} = \mu_t \left(\frac{\partial \widetilde{u}_i}{\partial x_j} + \frac{\partial \widetilde{u}_j}{\partial x_i} \right) - \frac{2}{3}\left(\mu_t \frac{\partial \widetilde{u_k}}{\partial x_k} + \overline{\rho}\widetilde{k} \right)\delta_{ij}. \tag{46}$$

where μ_t is the turbulent viscosity and k is the kinetic energy of turbulent fluctuation defined as

$$\widetilde{k} = \frac{1}{2}\widetilde{u_k " u_k "}. \tag{47}$$

It should be noted that the molecular exchange coefficients are local fluid properties while the turbulent coefficients are not fluid property but rather a property of

turbulence. The k-ε models calculate the turbulent viscosity in terms of two turbulence quantities: the turbulent kinetic energy and the energy dissipation rate

$$\mu_t = \bar{\rho} C_\mu \frac{k^2}{\varepsilon} \tag{48}$$

where C_μ is a dimensionless constant and usually has the value of 0.09 in standard models. The equation above shows that turbulent viscosity is evaluated by k and ε where these quantities are determined by solving the following transport equations:

$$\frac{\partial\left(\bar{\rho}\tilde{k}\right)}{\partial t} + \frac{\partial\left(\bar{\rho}\tilde{k}\tilde{u}_j\right)}{\partial x_j} = \frac{\partial}{\partial x_j}\left[\left(\mu + \frac{\mu_t}{\sigma_k}\right)\frac{\partial\tilde{k}}{\partial x_j}\right] + P + G - \bar{\rho}\tilde{\varepsilon} \tag{49}$$

$$\frac{\partial\left(\bar{\rho}\tilde{\varepsilon}\right)}{\partial t} + \frac{\partial\left(\bar{\rho}\tilde{\varepsilon}\tilde{u}_j\right)}{\partial x_j} = \frac{\partial}{\partial x_j}\left[\left(\mu + \frac{\mu_t}{\sigma_\varepsilon}\right)\frac{\partial\tilde{\varepsilon}}{\partial x_j}\right] + C_{\varepsilon 1}\frac{\tilde{\varepsilon}}{\tilde{k}}P + C_{\varepsilon 3}\frac{\tilde{\varepsilon}}{\tilde{k}}G - C_{\varepsilon 2}\bar{\rho}\frac{\tilde{\varepsilon}^2}{\tilde{k}} \tag{50}$$

where the right hand side of Equation (49) represents diffusion, productions of turbulent kinetic energy by mean deformation, productions of turbulent kinetic energy by body forces and dissipation, respectively.

The five empirical constants are not universal and must be adjusted to a specific problem. The following set of default values is used in the CFD solver FIRE:

$$C_{\varepsilon 1} = 1.44 \quad C_{\varepsilon 2} = 1.92 \quad C_{\varepsilon 3} = 0.8 \quad \sigma_k = 1.0 \quad \sigma_\varepsilon = 1.3 \,. \tag{51}$$

In case of the interaction of the gas phase with the liquid dispersed phase, additional terms appear in the transport equation for k and ε, which are given in section 4.3.

4 Spray Modelling

4.1 Simulation of Spray Processes

The current energy crisis highlights the need for the design of more powerful, fuel-efficient, and environmentally friendly combustion systems. A new design performance optimization of oil-fuelled combustion devices is one of the main goals of manufactures worldwide. There are challenges associated with the very short amount of time available for the fuel spray to atomize and form an adequate mixture for satisfactory combustion. Therefore, suitable fuel injectors are needed to provide sufficient control of the spray process and meet the basic requirements for atomization and the mixing process. High pressure injectors are one of the most commonly used injectors in commercial applications today. They operate at a relatively high pressure and their design improves the atomization process as well as the turbulence levels in the chamber for better mixing between the air and fuel. The understanding of the complex nature of spray formed by these high pressure fuel injectors in experimental investigations is limited, and this understanding can be significantly improved by numerical modelling and simulations.

Numerical modelling of spray processes is relevant in many engineering applications where the droplet-ambient interaction plays a decisive role in characterizing the efficiency of the system. For example, in combustion systems, droplet characteristics are the main contributors to increase efficiency of produced energy and reduce pollutant formation. Thus, numerical modelling and simulations of the spray behaviour are essential for an improved design, reliable performance optimization, and modern engineering devices. Computational capabilities have reached such a high level of sophistication that we are able to simulate the physics of multi-phase flows in practical combustion systems and related fuel-supply devices. Early comprehensive information, parametric studies and the initial conclusions that can be gained from computer simulation tools, such as Computational Fluid Dynamics (CFD), are very important to be able to handle modern technology requirements. Together with experiments and theory, CFD has become an integral component of spray research that can be used for understanding the complex phenomena occurring within the spray that

can, as a result, lead to an increase in performance and a reduction of cost. Although efforts to calculate spray flows are as old as CFD, the difficulty of in predicting of spray flows has proven to be considerable. Therefore, progress was slow and spray predictions were limited to very simple problems. Over the last few years, major progress has been achieved. An accurate description of the physics of multi-phase flows, where the liquid phase is dispersed in a cloud of different sized droplets that evaporate and can even further break-up, relies on the availability of adequate and efficient physical mathematical models. This consists of a set of models suitable to capture the complex nature of multiphase flow. These models tend to be simple due to the fact that the spray flow has to be modelled alongside the effects of turbulence, combustion and related phenomena in a realistic 3D environment. Therefore, the crucial precondition for spray modelling is to find a compromise between the complexity of the models and their computational efficiency. On the other side, the numerical modelling and simulation of the multiphase spray process is a very challenging task, especially when compared to a single phase flow. These challenges are due to fluid interfaces between the phases and property variations across the interfaces between phases. The unsteadiness and the highly non-linear interactions at an extensive range of time and length scales between the liquid and the gas phases makes the modelling very challenging. Thus, the spray models demand complicated techniques to couple the dynamics of the dispersed liquid and the carrier gas.

As mentioned previously, turbulence modelling is very important for the correct description of fluid flow in CFD modelling. The direct numerical simulations (DNS) of the turbulent break-up process is impossible for resolving all physical processes, except for a very simple configuration, due to resolution requirements. Large Eddy Simulation (LES) can be used as an alternative approach in order to reduce the computational cost by solving only the larger turbulent eddies, where the scales are larger than the grid size. The smaller scales are modelled by using an eddy viscosity based sub-grid model. The LES is still quite computationally demanding for solving the majority of practically relevant spray problems today and only limited work has been done regarding its applicability to two-phase flows [78][79]. Today, RANS is a much more effective method and the most common and favoured method in industrial applications.

4.2 Methods for Spray Modelling

Spray formed by high pressure fuel injectors consists of a large number of droplets where each of them has unique properties. The final atomized droplets are far too numerous, making it impossible to resolve each individual droplet in numerical simulation due to limited computer resources. Accordingly, a variety of strategies have been formulated during the last few years in order to address this problem. In general, most of these strategies fall into two basic formulation methods that are commonly used to couple the dynamics of the liquid phase and the gas phase: the Eulerian-Lagrangian method and the Eulerian-Eulerian method. Instead of modelling the details of flows around individual droplets these models are based on mass, momentum, and energy exchange between the liquid and gas phases. These exchange terms are based on semi-empirical correlations. Both methods treat the gas phase as a continuum, while either the Lagrangian or the Eulerian approach is used for the dispersed phase. The discretization of the liquid phase in both methods must be fine enough to achieve an adequate description of the liquid atomization and spray processes. In the Eulerian-Lagrangian approach a large number of parcels need to be tracked, while in the Eulerian multiphase approach a large number of transport equations need to be solved. In both cases the gas phase is calculated in the Eulerian framework.

The Eulerian-Lagrangian method, also referred to as the Discrete Droplet Model or Stochastic Particle Model, is most commonly used in simulation of sprays research. This method tracks the motion of the liquid droplets, indicating that the frame of reference is moving. The spray is discretized into finite numbers of droplet groups, known as parcels, which are supposed to be similar in size and have the same physical properties. The equations of motion for each parcel based on the Lagrangian approach are coupled with the Eulerian representation of the gas phase. This allows the decomposition of complicated and highly nonlinear systems of transport equations and describes the interactions between the control volumes and the system of equations that govern processes in individual control volumes, including the exchange between the liquid and the gas phase. The systems of these equations are mainly integrated using a much shorter time step than the global time steps that are used for calculation of the gas phase. The computational effort for this approach increases drastically with increasing parcel number, leaving its main use for sufficiently diluted spray where the volume

fraction of the dispersed phase is low enough to allow numerical simulation. In the dense spray region where the volume fraction of dispersed phase is very high the Discrete Droplet Method is not applicable, but another approach, the Eulerain multiphase method, can be used.

In the Eulerian multiphase method the dispersed liquid phases are treated as other continuous phases. This method regards the liquid phase and the gas phase as interpenetrating continua, where both phases are treated from the Eulerian point of view. Thus, this approach neglects the discrete nature of the dispersed phase and approximates its effect upon the continuous phase. The same discretization technique, similar numerical techniques and conservation equations are used for both phases. Furthermore, the liquid is divided into different droplet size classes; each represented by a separate droplet phase. The complete set of transport equations with some additional source terms accounting for the droplet dynamics have to be solved for each liquid phase under consideration. This leads to a great number of transport equations to be solved in order to describe the spray behaviour. The degree to which the spray description is accurate depends on the number of liquid phases. A higher number of liquid phases means better spray resolution, but computational effort is significantly influenced. This modelling approach is used in this study for the description of the fuel dense spray formed by high pressure diesel injectors and is described in the following sections.

4.3 Multiphase Conservation Equations

This section is focused on the details of the multiphase spray flow problem and its mathematical description. The conservation equations for mass, momentum and energy derived in section 3 are based on single phase flow. For multiphase flows, solving these equations is no longer a sufficient way to calculate the flow field for all involved phases. Multiphase flows are characterized by the presence of interfaces separating the phases, which considerably complicates the analysis of multiphase problems in comparison to single-phase flow. In the Eulerian multiphase approach, the phases share the same volume and penetrate each other in space and exchange mass, momentum and energy at these interfaces. This means that additional source terms have to be

incorporated into the conservation equations to account for the interaction between the gaseous and the dispersed liquid phases. The conservation equations, supplemented by turbulence model equations, have to be solved for all phases. The final result is a set of multi-phase conservation equations for mass, momentum, and energy, with exchange terms describing the interaction between the phases included. The inter-phase transfers between phases are often calculated using empirical closure relations. The purpose of this section is to describe these multi-phase conservation equations and their source terms for the Eulerian multiphase spray modelling approach.

The control volume is divided into gas and different droplet phases. The gas phase is considered to be the primary phase, while the secondary phases are droplet phases classified into different droplet size classes. This means that each droplet size is considered to form a separate droplet phase. The primary gaseous phase is a gas mixture composed by gas and vapor. All phases are treated as interpenetrating continua characterized by their phase volume fractions, determining what amount of phase exists in a given place at a given time.

Due to the complexities of interfaces and resultant discontinues in fluid properties the multiphase equations are derived by an ensemble averaging of the conservation equations for each phase in a multiphase flow.

4.3.1 Ensemble Averaging

Ensemble averaging is based on the probability that the flow field is being in a particular realization at a given time. If there are many different events possible, then the expected value is naturally an average of all of these events, or the ensemble of realizations. The ensemble average is generally the idea of adding the values of the variable for each realization and dividing by the number of observations. The techniques for doing what is described throughout this section are based on the theory of multi-component fluids by Drew and Drew and Passman [80][81].

The ensemble average of a property φ is an average of realizations

$$\overline{\varphi}(x_i,t) = \frac{1}{N}\sum_{n=1}^{N}\varphi(x_i,t) \tag{52}$$

where N is the number of times the experiment or process is repeated. In the limit of an infinite number of realizations, the above equation can be rewritten in the following form

$$\bar{\varphi}(x_i,t) = \int\limits_{all\Gamma} \varphi(x_i,t;\Gamma)\, d\left[m(\Gamma)\right] \tag{53}$$

where $\varphi(x_i,t;\Gamma)$ is the realization of $\varphi(x_i,t)$ over all possible realizations, $all\Gamma$, and $m(\Gamma)$ is the probability that the realization $\varphi(x_i,t)$ will occur.

As mentioned above, multiphase flows are characterized by the presence of phase interface and to distinguish the phases during the averaging operation, the phase indicator function, $X_k(x_i,t)$, is introduced. For a given realization of the flow Γ, the phase indicator function takes the value 1 if phase k is present at point x and at time t. Otherwise, it takes the value zero.

$$X_k(x_i,t) = \begin{cases} 1 & if\ x_i\ is\ in\ phase\ k\ at\ time\ t \\ 0 & otherwise \end{cases} \tag{54}$$

The volume fraction of phase k can be defined as the average of the phase indicator function X_k as

$$\alpha_k = \bar{X}_k \tag{55}$$

where α_k denotes in fact the probability of phase k.

The sum of the volume fractions of all phases must be

$$\sum_{k=1}^{n_{ph}} \alpha_k = 1. \tag{56}$$

All the remaining variables are either component-weighted or mass-weighted (or Favre) averaged. The averaged density of phase k is defined by

$$\bar{\rho}_k = \frac{\overline{X_k\rho}}{\alpha_k} \quad, \tag{57}$$

which denotes component-weighted variables. The averaged velocity of phase k is defined by

$$\overline{\mathbf{u}}_k = \frac{\overline{X_k \rho \mathbf{u}}}{\alpha_k \overline{\rho}_k} \tag{58}$$

which denotes mass-weighted (Favre) variables.

The basic equation of the multi-phase model, based on the above definition, will be presented in the next sections. In addition to the classic single-phase flow equation, the multi-phase flow equations are based on the concept of volume fraction, which represents the amount of a phase at a given place and time. Each term is multiplied by the volume fraction of the phase in question. An additional exchange terms are added to describe the spray physics and to make an interaction between the liquid phases and the gas phase. The final result is a set of multi-phase transport equations.

In the mathematical description that follows, the averaging bars are omitted for the purpose of simplification. The notation used is in Cratesian tensor form, where the lower case subscripts (*i, j, ij* etc.) denote the vector or tensor components. The lower case subscript (*k*) is used to denote the property of a specific phase, while two lower case subscripts (*lk*) are used to indicate the difference between the phases.

4.3.2 Mass Conservation Equation

One transport equation is required to represent the gas phase, while a number of mass conservation equations, *k,* are required to represent the droplet phases to account for a range of droplet size classes.

The mass conservation equation for the three dimensional multiphase flow for phase *k* can be written as

$$\frac{\partial}{\partial t}(\alpha_k \rho_k) + \frac{\partial}{\partial x_j}\left(\alpha_k \rho_k u_{kj}\right) = \sum_{l=1, l \neq k}^{n_{ph}} \Gamma_{kl} \tag{59}$$

where α denotes the volume fraction of the phase under consideration. The volume fraction accounts for the fact that each cell is occupied by phases, where each phase occupies a certain volume fraction of the cell. The conservation laws of mass are

satisfied by each phase individually. The volume fractions represent unknowns which have to be solved as other unknowns. Finally, the sum of all volume fractions must be:

$$\sum_{k=1}^{n_{ph}} \alpha_k = 1 \tag{60}$$

The source term on the right hand side is the interfacial mass transfer between phases k and l as the droplets move from one size group to another. Such mass exchange would is strongly coupled with the interfacial heat exchange, which is discussed in later sections.

4.3.3 Momentum Conservation Equation

The momentum conversation equations for gaseous and droplet phases k are respectively

$$\frac{\partial}{\partial t}\left(\alpha_k \rho_k u_{ki}\right) + \frac{\partial}{\partial x_j}\left(\alpha_k \rho_k u_{ki} u_{kj}\right) = -\alpha_k \frac{\partial p}{\partial x_i} + \frac{\partial}{\partial x_j}\left[\alpha_k (\tau_{kij} + \tau_{kij}^t)\right]$$
$$+\alpha_k \rho_k f_i + \sum_{l=1,l\neq l}^{n_{ph}} \mathrm{M}_{kli} + u_{ki} \sum_{l=1,l\neq k}^{n_{ph}} \Gamma_{kl} \tag{61}$$

where the n_{ph} momentum equations are needed to represent a range of droplet size classes, given that different velocities are known to develop between droplets of different size for the spray flows investigated here. The first term on the left hand side is the rate of change of momentum within the control volume. The convection term on the left hand side is the same as for single-phase with an addition of the volume fraction. The terms on the right hand side are the volume and surface forces acting on phase α. The volume force f is gravity acting on the fluid. The surface forces occur due to viscous stresses which are similar to those find in a single phase. The first term on the right hand side is the pressure gradient, i.e., the net pressure force acting on phase α. The pressure term on the right hand side is obtained accounting for the pressure force that exists internally in the control volume, not just at the boundaries. Therefore, to get the correct representation of pressure forces on each phase, te interfacial pressure forces must be added to the original term that represents the change in pressure forces

acting over the control volume,. The interested reader can find detailed information regarding derivation of this equation in Drew & Passman [81]. The second term is viscous stress denoted by shear stress due to the molecular viscosity τ_k and Reynolds stress τ^t_k. The third term is the gravity force; where M represents the interfacial momentum transfer from the k phase to the gas phase by phenomena such as drag forces, lift forcey etc. In most cases the lift forces are insignificant when compared to the drag forces. The term $u_{ki}\Gamma_{kl}$ denotes the momentum addition by the mass transfer between the droplet phases. It is assumed that all phases share the same pressure field:

$$p_k = p \tag{62}$$

For phase k the viscous stress tensor τ_{kij} is defined as

$$\tau_{kij} = \mu_k \left[\left(\frac{\partial u_{kj}}{\partial x_i} + \frac{\partial u_{ki}}{\partial x_j} \right) - \frac{2}{3}\delta_{ij}\frac{\partial u_{km}}{\partial x_m} \right] \quad . \tag{63}$$

Here μ_k is the molecular dynamic viscosity of phase k. Reynolds stress τ^t_{kij} is defined as

$$\tau^t_{kij} = \mu^t_k \left[\left(\frac{\partial u_{kj}}{\partial x_i} + \frac{\partial u_{ki}}{\partial x_j} \right) - \frac{2}{3}\delta_{ij}\frac{\partial u_{km}}{\partial x_m} \right] - \frac{2}{3}\delta_{ij}\rho_k k_k \quad . \tag{64}$$

Turbulent viscosity μ^t_k in the equation above is obtained from the turbulence model, similar to single phase flow:

$$\mu^t_k = \rho_k C_\mu \frac{k_k^2}{\varepsilon_k} \quad . \tag{65}$$

4.3.4 Energy Conservation Equation

The third fundamental conservation principle derived for multiphase flow is the energy equation. The total enthalpy h_k is used as an energy representative and a separate equation can be expressed for each phase:

$$\frac{\partial}{\partial t}\left(\alpha_k \rho_k h_k\right) + \frac{\partial}{\partial x_j}\left(\alpha_k \rho_k u_{kj} h_k\right) = \frac{\partial}{\partial x_j}\left[\alpha_k \left(q_{kj} + q_{kj}^t\right)\right] + \alpha_k \rho_k \theta_k + \alpha_k \rho_k f_j u_{ki}$$

$$+ \frac{\partial}{\partial x_j}\left[\alpha_k u_{ki}\left(\tau_{kij} + \tau_{kij}^t\right)\right] + \alpha_k \frac{\partial p}{\partial t} + \sum_{l=1, l \neq k}^{n_{ph}} \mathrm{H}_{kl} + h_k \sum_{l=1, l \neq k}^{n_{ph}} \Gamma_{kl} .$$

(66)

H_{kl} denotes the interfacial (inter-phase) enthalpy transfer between phases k and l by phenomena such as evaporation, while θ_k is specific enthalpy sources. Heat flux vector q_{kj} is given by

$$q_{kj} = \frac{\kappa_k}{c_{p,k}} \frac{\partial h_k}{\partial x_j}$$

(67)

here κ_k is phase k thermal conductivity. The turbulent heat flux vector q_{kj}^t is given by

$$q_{kj}^t = \frac{\mu_k^t}{\sigma_T} \frac{\partial h_k}{\partial x_j}$$

(68)

where u_k' represents the fluctuating part of the velocity, h_k' is the fluctuating part of the turbulent enthalpy and σ_T is the turbulent Prandtl number.

4.3.5 Turbulence Multiphase Model

As mentioned previously, turbulence modelling is important for the correct prediction of multiphase flow. In comparison with single-phase flows, the multiphase flows, featured by complicated interface dynamics, require a higher number of terms that should be modelled, and the modelling itself is very difficult [82]. The k-ε model has proven to be the most usable with respect to multiphase extension. Therefore, the turbulence modelled in this work is the extension of the standard k-ε model for a single-phase flow. Other, more sophisticated models exist, but the k-ε model is chosen here because it has gained significant popularity by offering numerical stable calculations with reasonable accuracy at low computational cost. The k-ε model introduces into the calculation two additional transport equations for each phase, one for the calculation of

turbulent kinetic energy and one for the calculation of turbulent dissipation. The conservation equation for the turbulent kinetic energy k is given by:

$$
\frac{\partial \alpha_k \rho_k k_k}{\partial t} + \frac{\partial}{\partial x_j}\left(\alpha_k \rho_k u_{kj} k_k\right) = \frac{\partial}{\partial x_j}\left[\alpha_k\left(\mu_k + \frac{\mu_k^t}{\sigma_k}\right)\frac{\partial k_k}{\partial x_j}\right] + \alpha_k \mathbf{P}_k - \alpha_k \rho_k \varepsilon_k
$$
$$
+ \sum_{l=1,l\neq k}^{n_{ph}} \mathbf{K}_{kl} + k_k \sum_{l=1,l\neq k}^{n_{ph}} \Gamma_{kl}
$$

(69)

where the term $\mathbf{P}_k$ stands for production of turbulent kinetic energy for phase k and it is defined as

$$
\mathbf{P}_k = \tau_{kij}^t \frac{\partial u_{ki}}{\partial x_j} \quad .
$$

(70)

An analogous equation for the turbulent dissipation rate is given by

$$
\frac{\partial \alpha_k \rho_k \varepsilon_k}{\partial t} + \frac{\partial}{\partial x_j}\left(\alpha_k \rho_k u_{kj} \varepsilon_k\right) = \frac{\partial}{\partial x_j}\left[\alpha_k\left(\mu_k + \frac{\mu_k^t}{\sigma_\varepsilon}\right)\frac{\partial \varepsilon_k}{\partial x_j}\right] + \sum_{l=1,l\neq k}^{n_{ph}} \mathbf{D}_{kl} + \varepsilon_k \sum_{l=1,l\neq k}^{n_{ph}} \Gamma_{kl}
$$
$$
+ \alpha_k C_{\varepsilon 1} \mathbf{P}_k \frac{\varepsilon_k}{k_k} - \alpha_k C_{\varepsilon 2} \rho_k \frac{\varepsilon_k^2}{k_k} - \alpha_k C_{\varepsilon 4} \rho_k \varepsilon_k \frac{\partial u_{kj}}{\partial x_j} \quad .
$$

(71)

The terms $\mathbf{K}_{kl}$ and $\mathbf{D}_{kl}$ are the exchange terms accounting for turbulence modification by the presence of droplets. For the modelling calculation, performed as part of this work, the model relies on the assumption that the level of turbulence of the dispersed phases are equal to the continuous phase level of turbulence and that the interaction between the two phases is neglected [83]. Finally, the employed closure coefficients for turbulent kinetic energy and turbulent dissipation equations are:

$$
C_{\varepsilon 1} = 1.44 \quad C_{\varepsilon 2} = 1.92 \quad C_{\varepsilon 3} = 0.09 \quad C_{\varepsilon 4} = -0.33 \quad \sigma_k = 1.0 \quad \sigma_\varepsilon = 1.3 \; .
$$

(72)

4.3.6 Vapor Transport Equation

The first phase is the primary gaseous phase, gas mixture, which is composed of two species namely gas and vapour. Hence, the vapor mass fraction needs to be transported by a separate scalar transport equation within the gaseous phase as

$$\frac{\partial}{\partial t}(\alpha_1 \rho_1 Y_i) + \frac{\partial}{\partial x_j}(\alpha_1 \rho_1 \mathbf{v}_1 Y)_i = \frac{\partial}{\partial x_j}\left(\alpha_1 (\rho_1 D_{Y_i} + \frac{\mu_1^t}{Sc^t})\frac{\partial}{\partial x_j} Y_i\right) + S_{Y_i}. \tag{73}$$

The source term on the right hand side S_{Yi} is determined by the sum of the evaporated liquid masses of all droplet phases.

4.4 Spray Sub-Models

In the presence of liquid spray there are mass, momentum, energy and turbulence transfers between the phases. These transfers are denoted as source terms (interfacial exchange terms) on the right hand side of the multiphase conservation equations, representing the interaction and coupling between the phases. The source terms are determined by the spray sub-models, accounting for the appropriate physics of the spray, such as break-ups and evaporation. The interfacial mass exchange between the gaseous phase and the liquid phase includes primary break-up, secondary break-up and droplet evaporation, while the interfacial momentum exchange includes drag forces and turbulent dispersion forces. The interfacial heat exchange is determined by the evaporation model.

4.4.1 Primary Break-up Models

The nature of the break-up process depends on the spray region. In the case of high-pressure injection conditions, the primary break-up of the liquid jet starts directly at the nozzle exit. The liquid jet disintegrates into fragments and large drops which forms dense spray region. It is assumed that the main mechanisms for the primary break-up of liquid jet are the turbulence generated inside the injection nozzle and the aerodynamic interaction with the surrounding air outside the nozzle, as described in section 2. Therefore, the primary break-up model used in present study takes into account the effects of turbulence and aerodynamic surface instabilities, according to the model of Bianchi & Pelloni [84]. The model assumes that the turbulent forces within the liquid emerging from the nozzle cause the surface waves to grow and break-up with the characteristic atomization length scale L_A. and the time scale τ_A. The wavelength of the unstable surface wave is defined by the turbulent length scale that is used to calculate the atomization characteristic length scale.

In addition, two time scales of atomization are evaluated, the mean turbulent time scale and the aerodynamic time scale. The break-up time scale is then calculated as the linear function of these two time scales:

$$\tau_A = C_1\tau_T + C_3\tau_W \tag{74}$$

where C_1 and C_3 are model constants. The τ_T is the turbulent time scale and τ_W is the aerodynamic time scale. The liquid jet turbulent time scale τ_T is determined as

$$\tau_T = c_\mu \frac{k_{avg}}{\varepsilon_{avg}} \tag{75}$$

where the liquid jet average turbulent kinetic energy k_{avg}, and its dissipation rate ε_{avg} at the injection nozzle exit are used for the calculation. The constant c_μ is given by the standard $k - \varepsilon$ model. The aerodynamic time scale is derived from the Kelvin-Helmholtz instability model, where the viscous forces between the liquid and the gas produces an unstable wave growth on the liquid jet surface. The aerodynamic time scale (wave growth time scale) can be expressed according to the KH instability theory as

$$\tau_W = \frac{L_W}{\left[\dfrac{\rho_N \rho_g |u_{rel}|^2}{(\rho_N + \rho_g)^2} - \dfrac{\sigma}{(\rho_N + \rho_g) L_W} \right]^{0.5}}. \tag{76}$$

The liquid jet aerodynamic length scale is estimated to be proportional to the liquid jet turbulent length scale:

$$L_W = 2L_T. \tag{77}$$

The liquid jet turbulent length scale is related to the average turbulent kinetic energy and the energy dissipation rate at the nozzle exit

$$L_T = c_2 c_\mu \frac{k_{avg}^{3/2}}{\varepsilon_{avg}} \tag{78}$$

where this length scale is used as the atomization length scale L_A. In the equation above k_{avg} and ε_{avg} are estimated [84] as follows:

$$k_{avg} = \frac{u_{inj}^2}{8 L_{noz} / D_{noz}} \left[\frac{1}{c_7^2} - c_4 - (1 - c_6^2) \right] \tag{79}$$

$$\varepsilon_{avg} = c_5 \frac{u_{inj}^3}{2L_{noz}} \left[\frac{1}{c_7^2} - c_4 - (1 - c_6^2) \right] \tag{80}$$

where c_7 is the discharge coefficient, $c_4 = 0.45$ and $c_5 = 0.27$, c_6 is the flow area contraction coefficient, L_{noz} is the nozzle hole length and D_{noz} is the diameter of the nozzle hole.

The radius of the injected droplet is assumed to decrease continuously with time as

$$\frac{dr}{dt} = -\frac{L_A}{\tau_A}. \tag{81}$$

The mass exchange rate per droplet surface due to primary break-up is expressed as

$$M_N = \rho_N \frac{dr}{dt} \tag{82}$$

while the final mass exchange is calculated as

$$\frac{dm}{dt} = 4\pi r_N^2 \rho_N \frac{dr}{dt}. \tag{83}$$

The model is based on the Eulerian multiphase approach. The liquid jet is classified as a bulk liquid phase that is introduced as a number of spherical large drops, known as blobs. The diameter of these blobs equals the nozzle hole diameter. The primary break-up of the liquid jet occurs between the bulk liquid phase N and the liquid droplet phases from 2 to $N-1$.

The mass exchange rate due to primary break-up, mass loss per unit volume for the bulk liquid phase N to the liquid droplet phases k, is calculated as

$$\Gamma_{P,Nk} = 4\pi r_N^2 \rho_N N_N \left(\frac{dr_N}{dt} \right)_{primbr} = \rho_N \frac{3\alpha_N}{r_N} \left(\frac{dr_N}{dt} \right)_{primbr} = -\Gamma_{P,kN} \tag{84}$$

where N_N is derived assuming spherical droplets with radius r_N:

$$\frac{4\pi r_N^3}{3} N_N = \alpha_N \rightarrow N_N = \frac{3\alpha_N}{4\pi r_N^3}. \tag{85}$$

It is noteworthy, however, that in this model the effects of cavitation are not included and the use of this model is limited to spray from non-cavitating turbulent nozzle hole flows.

4.4.2 Secondary Break-up Models

Once the liquid droplets are formed from the liquid jet after the primary break-up they may further break-up into smaller droplets due to aerodynamic forces that are induced by the relative velocity between droplets and ambient gas. These forces cause an unstable wave growth on the surface of the droplet that can eventually lead to break-up. This phenomenon is known as the secondary break-up, or the droplet break-up. A variety of secondary break-up models have been proposed in literature, but there are a few popular models that are extensively used in modelling, including RD (Reitz and Diwakar), WAVE, TAB (Taylor Analogy Break-up) and FIPA (Fractionnement Induit Par Acceleration) etc. It is exceedingly difficult to choose which of these models should be utilized for a specific simulation task. It turns out that practically all of these models are capable of reproducing measured data, as long as the model constants are properly chosen. Therefore, the standard WAVE model [85], which is appropriate for a very high speed injection, is used in this study to account for the droplet break-up processes. This model is based on the Kelvin-Helmholtz instability of a liquid jet, where the viscous forces produce waves on the liquid surface and new droplets are formed from the surface waves. Waves grow on the droplet surface with a growth rate Ω and a wavelength Λ, and the sizes of the new-formed droplets are determined from the wavelength and growth rate of this instability. Due to the break-up and production of new droplets, the size of the parent droplets is reduced and the rate of change of this parent droplets is given by

$$\frac{dr_k}{dt} = -\frac{r_k - r_{stable}}{\tau_a}, r_{stable} \leq r_k \tag{86}$$

where r_k is the radius of the droplet size class and the break-up droplet radius r_{stable} is assumed to be proportional to wavelength of the fastest-growing unstable wave

$$r_{stable} = B_0 \Lambda$$

where $B_0 = 0.61$ is the model constant. The break-up time is given by

$$\tau_a = 3.726 B_1 \frac{r_k}{\Lambda_k \Omega_k} \tag{87}$$

where B_1 is an adjustable model constant including the effects of the nozzle hole flow. The recommended values of this constant range from 1.73 to 30 [85][86]. A small value of B_1 leads to increased break-up and reduces the penetration length, while a higher value of B_1 causes reduced break-up and increases the penetration length.

The growth rate Ω and wave-length Λ is given by Reitz [85]as

$$\Lambda_k = 9.02 r_k \frac{\left(1 + 0.45 \cdot Oh^{0.5}\right)\left(1 + 0.4 \cdot T^{0.7}\right)}{\left(1 + 0.87 \cdot We_1^{1.67}\right)^{0.6}} \tag{88}$$

$$\Omega_k = \left(\frac{\rho_k r_k^3}{\sigma}\right)^{-0.5} \frac{0.34 + 0.38 \cdot We_1^{1.5}}{\left(1 + Oh\right)\left(1 + 1.4 \cdot T^{0.6}\right)} \tag{89}$$

where r_k is the droplet radius of the break-up phase, Oh is the Ohnesorge number, T is the Taylor number and We is the Weber number.

The mass exchange rate per droplet surface due to secondary break-up is expressed:

$$M_k = \rho_k \frac{dr_k}{dt} \tag{90}$$

while the final mass exchange is calculated as

$$\frac{dm_k}{dt} = 4\pi r_k^2 \rho_k \frac{dr_k}{dt}. \tag{91}$$

The mass exchange rate due to secondary break-up, mass loss per unit volume of phase k, is calculated as

$$\Gamma_{S,kl} = 4\pi r_k^2 \rho_k N_k \left(\frac{dr_k}{dt}\right)_{\sec br} = \rho_k \frac{3\alpha_k}{r_k}\left(\frac{dr_k}{dt}\right)_{\sec br} \tag{92}$$

where N_k is derived assuming spherical droplets with radius $r_{k:}$

$$\frac{4\pi r_k^3}{3} N_k = \alpha_k \rightarrow N_k = \frac{3\alpha_k}{4\pi r_k^3}.$$

(93)

The secondary break-up model is applied in each cell of the spray region. If the predicted size of the new droplets r_l is less than the parent droplet radius r_k, then mass will be transferred according to the break-up rate into the corresponding droplet size class.

4.4.3 Evaporation Model

In addition to the primary and secondary break-up, the fuel evaporation of droplets is of great importance in predicting the performance of spray injections systems. It has a significant impact on effective fuel-air mixing, combustion and the emission formation process. An understanding of fuel evaporation is a prerequisite for assessing the quality of the mixture formation and must be included in the calculation of spray heat and the mass transfer process. This means that in the interfacial mass exchange, represented by the term Γ_{kl}, an additional contribution from droplet evaporation, as well as in the interfacial enthalpy exchange term H_{kl} needs to be incorporated. The fact that droplets exchange heat and mass simultaneously with the gaseous phase highlights the complex nature of these interdependent processes. Therefore, accurate numerical simulation of spray processes, besides break-up mechanisms, requires the modelling of droplet evaporation. The evaporation of a droplet in the spray is influenced by neighbouring droplets, but it is usually assumed that the droplets behave as if they were isolated from each other in a gas environment.

This work investigates the high pressure diesel injections where the fuel evaporates after the spray has broken into small droplets. This occurs because the liquid fuel is injected through the nozzle hole into the combustion chamber below its boiling temperature and the specific surface area is very small before dispersion. Thus, evaporation of droplets is a vital part in the modelling of spray evaporation. This work assumes that the overall spray behaviour is obtained by summing the behaviour of isolated droplets dynamics inserted into the hot gas flow. The heat arrives at the droplet from the hot gas by conduction, convection, and radiative heat transfer, producing the

fuel vapour that leaves into the gas by convection and diffusion. Hot chamber gases transfer the heat to colder droplets, affecting the droplet temperature change, and the velocity and phase change from liquid to vapour. It is assumed that the droplets are spherical. It is also assumed that the liquid fuel temperature is uniform throughout the droplet and that the pressure drop in the gas is negligible. The radiative heat transfer is small compared with convection and can be neglected. The mathematical model used to perform the calculation of the evaporation processes is Abramzon/Sirignano [87]. The heat and mass transfer processes in the gas phase near the surface of droplets are derived by the mass evaporation rate m_d and the heat transferred into the droplet Q_d. Droplet evaporation is described by the empirical Nusselt and Sherwood laws derived from experiments using single droplets under certain conditions. Consequently, the droplet evaporation rate is given as

$$m_d = 2\pi\overline{\rho}_g\overline{\beta}_g r_d Sh^* \ln(1+B_M) \tag{94}$$

and

$$m_d = 2\pi\frac{\overline{k}_g}{\overline{c}_{pF}} r_d Nu^* \ln(1+B_T) \tag{95}$$

where r_d is the droplet diameter, and $\overline{\rho}_g, \overline{\beta}_g, \overline{k}_g$ are the density, binary diffusion coefficient and thermal conductivity of the gas mixture at reference conditions, respectively. $\overline{c}_{pF}$ is the specific heat capacity of the vapor and B_M and B_T are mass and heat transfer numbers, also called also Spalding numbers. The mass transfer number is given as

$$B_M = \frac{Y_{FS} - Y_{F\infty}}{1-Y_{FS}} \tag{96}$$

where Y_F is the fuel mass fraction and index S denotes the condition at droplet surface, while index ∞ denotes the ambient condition. The non-dimensional heat and mass transfer coefficients Nu^* and Sh^* are modified Nusselt and Sherwood numbers, which are given as

$$Nu^* = 2+(Nu_0 - 2)/F_T \tag{97}$$

$$Sh^* = 2 + (Sh_0 - 2)/F_M \tag{98}$$

where Nu_0 and Sh_0 are appropriate, non-dimensional parameters of the non-evaporating droplet proposed by Clift [88]:

$$Nu_0 = 2 + 0.552\,\mathrm{Re}^{0.5}\,\mathrm{Pr}^{0.33} \tag{99}$$

$$Sh_0 = 2 + 0.552\,\mathrm{Re}^{0.5}\,Sc^{0.33}. \tag{100}$$

The diffusional film correction factors F_M and F_T are expressed as functions of mass and heat transfer numbers:

$$F_M = F(B_M); F_T = F(B_T) \tag{101}$$

representing the relative change of film thicknesses due to Stefan law [87]. $F(B)$ is the universal function for both correction factors F_M and F_T:

$$F(B) = (1 + B)^{0.7}\frac{\ln(1 + B)}{B}. \tag{102}$$

The calculation procedure of the evaporation rate m_d and the heat penetrating into the droplet phases Q_d is:

1. Calculation of the mass fraction of fuel vapour Y_{FS} at the droplet surface.
2. Calculation of the average physical properties in the gas film using the reference temperature and the fuel concentration. The reference values are calculated according to the 1/3 rule recommended by [89] as

$$\bar{T} = T_S + \frac{(T_\infty - T_S)}{3} \tag{103}$$

$$\bar{Y}_S = Y_{FS} + \frac{(T_{F\infty} - T_{FS})}{3} \tag{104}$$

3. Calculation of the Nusselt and Sherwood number, Nu_0 and $Sh_{0,}$, for a non-evaporating droplet.
4. Calculation of the mass transfer number B_M, correction factor F_M, and modified Sherwood number Sh^*.
5. Calculation of the mass evaporation rate according to Equation (94).

6. Calculation of the heat transfer number, B_T^{old}, from a previous time step and correction factor F_T.

7. Calculation of the modified Nusselt Nu^* and correction of the heat transfer number by comparing the value of the mass evaporation rate from Equation (94) and (95) and

$$B_T = (1 + B_M)^\Phi - 1.$$

()

The parameter Φ is

$$\Phi = \frac{\overline{c}_{pF}}{\overline{c}_{pg}} \frac{Sh^*}{Nu^*} \frac{1}{Le}.$$

(105)

8. Calculation of the heat transferred into the droplet Q_d is:

$$Q_d = m_d \left(\overline{c}_{pF} \frac{T_\infty - T_S}{B_T} - L(T_S) \right).$$

(106)

In the Eulerian multiphase approach the droplet evaporation occurs between the gaseous phases 1 and the droplet phases 2 to N. The total evaporation mass flux from all droplets of class k in one control volume is calculated as

$$\Gamma_{E,kg} = \frac{-6\alpha_k m_d}{\pi d_k^3} = -\Gamma_{E,gk}$$

(107)

while the total mass flux from all droplet phases to the gas phase is given as:

$$\Gamma_{E,1l} = 6 \sum_{k=2}^{k=N} \frac{\alpha_k m_d}{\pi d_k^3}.$$

(108)

The amount of heat penetrating into the droplet interior from hot gases to droplet phases can be expressed in a similar way as for mass transfer process as

$$H_{E,kg} = \frac{6\alpha_k Q_d}{\pi d_k^3} = -H_{E,gk}$$

(109)

$$H_{E,1l} = -6 \sum_{k=2}^{k=N} \frac{\alpha_k Q_d}{\pi d_k^3}.$$

(110)

In this way the evaporation model determines the interfacial enthalpy exchange H_{kl} in Equation (66).

4.4.4 Momentum Exchange Model

The phases interact with one another at the interfaces separating the phases. If the gas has higher velocity than the liquid droplets, it will create a drag force acting on the droplet at the interface. An equal drag force of opposite sign will act on the gas. This interaction at the inter-phases is described as an interfacial momentum exchange.

The drag forces (shear force) and turbulent dispersion forces determine the momentum exchange between the gas phase *1* and the liquid phases *k* from *2* to *N*.

4.4.4.1 Drag Force

The three-dimensional character of the droplets is accounted for by drag forces. The drag force F_D acting on the droplets is caused by the droplet movement relative to the ambient gas phase. The equation of motion of a spherical droplet moving with a velocity u_{rel} relative to the gas may be written as follows:

$$\mathbf{F}_D = \frac{\rho_g}{2} c_D A_d \mathbf{u}_{rel} u_{rel} \tag{111}$$

where ρ_g is the fluid density, c_D is the drag coefficient, and A_d is the surface area of the droplets, assuming spherical shape.

The drag coefficient c_D for the droplet is usually an empirically determined parameter which is usually given as a constant or as a function of a Reynolds number. At the low Reynolds number,

$$c_D = \frac{24}{Re} \tag{112}$$

is given by the well known Stoke's law, where *Re* is the relative Reynolds number for the gaseous phase *g* and liquid phase *k* is

$$Re = \frac{\rho_g \left| u_{rel} \right| d_k}{\mu_g} \quad . \tag{113}$$

For a higher Reynolds number $Re \leq 1000$ the drag coefficient often specified as a function of the droplet Reynolds number is defined as

$$c_D = \frac{24}{Re}(1+0.15 Re^{0.687}) \tag{114}$$

while for Re > 1000 and according to Newton's law, the drag coefficient is defined as constant:

$$c_D = 0.44. \tag{115}$$

In this thesis for multiphase simulation the following correlation [90] is used:

$$c_D = \frac{24}{Re}\left[\left(1-\alpha_k\right)^{-2.65} + \frac{Re^{0.667}}{6}\left(1-\alpha_k\right)^{-1.78} \right] \tag{116}$$

where α_k is the dispersed phase volume fraction. This equation was given by O'Rouke and Bracco and comes from experimental data [91].

For higher Reynolds and Weber numbers the liquid droplets are deformed and are not longer spherical. Thus, the drag coefficients should be a function of oscillation amplitude. Correlations for the drag coefficients of deformed liquid droplets have been considered by Liu [92]. The TAB model is usually used to estimate the droplet distortion [93].

The drag force per unit volume between the gaseous phase g and the liquid phases k is given by:

$$\mathbf{M}_{D,kg} = N''' \, \mathbf{F}_D \tag{117}$$

where N''' denotes the number of droplets per unit volume

$$N''' = \frac{6 \, \alpha_k}{\pi \, d_k^3} \quad . \tag{118}$$

Finally, the drag force can be expressed as

$$\mathbf{M}_{D,kg} = \frac{6\alpha_k}{d_k^3 \pi} \mathbf{F}_D = \frac{3}{4} c_D \frac{\alpha_k \rho_g}{d_k} \left| \mathbf{u}_g - \mathbf{u}_k \right| \left(\mathbf{u}_g - \mathbf{u}_k \right) = -\mathbf{M}_{D,gk} \quad . \tag{119}$$

The drag force of all droplets in a control volume is obtained by multiplying of $\mathbf{M}_{D,kg}$ by the certain control volume of the computational cell. It is assumed that the velocity is uniform for all droplets in the control volume and an average uniform droplet diameter is also assumed.

4.4.4.2 Turbulent Diffusion Force

The relative velocity between the gaseous phase and the dispersed phase results not only in the deceleration and deformation of droplets, but also in the diffusion or dispersion of droplets by turbulence. Hence, the turbulent transport of a dispersed liquid phase by turbulence presents an important mechanism in multi-phase flows that must be taken into account. One of the approaches [94] for predicting the droplet dispersion in turbulence is based on the turbulent diffusion force that is constituted within the context of the k-ε model:

$$\mathbf{M}_{T,kg} = c_{T,kg} k_g \nabla \alpha_k = -\mathbf{M}_{Tgk} \quad . \tag{120}$$

The coefficient $c_{T,kg}$ may be used as a constant value $c_{T,kg} = 0.1 \sim 1$ or may be calculated from the droplet relaxation time and turbulence time scales [77].

5 Chemistry Modelling

5.1 Combustion Modelling

Combustion can be defined as significant release of heat caused by the chemical reaction between the fuel and an oxidizer. Combustion modelling requires some understanding of elementary chemical reactions, reactions rates and temperature and pressure dependence. All of this information is embedded in a reaction chemical mechanism that is relevant for combustion modelling. The smallest mechanism encountered in combustion modelling describes the oxidation of hydrogen. Nine species and approximately fifty elementary reactions are involved in this mechanism. For combustion of hydrocarbon fuels, as simple as methane CH_4, the number of elementary reactions in the mechanism is much larger. Furthermore, for combustion of higher hydrocarbons, for example Diesel fuel, hundreds of species are present and several thousands of elementary reactions are involved in the chemical mechanism. The interactions of these elementary reactions govern the combustion process. However, such large mechanisms require significant computational power in the simulation of practical combustion systems. This computation cost is directly proportional to the number of species, reactions, and cells in the computational domain. Thus, different approaches have been addressed to reduce the computational expense due to reaction mechanisms [5][95][96][97][98][99].

There are two main categories of flames: premixed flames and non-premixed flames. These flame types are determined by the way in which the fuel and oxidizer are mixed and burned. In premixed flames the fuel and oxidizer are mixed first and burned later, while in non-premixed flames the fuel and oxidizer are mixed during the combustion process. Furthermore, these categories can be subdivided based on whether the fluid flow is laminar or turbulent. Chemical reactions are the same in laminar and turbulent flows, but the physical flow properties are changed, influencing the combustion. Different combustion modelling approaches with varying degrees of complexity have been proposed in the last two decades. An excellent review summarizing a non-premixed combustion modelling of turbulent diffusion flames can be found in [96], while a review of premixed combustion modelling has been provided

by Brewster [100]. A Bilger et al. [101] recently provided a strong review for both non-premixed and premixed combustion modelling techniques, as well for partially premixed turbulent combustion. However, the principle description of all combustion processes is based on the fundamental conservation equations: the mass conservation equation, the momentum conservation equations, the energy conservation equation and the species mass fraction conservation equations. Other sub-models are coupled with these equations to account for species mixing and chemical reactions.

Combustion modelling is a broad subject, making it impossible to review all likely aspects of combustion modelling. This section is intended to give only the basic definitions and concepts, which shall be referred to throughout this work. For more information on the combustion fundamentals one is referred to the standard literature [5][95].

5.1.1 Simplified Combustion

The combustion process can be simplified to a single overall reaction as

$$\text{F} + \text{Ox} \rightarrow \text{Pr} \tag{121}$$

where F is fuel, Ox is oxidizer and Pr is products. The equation above is known as the general global reaction mechanism, and assumes that the reaction between fuel and oxygen is complete and no intermediated species concentration can be calculated. The rate of the reaction is given as:

$$\frac{d[F]}{dt} = -k(T)[F]^n[Ox]^m \tag{122}$$

where k is the global reaction rate coefficient, n and m are reaction orders determined from experimental data and $[F]$ and $[Ox]$ denote mass fraction of the fuel and oxidizer, respectively. Chemical reaction rate coefficients from the above equation can be calculated according to modified Arrhenius law

$$k = AT^{\beta} \exp\left(-\frac{E}{RT}\right). \tag{123}$$

The coefficients A, β and E are determined from experimental data. It can be noticed that the reaction rate depends nonlinearly on the temperature T and the activation energy E. In this combustion modelling approach the burning rate depends significantly on the chemical kinetics while the effects of turbulent fluctuations are ignored. An alternative approach to this model, described by Magnussen and Hjertagre [102], can be used for chemistry modelling of turbulent flames. This model employs the eddy break-up model suggested by Spalding [103] and assumes that reaction rates are controlled by turbulence while chemical kinetics are neglected. The fuel consumption rate (reaction rate) is assumed to be inversely proportional to the turbulent mixing time scale (k/epsilon) and can be expressed in accordance with Magnussen and Hjertager as

$$w_F = A \frac{\varepsilon}{k} \min\left(Y_F, \frac{Y_{Ox}}{S}, B \frac{Y_{Pr}}{1+S} \right) \tag{124}$$

where Y denotes the local mean mass fraction of fuel, oxygen and product, while S is the relationship in the stoichiometric fuel/air reaction in Equation (124), and A and B are empirical coefficients that are not generalized, but rather established for each reactive flow application. The chemical reaction is controlled by the limited species which are either fuel, oxidizer, or product. Generally, it is possible to assimilate both of these approaches where both the Arrhenius and eddy dissipation reaction rates can be calculated, and the smallest rate is assumed to be the burning rate. This means that three different reaction rates are calculated and the smallest rate is used for combustion modelling. The first rate is calculated according to the Arrhenius reaction rate, the second calculated reaction rate represents the rate of dissipation of turbulent reactant eddies, while the third reaction rate is the rate of dissipation of turbulent eddies with products according to Equation (124). Although this approach can give satisfactory results when compared with measurements, the combustion modelling with global reaction approach simply provides a basis for understanding what is happening and has limited use in combustion.

5.1.2 Detailed Combustion Modelling

The oxidation of fuel is composed by many elementary steps, which can be described by the detailed reaction mechanism that involves a collection of elementary reactions. In contrast to an overall chemical reaction, an elementary chemical reaction cannot be further broken into constituent reactions. The reaction mechanisms describe the chemistry - how it occurs on a molecular level and which bonds are broken or formed.

A general set of elementary reactions, making the detailed reaction mechanism, can be represented as

$$\sum_{i=1}^{N_{spec}} \mathbf{v}'_{ij} M_i \underset{k_{b,j}}{\overset{k_{f,j}}{\rightleftharpoons}} \sum_{i=1}^{N_{spec}} \mathbf{v}''_{ij} M_i \tag{125}$$

where M_i is the species i involved in an elementary reaction j, $\mathbf{v}'_{ij}$ are stoichiometric coefficients of the reactants, and $\mathbf{v}''_{ij}$ are stoichiometric coefficients of the products for reaction j. The above equation is valid for both reversible and non-reversible reactions, where $k_{f,j}$ and $k_{b,j}$ denote the forward and backward rate constant for reaction j, respectively. The forward rate coefficients $k_{f,j}$ are obtained from the Arrhenius expressions as:

$$k_{f,j} = A_j T^{\beta_j} \exp\left(-\frac{E_j}{RT}\right). \tag{126}$$

All of the elementary reactions have their own values for A_j, β_j and E_j which are obtained from experimental data [95]. If the reaction is reversible, the backward rate constants $k_{b,j}$ are calculated from the forward constants $k_{f,j}$ using the following expression:

$$k_{b,j} = \frac{k_{f,j}}{K_j} \tag{127}$$

where K_j is the equilibrium constant for the j reaction and can be calculated as

$$K_j = \prod_{i=1}^{N_{spec}} \left[X_{i,eq} \right]^{\left(\mathbf{v}_{ij}^{''} - \mathbf{v}_{ij}^{'} \right)}$$ (128)

where $\left[X_{i,eq} \right]$ denotes the molar concentration of the species i at equilibrium. The mole fraction of species is usually used in chemical kinetics and can be easily related with mass fraction as

$$\left[X_i \right] = \rho \frac{Y_i}{W_i}$$ (129)

where W_i is the molecular weight of species i.

The rate of the reaction ω_i for species i is given by:

$$\omega_i = W_i \sum_{j=1}^{N_{reac}} \left(\mathbf{v}_{ij}^{''} - \mathbf{v}_{ij}^{'} \right) \left[k_{f,j} \prod_{i=1}^{N_{spec}} \left[X_i \right]^{v_{ij}^{'}} - k_{b,j} \prod_{i=1}^{N_{spec}} \left[X_i \right]^{v_{ij}^{''}} \right]$$ (130)

where ω_i represents the source term in the species equation.

5.1.3 Mixture Formation Models

In contrast to the classical combustion modelling approach, the transport equation for the individual species is not solved in the combustion domain in the mixture formation approach. Instead, only one or two transport equations for the conserved scalar variable, called the mixture fraction, have to be solved. In this case the only description required is the process of mixing, while the reaction chemistry is calculated using an equilibrium assumption or flamelet model, where turbulence-chemistry interactions are pre-processed and stored in look-up tables. Instead of the species, only the mixture fraction Z (conserved scalar)

$$Z = \frac{\dot{m}_F}{\dot{m}_F + \dot{m}_O}$$ (131)

is tracked. For the case where there are two inlet streams the fuel stream and oxidant, the mixture fraction defines the degree of the mixing process. A conservation equation for the mean mixture fraction can be written as

$$\frac{\partial\left(\bar{\rho}\tilde{Z}\right)}{\partial t}+\frac{\partial\left(\bar{\rho}\tilde{Z}\tilde{u}_j\right)}{\partial x_j}=\frac{\partial}{\partial x_j}\left(\frac{\mu_t}{\mathrm{Sc}_{t1}}\frac{\partial\tilde{Z}}{\partial x_j}\right) \tag{132}$$

which is similar in form to the other conservation equations. In the above equation above the term concerning molecular diffusion is ignored since it is usually negligible when compared with other terms. This equation has no chemical source terms and thus Z is a conserved scalar. Since that combustion process is usually turbulent, the mixture fraction will fluctuate about its mean value at every point in the combustion chamber. To characterize the mixing process and related chemical reactions a variance of the mixture fractions, second moment about the mean, is required as the closure model:

$$\frac{\partial\left(\bar{\rho}\widetilde{Z''^2}\right)}{\partial t}+\frac{\partial\left(\bar{\rho}\widetilde{Z''^2}\tilde{u}_j\right)}{\partial x_j}=\frac{\partial}{\partial x_j}\left(\frac{\mu_t}{\mathrm{Sc}_t}\frac{\partial\widetilde{Z''^2}}{\partial x_j}\right)+2\frac{\mu_t}{\mathrm{Sc}_t}\left(\frac{\partial\tilde{Z}}{\partial x_j}\right)^2-\bar{\rho}\tilde{\chi}\ . \tag{133}$$

The turbulent Schmidt number in this work is chosen $\mathrm{Sc}_{t1}=\mathrm{Sc}_{t2}=0.7$ [104]. The last term on the right hand side is the sink and can usually be modelled as

$$\bar{\chi}=C\frac{\varepsilon}{k}\widetilde{Z''^2}\ . \tag{134}$$

This modelling approach ensures that the chemistry is reduced to the transport equations for the mixture fraction and its variance that are solved in the standard CFD procedure, while species mass fractions, temperature and density are then derived from the calculated mixture fraction fields. The reaction chemistry can be calculated using an equilibrium algorithm or laminar flamelet approach, where turbulence-chemistry interactions are pre-processed and stored in look-up tables. The probability density function (PDF) is used to calculate time mean values because the temperature and the species mass fractions in the turbulent mixing flow are random functions of space and time, and thus turbulent fluctuations must be taken into account in terms of PDF. There are different ways to obtain this statistical approach. In the full PDF approach [105] Monte-Carlo algorithms are commonly used to solve transport equations. either for velocity-composition joint PFD or just for the composition joint PDF. This approach requires significant computer power and therefore a simpler approach such as presumed PDF is typically used. The PDF shape is assumed a priori and the parameters of PDF

are calculated using the mixture fraction moments from their respective transport equations. The PDF shape is assumed from experimentally observed fluctuations in flames [5][96], and can be assumed to be beta function, Gaussian function or Dirac-delta function [5]. The beta PDF was used in this thesis to take into account the fluctuations associated with a turbulent combustion. The shape of PDF used here is described in section 5.2.3.

As already mentioned, in mixture formation combustion models the chemistry can be calculated in the pre-processor step and tabulated by different approaches, for example by the chemical equilibrium or chemical non-equilibrium approach. In both cases chemistry is in interaction with the PDF approach in order to take into account turbulence. The equilibrium approach assumes that the chemistry is rapid enough and that the species and the products reach their equilibrium values as soon as they mix. In the chemical non-equilibrium approach, such as laminar flamelet model, the detailed, more realistic chemical kinetics are incorporated in the combustion prediction. In the case of Steady Laminar Flamelet Model – SLFM [104][106], which is also used in this thesis, the following equations for the instantaneous values of the species mass fractions and temperature are solved in the pre-processor step by CSC solver [107][108]:

$$\rho \frac{\partial Y_i}{\partial \tau} - \rho \frac{\chi}{2} \frac{\partial^2 Y_i}{\partial Z^2} - \dot{\omega}_i = 0 \tag{135}$$

$$\rho \frac{\partial T}{\partial \tau} - \rho \frac{\chi}{2} \frac{\partial^2 T}{\partial Z^2} - \rho \frac{\chi}{2 c_p} \frac{\partial T}{\partial Z} \frac{\partial c_p}{\partial Z} - \sum_{i=1}^{N_{spec}} \rho \frac{\chi}{2} \frac{c_{pi}}{c_p} \frac{\partial Y_i}{\partial Z} \frac{\partial T}{\partial Z} + \frac{1}{c_p} \sum_{i=1}^{N_{spec}} h_i \dot{\omega}_i - \frac{q_R}{c_p} = 0 \tag{136}$$

where Z is the mixture fraction, T is temperature, Y_i, $\dot{\omega}_i$ and h_i are the mass fraction, chemical reaction rate and specific enthalpy of species i, respectively, c_p is the specific heat coefficient, while q_r is the radiative heat gain/loss.

The scalar dissipation rate $\chi = \chi(Z)$ is a variable that is given in a parameterized form as [106]:

$$\chi = \chi(Z) = \chi_{st} \frac{\exp\left\{-2\left[erfc^{-1}(2Z)\right]^2\right\}}{\exp\left\{-2\left[erfc^{-1}(2Z_{st})\right]^2\right\}} \tag{137}$$

72

For given values of the stoichiometric scalar dissipation rate parameter $\chi_{st}(0 < \chi_{st} < \chi_{st,extinction})$ the flamelet equations are solved in the pre-processing step until the stationary solutions are obtained. The combustion-turbulence interaction is accomplished via the presumed beta probability density function (beta PDF) as:

$$\widetilde{Y}_i = \int_0^1 Y_i(Z, \chi_{st}) P(Z) dZ \tag{138}$$

$$\widetilde{T} = \int_0^1 T(Z, \chi_{st}) P(Z) dZ \tag{139}$$

where $\widetilde{Y}_i$ is a time-mean mass fraction of the species i, and $\widetilde{T}$ is time-mean temperature. Consequently, combustion modelling for non-premixed flames can be based on the mixture formation models, for example the steady laminar flamelet model, where stationary flamelet profiles and appropriate Probability Density Function (PDF) tables were created in the pre-processor step. A detailed chemical reaction mechanism is used for fuel oxidation, while turbulence fluctuations are taken into account by using presumed PDF. These PDF tables with the mean values of the chemical quantities can then be used in as many subsequent CFD calculations as necessary. The main advantage of this modelling approach is the reduction of transport equations, related only to the mixture fraction and its variance, that are solved in the standard CFD procedure. The CFD code then looks up the pre-processed values that are derived from the predicted mixture fraction fields and uses them to modify the cell values throughout the entire calculation domain.

5.2 NO$_x$ Modelling

Nitrogen oxides (NO$_x$) are among the main pollutants in the atmosphere. A significant amount of NO$_x$ emissions is attributable primarily to human activities, in particular the combustion of fossil fuels. Motor vehicles, electric power plants, and other industrial, commercial, and residential sources that burn fuels account for most of the nitrogen pollutant emissions. Nitrogen oxides emitted from these combustion systems are a major environmental problem since they contribute to photochemical smog, acid rain,

corrosion problems, global warming and depletion of the stratospheric ozone. As the awareness of these harmful effects has risen, emissions of NO_x have become subject to increasingly stringent regulations in order to protect human health, air quality and vegetation. These regulations have driven and continue to drive the development of various combustion techniques used to reduce NO_x emissions from combustion systems. In response to these regulations, understanding the NO_x reaction processes in combustion systems continues to be a major challenge for R&D.

Dramatic improvements in computer hardware performance and advance in the science of NO_x chemical reaction mechanisms have made modelling of NO_x formation a valuable tool that can be used to investigate and improve understanding of the NO_x formation in practical combustion systems [41][48]. Hundreds of elementary reactions are involved in a detailed description of the formation and destruction of oxides of nitrogen in combustion systems. However, it is not currently feasible to use such detailed reaction mechanisms to model a turbulent reacting system in which large reaction kinetics schemes are coupled with turbulent fluid dynamics [48]. Consequently, the modelling work in this thesis is based on a reduced chemical reaction mechanism which is used in the CFD code FIRE to describe the NO_x reaction process in the combustion of gaseous and liquid hydrocarbon fuels. Two chemical reaction mechanisms, thermal and prompt, are incorporated in the model in order to predict NO_x formation in the combustion systems. Each of these mechanisms is described subsequently in the following section. This modelling work has involved an approach that couples a simplified description of the NO_x reaction process with a detailed description of the combustion and flow process. A joint solution of a detailed CFD equation for turbulent flow, combined with a NO_x reduced chemical reaction mechanism. is required for this approach, and is referred to in this thesis as comprehensive NO_x modelling.

5.2.1 Environmental Impact of NO_x

The combustion of fossil fuels used to meet the society's demands for energy release large quantities of pollutants into the environment. Among these pollutants are the nitrogen oxides (NO_x), which are considered important pollutants in the air because

they can cause environmental problems and can be harmful to human health. The negative influence to the environment and human health is caused by the contribution to a photochemical smog, acid rain, corrosion problems, global warming and the destruction of ozone in the stratosphere.

Photochemical smog is a type of pollution that occurs in the urban troposphere in metropolitan areas. In the presence of sunshine, NO_x can react with hydrocarbons to make ground-level ozone. The photochemical smog is responsible for reduced visibility in urban areas and can cause serious respiratory problems and eye irritation for humans, and can also damage vegetation. Ground-level ozone inhibits the ability of plants to produce and store food, so that growth, reproduction and plant health are impaired.

NO_x reacts with moisture in the atmosphere to form acid rain. Once emitted into air, nitrogen oxides form nitrates, which are the principle components that change the pH of rainwater from neutral to dangerously acidic. The acid in rain, clouds, and fog damages forests and water ecosystems and contributes to the deterioration of buildings, cars and other man-made constructions. Furthermore, nitrogen oxides contribute to the greenhouse effect in the troposphere and emitted NO_x substances at ground level can be transported to the stratosphere, contributing to ozone depletion and leading to enhanced UV irradiation.

The generic designation NO_x refers to the summation of all oxides of nitrogen, namely NO, NO_2, N_2O, N_2O_2, N_2O_3, N_2O_4 and N_2O_5. The family of NO_x compounds and some of their physical properties are listed in Table 5.1.

Table 5.1: Nitrogen oxides

Formula	Name	Properties
NO	nitric oxide	color-less slightly water-soluble gas
NO_2	nitrogen dioxide	redish-brown very water-soluble gas
N_2O	nitrous oxide	colorless water soluble gas
N_2O_2	dinitrogen dioxide	colorless slightly-water soluble gas
N_2O_3	dinitrogen trioxide	black water-soluble solid
N_2O_4	dinitrogen tetroxide	redish-brown very water-soluble gas
N_2O_5	dinitrogen pentoxide	white very water-soluble solid

The most damaging of the hazardous nitrogen compounds formed during combustion are nitrogen monoxide, or nitric oxide (NO), and nitrogen dioxide (NO_2). However, combustion sources emit NO_x mostly in the form of nitric oxide with NO representing 90 to 95 percent of the total NO_x emissions. NO is formed at elevated temperatures while low temperatures favour the formation of NO_2. In the atmosphere a large part of NO is oxidized to NO_2, as the latter is more stable at lower temperatures. Considering that most of the NO_x emitted by combustion sources is NO with only a small fraction appearing as NO_2, and that other nitrogen oxides are emitted in negligible concentrations, the presence and effects of NO_2, N_2O, N_2O_2, N_2O_3, N_2O_4 and N_2O_5 during combustion processes are ignored in this work.

5.2.2 Mechanisms for NO_x Formation in Combustion Systems

As already described in a previous section, as far as air pollution is concerned NO and NO_2 are the most important. It is mainly NO which arises during the combustion process, but it is converted to NO_2 in the atmosphere due to the further oxidation of NO. Consequently, this thesis is focused on the modelling of nitric oxide (NO) formation in combustion processes.

The formation of NO from a specific combustion device is determined by the interaction of chemical and physical processes occurring within the combustion chamber. In practical combustion systems, NO can be formed from two different sources: the molecular nitrogen (N_2) present in the combustion air and the nitrogen bound in a fuel. There are three fundamentally different chemical mechanisms of NO formation: the thermal NO mechanism, the prompt NO mechanism and the fuel NO mechanism. The thermal NO mechanism arises from the thermal dissociation and the subsequent reaction of nitrogen and oxygen molecules in combustion air at relatively high temperatures in a fuel-lean environment. This process is described by a set of chemical reactions known as the extended Zeldovich mechanism. The prompt NO mechanism forms NO from nitrogen much earlier in the flame than the thermal NO mechanism. This mechanism, only significant in fuel-rich regions of flames, involves the intermediate formation of hydrogen cyanide (HCN), followed by the oxidation of HCN to NO. Finally, if the fuel contains organically bound nitrogen, as for example in

the case of heavy oil or coal, then the fuel NO is formed during the combustion process. The nitrogen that is bound into fuel molecules is released in the flame region, and some is oxidized to form fuel NO. Natural gas and most distillate oils have no chemically bound fuel nitrogen and essentially all NO formed from the combustion of these fuels is thermal NO and prompt NO. Therefore, only these two mechanisms are described in more detail in the following sections.

5.2.2.1 Thermal NO Mechanism

The thermal NO mechanism involves a reaction between atmospheric nitrogen and the atomic oxygen produced in the high temperature regions of the flame and the subsequent reactions with the atomic nitrogen. The major factors that influence thermal NO formation are temperature, atomic oxygen, concentrations of nitrogen, and residence time. Of these four factors, temperature is the most important because the dependencies on oxygen concentration and residence time are less pronounced than the temperature dependency. The production of NO is only significant at temperatures exceeding approximately 1550°C due to high activation energy [108][110]. Actually, atmospheric nitrogen has a strong triple bond and is extremely stable. Thus, it can only be decomposed at very high temperatures within the flame. At temperatures lower than 1000°C, the amount of thermal NO formed is reduced, while at temperatures below 760°C NO is either generated in much lower concentrations or not at all.

This process is determined by a set of chemical reactions, which was first described by Zeldovich (1946) as a two-step mechanism:

$$N_2 + O \overset{k_1}{\leftrightarrow} NO + N \tag{140}$$

$$N + O_2 \overset{k_2}{\leftrightarrow} NO + O \tag{141}$$
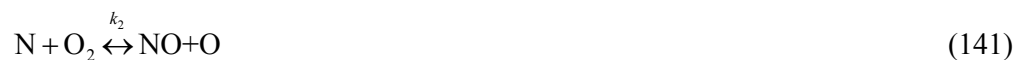
The initial step is the rate determining step in the mechanism, influencing the amount of NO that is formed. In the high temperature flame region and in near-stoichiometric conditions, the oxygen molecules are decomposed into individual oxygen atoms. These atoms react with the nitrogen molecules from the combustion air

to form NO molecules and nitrogen atoms. The rate of the reaction with N_2 is highly dependent on temperature because of the energy required to split the strong triple bond in the N_2 molecule, reflecting the high activation energy of the $O + N_2$ reaction. The first reaction is extremely slow at low combustion temperatures, but increasing the temperature rapidly increases the rate of the reaction. The resultant nitrogen atoms from reaction (1) are unstable and will proceed rapidly to form NO. Since the activation energy for the oxidation of nitrogen atoms is small, the rate of NO formation is controlled by the kinetics of dissociation of the nitrogen molecule.

The original Zeldovich mechanism is extended to more accurately describe thermal NO formation under fuel-rich conditions by including an additional elementary reaction:

$$N + OH \overset{k_3}{\leftrightarrow} NO + H \tag{142}$$
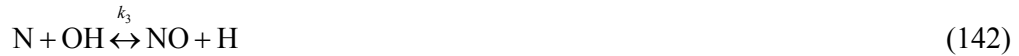
The nitrogen atoms released at reaction (1) are oxidized to nitric oxide mainly by the hydrogen radical at a near-stoichiometric condition and in fuel-rich conditions. This reaction mechanism is known as the extended Zeldovich mechanism, which considers the effect of oxygen and hydrogen radicals on NO formation.

From the extended Zeldovich mechanism a following expression can be derived to approximate the rate of thermal NO formation:

$$\frac{dc_{NO}}{dt} = k_{1f}c_O c_{N_2} + k_{2f}c_N c_{O_2} + k_{3f}c_N c_{OH} - k_{1b}c_{NO}c_N - k_{2b}c_{NO}c_O - k_{3b}c_{NO}c_H \tag{143}$$

The reaction rate coefficients k_{1f}, k_{1b}, k_{2f}, k_{2b}, k_{3f}, k_{3b} for the forward reactions and the corresponding backward reactions can be expressed according to the Arrhenious law:

$$k = AT^{\beta} \exp\left(-\frac{E_{\beta}}{RT}\right) \tag{144}$$

where A is the pre-exponential factor, β indicates the order for the temperature dependence of the pre-exponential factor, E_{β} is the activation energy, T is the temperature, and R is the universal gas constant. There have been indirect and direct measurements of the rate coefficients of these three reactions, this data has been critically evaluated by Blauch and Hanson [41][111].

The overall NO formation rate for these three reactions can be expressed as:

$$\frac{dc_{NO}}{dt} = 2k_{1f}c_Oc_{N_2}\frac{\left(1-\dfrac{k_{1b}k_{2b}c_{NO}^2}{k_{1f}c_{N_2}k_{2f}c_{O_2}}\right)}{\left(1+\dfrac{k_{1b}c_{NO}}{k_{2f}c_{O_2}+k_{3f}c_{OH}}\right)} \tag{145}$$

where the values k_{1f}, k_{1b}, k_{2f}, k_{2b}, k_{3f}, k_{3b} are determined by experiments [111]:

Since the thermal NO mechanism involves O and OH radicals, it is necessary to couple the thermal NO reactions to the fuel oxidation reactions. However, compared to the fuel oxidation reactions, the overall rate of NO formation by the thermal mechanism is slow, and it can be assumed that thermal formation reactions can be decoupled from the fuel oxidation mechanism [41]. In this situation, the equilibrium values of temperature and concentrations of O_2, N_2, O and OH are assumed. Using this approach, oxygen atoms are assumed to be in equilibrium with O_2 [48]:

$$c_O = k_{eq}c_{O_2}^{0.5} \tag{146}$$

An improvement to this method can be made by other methods to estimate O and OH concentration. The value for O and OH can be obtained using the partial equilibrium assumption or using O and OH radical concentration when they are accurately predicted using and advance chemistry model [48].

In the partial equilibrium assumption, the concentration of O and OH can be expressed [99]:

$$c_O = 36.64\,T^{0.5}c_{O_2}^{0.5}\exp\left(\frac{-27123}{T}\right) \tag{147}$$

$$c_{OH} = 2.129\times10^2\,T^{-0.57}\exp\left(-\frac{4595}{T}\right)c_O^{0.5}c_{H_2O}^{0.5} \tag{148}$$

The NO source term resulting from thermal NO mechanism can be written as:

$$S_{\text{NO},t} = M_{\text{NO}} 2k_{1f} c_{\text{O}} c_{\text{N}_2} \frac{\left(1 - \dfrac{k_{1b} k_{2b} c_{\text{NO}}^2}{k_{1f} c_{\text{N}_2} k_{2f} c_{\text{O}_2}}\right)}{\left(1 + \dfrac{k_{1b} c_{\text{NO}}}{k_{2f} c_{\text{O}_2} + k_{3f} c_{\text{OH}}}\right)} \tag{149}$$

where M_{NO} is the molecular weight of nitric oxide.

5.2.2.2 Prompt NO Mechanism

Prompt NO is observed by many authors. It was first identified by Fenimore (1971) that the rate of NO generated during the combustion of hydrocarbon substances is considerably higher than that predicted by the Zeldovich mechanism. This enhanced NO formation is attributed to the presence of hydrocarbon species, which result from fuel fragmentation during the combustion process. Prompt NO is formed by the reaction of atmospheric nitrogen with hydrocarbon fragments, which is subsequently oxidized to form NO. The prompt NO mechanism forms NO from nitrogen in the flame much earlier than the thermal NO mechanism, as its name suggests.

A number of hydrocarbon radicals are responsible for prompt NO, but CH and CH_2 are suggested as the major contributors [41][48]. The following reactions are the most likely initiating steps for prompt NO:

$$\text{Fuel} \rightarrow \text{CH}, \text{CH}_2 ... \tag{150}$$

$$\text{CH} + \text{N}_2 \leftrightarrow \text{HCN} + \text{N} \tag{151}$$

$$\text{CH}_2 + \text{N}_2 \leftrightarrow \text{HCN} + \text{NH} \tag{152}$$

The model used in the present study to predict prompt NO concentration was an overall approximate prompt reaction, proposed by De Soete [112]. A global kinetics mechanism was used to predict the rate of prompt NO:

$$\frac{dc_{\text{NO}}}{dt} = kf c_{\text{O}_2}^b c_{\text{N}_2} c_{fuel} \exp\left(-\frac{E}{RT}\right) \tag{153}$$

where c denotes the concentration, k is the pre-exponential factor, f is the correction factor, b is the order of reaction for molecular oxygen and E is the activation energy. Values k and E are experimental constants [113].

Bachmaier et al. [114] experimentally determined the prompt NO levels as a function of the equivalence ratio for different fuel types in laminar premixed flames, including methane, ethane, ethylene, acetylene, propane, n-butane, n-hexane, iso-octane etc. The predicted results indicated that the model performance declined significantly under fuel-rich conditions and for higher hydrocarbon fuels. In order to minimize this error and predict the prompt NO adequately in all conditions, the De Soete model was modified using the available experimental data by correction factor f, which takes into account both the type of fuel and air/fuel ratio effects [99]:

$$f = 4.75 + A_1 n - B_2 \phi + B_3 \phi^2 - B_4 \phi^3 \tag{154}$$

where n is a number of carbon atoms in the fuel and Φ is the equivalence ratio. A_1, B_2, B_3 and B_4 take the values 0.082, 23.2, 32, 12.2, respectively. An empirical function $f(\Phi)$ is determined using measurement data and assumes negligible prompt NO formation at an equivalence ratio below 0.6 and above 1.6.

Oxygen reaction b order depends on flame conditions. According to De Soete [112], oxygen reaction order is uniquely related to the oxygen mole fraction in the flame:

$$
\begin{aligned}
X_{O_2} &\leq 4.1 \times 10^{-3} \rightarrow b = 1.0 \\
4.1 \times 10^{-3} &\leq X_{O_2} \leq 1.11 \times 10^{-2} \rightarrow b = -3.95 - 0.9 \ln X_{O_2} \\
1.11 \times 10^{-2} &< X_{O_2} < 0.03 \rightarrow b = -0.35 - 0.1 \ln X_{O_2} \\
X_{O_2} &\geq 0.03 \rightarrow b = 0
\end{aligned}
\tag{155}
$$

The NO source term resulting from prompt NO mechanism can be written as:

$$S_{NO,pr} = M_{NO} k f c_{O_2}^b c_{N_2} c_{fuel} \exp\left(-\frac{E}{RT}\right) \tag{156}$$

5.2.3 Chemistry-Turbulence Interaction

The combustion process typically occurs in a turbulent environment, which requires special consideration when predicting NO concentrations. There is a difference between the NO profiles predicted using the mean temperature and densities, and those predicted by the temperature and density fluctuations caused by turbulence [48]. Therefore, incorporating the effects of the turbulent fluctuations on the presented NO pollutant reaction process is important. Time-mean reaction rates of NO cannot be calculated from the time-mean value of temperature because the relationship among NO kinetic rates and temperatures are highly nonlinear. The presumed probability density function (PDF) approach is used to account for the effects of turbulent fluctuations on the kinetic rates of NO, integrating the kinetic rates with respect to the fluctuating temperature:

$$\overline{S}_{NO} = \int_0^1 P(T) S_{NO}(T) dT \tag{157}$$

where $P(T)$ is the probability density function of the normalized temperature T, and S_{NO} is the instantaneous NO source. The probability density function is completed defined by the mean value and variance of temperature.

The PDF is assumed to be a two-moment beta function, which is suitable for the combustion calculations. The beta probability density function for a given value T, and a given pair of values α and β is:

$$P(T) = \frac{1}{B(\alpha, \beta)} T^{\alpha-1} (1-T)^{\beta-1} \tag{158}$$

where $B(\alpha, \beta)$ is beta function.

Equation (152) computes the probability density $P(T)$ at T for a beta distribution with parameters α and β. The parameters in α and β must all be positive, and the value T must lie on the interval [0, 1]. Thus, this variable T must be normalized.

The beta function is defined as:

$$B(\alpha, \beta) = \int_0^1 T^{\alpha-1} (1-T)^{\beta-1} dT \tag{159}$$

where beta function can be also defined in terms of gamma function:

$$B(\alpha,\beta) = \frac{\Gamma(\alpha)\Gamma(\beta)}{\Gamma(\alpha+\beta)} \tag{160}$$

The gamma function of some variable z is defined by the integral:

$$\Gamma(z) = \int_0^\infty e^{-t} t^{z-1} dT \tag{161}$$

Parameters α and β depend on the mean value of the temperature from the main combustion calculation and its variance $\widetilde{T''^2}$:

$$\alpha = \tilde{T}\left[\frac{\tilde{T}\left(1-\tilde{T}\right)}{\widetilde{T''^2}} - 1 \right] \tag{162}$$

$$\beta = \left(1-\tilde{T}\right)\left[\frac{\tilde{T}\left(1-\tilde{T}\right)}{\widetilde{T''^2}} - 1 \right] \tag{163}$$

Parameters α and β must always be positive; $\alpha,\ \beta\ >\ 0$. Therefore $\overline{T}\ >\ 0$. The requirement $\alpha > 0$ shows that $\widetilde{T''^2}\ <\ \overline{T}\left(1-\overline{T}\right)$. This requirement is the upper limit of the temperature variance $\widetilde{T''^2}$. The lower limit of the temperature variance must be that $\widetilde{T''^2}\ > 0.002$, enabling calculation of gamma function.

The temperature variance $\widetilde{T''^2}$ can be calculated by solving a transport equation during the combustion calculation stage, or after the main combustion calculation has been completed.

$$\frac{\partial}{\partial t}\left(\overline{\rho}\widetilde{T''^2}\right) + \frac{\partial}{\partial x_i}\left(\overline{\rho}\tilde{u}_i\widetilde{T''^2}\right) = \frac{\partial}{\partial x_i}\left(\overline{\rho}\frac{v_t}{\sigma_t}\frac{\partial \widetilde{T''^2}}{\partial x_i}\right) + 2\overline{\rho}\frac{v_t}{\sigma_t}\left(\frac{\partial \tilde{T}}{\partial x_i}\right)^2 - 2\overline{\rho}\frac{\tilde{\varepsilon}}{\tilde{k}}\widetilde{T''^2} \tag{164}$$

where the constants σ_t, C_g i C_d have the values σ_t=0.85, C_g=2.86 i C_d=2.0.

Equation (157) must be integrated at every node and at every iteration. The number of points of the beta function integral is specified by the user. A larger number of points yields a more accurate calculation of the PDF function, but takes longer to compute.

5.2.4 Solution Approach

The formation of NO in the combustion processes is characterized by using the following transport equation for the NO mass fraction:

$$\frac{\partial(\overline{\rho}\tilde{Y}_{NO})}{\partial t} + \frac{\partial(\tilde{u}_i\overline{\rho}\tilde{Y}_{NO})}{\partial x_i} = \frac{\partial}{\partial x_i}\left(\overline{\rho}D_t\frac{\partial \tilde{Y}_{NO}}{\partial x_i}\right) + \overline{S}_{NO} \tag{165}$$

where $\tilde{Y}_{NO}$ is the mean mass fraction of NO, and $\overline{S}_{NO}$ is the mean turbulent source of nitric oxide by different mechanisms.

6 Numerical Simulations and Results

6.1 Eulerian Multiphase Spray Simulation

As stated in the introduction, one objective of this thesis has been the application, optimisation and validation of the Eulerian multiphase spray modelling concept for spray in the dense spray region. This section illustrates the capabilities of the verified and validated Eulerian multiphase approach for modelling and numerical simulation of high pressure-high temperature spray, which can be further applied for to a coupled simulation with the existing classic Lagrangian DDM spray modelling approach.

Validation of the Eulerian multiphase spray model against the experimental data represents one of the basic requirements for the accurate prediction of spray flows due to the complex nature of these physical processes. Therefore, it is necessary to carefully perform the spray model verification and validation, which can be used for further improvement and development of the physical spray models. Several simulations of high pressure diesel injections, combined with different chamber pressures, using an approach with fixed droplet size classes, were carried out and compared with experimental data.

6.1.1 Experimental Configuration

Experimental measurements of spray development were made in the high temperature-high pressure injection chamber in order to have a similar injection temperature and similar pressure conditions as are found in a in realistic engine. Under such conditions, the spray characterization was aimed to produce reference data for CFD spray model validation. The diesel fuel was injected into the high pressure chamber by the 1- hole nozzle with an orifice diameter of 205 μm, and into an N_2 environment. The flow within the nozzle is controlled through the fast opening and closing of the needle valve and shaped by the nozzle itself. The jet flow exits the nozzle in the form of a high-speed jet in the high temperature-high pressure chamber and starts to break-up into conical spray. The injection rates were measured for the values of injection pressures 50, 80, and 120

MPa as shown in Figure 6.1. The chamber was filled with N_2 and the initial conditions were 5.4 MPa or 7.2 MPa at a temperature of 900K.
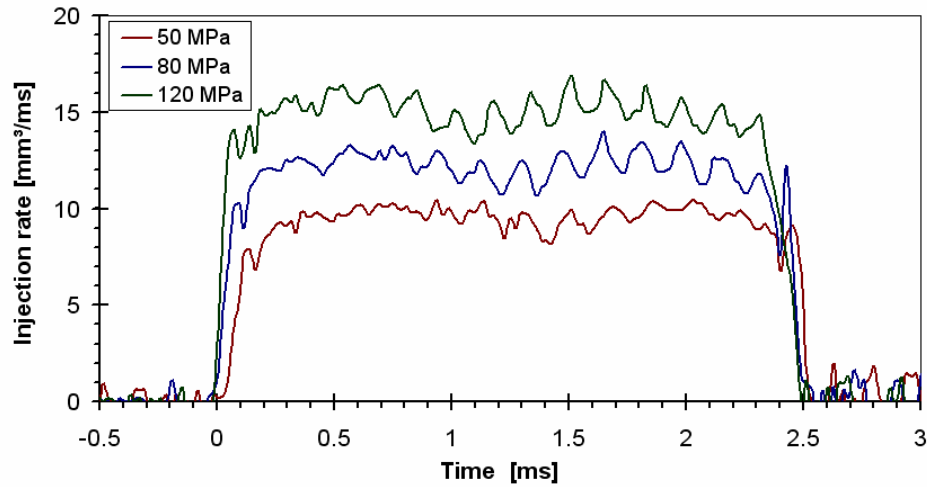
Figure 6.1: Injection rates for different injection pressures

The spray tip penetration behaviour was measured for the combination of the rail pressure with the ambient pressures. The penetration of the liquid phase and the vapour phase of the spray were visualised with an optical set-up for combined Schlierean and Mie- scattering filming of the spray. The strong influence of injection pressure on the penetration of the vapour phase for chamber pressure of 7.2MPa is shown in Figure 6.2. In contrast, the influence of injection pressure on liquid penetration is much smaller.

The measurements obtained with the variation of different injection pressures with a strong impact on the penetration of the vapour phase were chosen and compared with simulation results in this work in order to find appropriate correlations and coefficients, for the purpose of forming a suitable model and gaining confidence in the Eulerian model spray predictions.
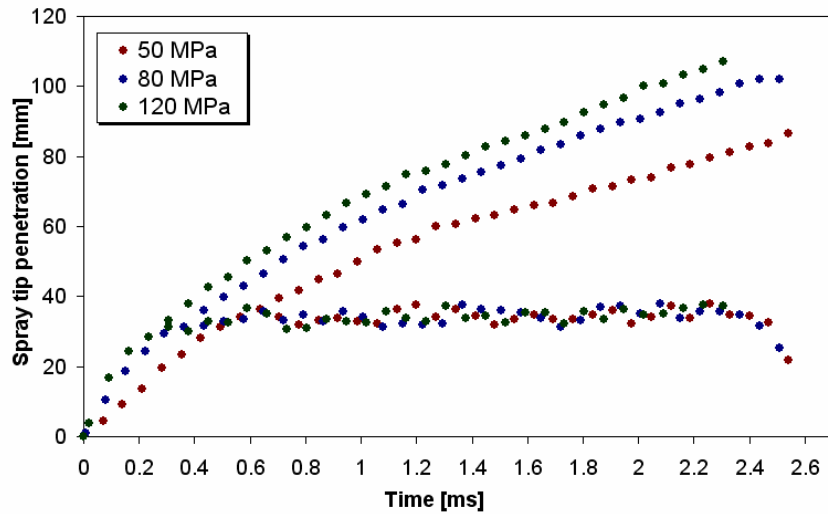
Figure 6.2: Measured liquid and vapour penetration at 7.2 MPa for injected pressure of 50, 80 an 120 MPa

6.1.2 Numerical Simulation

All numerical simulations performed in this section were based on the Eulerian multiphase spray approach. Eulerian multiphase spray modelling treats all phases, gas and liquids, as interpenetrating multi-fluids represented by their volume fractions. Volume fraction is a key quantity in this approach, which represents that each control volume is occupied by phases, where each occupies a certain volume fraction of the control volume. The gas phase was treated as the primary phase, while the spray droplets were treated as the secondary phases. The droplets were classified into different size classes by volume fractions and diameters. The phase specification of the model is given in Table 6.1. The first phase was the primary gaseous phase, gas mixture, which was composed of two species, namely gas and vapor, in addition to the mass fraction equation of the fuel vapour in the gaseous phase. Hence, the vapor mass fraction was transported by a separate scalar transport equation within the gaseous phase. The phases from 2 to N-1 are the droplet phases where a constant droplet class diameter was assigned to each of the phases. The droplet phases were sorted in an ascending manner where phase *2* is the phase with the smallest droplet diameter, while phase N-1 presents the phase with the largest droplet diameter. The last phase, N, is the

87

bulk liquid phase from the nozzle, which disintegrates into various droplet phases due to the break-up process.

Table 6.1: The phase specification of the Eulerian multiphase spray model

Phase	1	2, …, *N*-1	*N*
Content	Gas mixture	Droplets	Bulk liquid

A separate set of complete conservation equations, with some additional source terms accounting for the droplet dynamics, was solved for each phase with the same discretization, and similar numerical techniques for the gas and liquid phases. The interactions between the phases were calculated using empirical closure relations by interfacial exchange terms. The interfacial mass exchange between the gaseous phase and the liquid phases includes droplet evaporation, primary break-up and secondary break-up, while the interfacial momentum exchange includes drag forces and turbulent dispersion forces. The interfacial heat exchange between the gaseous phase and the droplet phases was determined by the evaporation of droplets as stated in the model description. The interfacial exchange terms in turbulence kinetic energy and turbulence energy dissipation balance equations were ignored, while both equations were solved for gas and droplet phases.

In the case of high-pressure injection conditions, the mass transfer within the spray region starts directly at the nozzle exit where the liquid jet is disintegrated first into ligaments and then large droplets. This was calculated by the primary break-up model by the diameter change rates where the bulk liquid phase, *N,* is disintegrated into the liquid droplet phases 2 to *N*-1. The model uses the turbulent length scale to determine the atomization length scale, and also uses the turbulent and aerodynamic time scale to determine the break-up scale, as addressed in section 4.4.1. The droplets produced from the primary break-up process further break-up into smaller droplets due to aerodynamic forces acting on the droplet, which is induced by relative velocity between the droplets and ambient gas. In the break up of droplets, secondary break up, every droplet phase may disintegrate into droplets with smaller size class diameter. The diameter change rate of the blob, due to secondary break-up, was modelled with the appropriate model for a very high speed injection, the standard WAVE model, as described in section

4.4.2. In addition, the contribution from the droplet evaporation, between phases from 2 to N and the gaseous phase $1,$ was incorporated in the interfacial mass exchange. The droplet evaporation was determined by summing evaporation behaviour of the single, isolated droplet dynamics inserted into hot gas flow, as described in section 4.4.3.

The momentum exchange between the gaseous phase 1 and liquid phases k (2 to N) was determined by drag forces acting at the inter-phase on the droplets, induced by the droplet movement relative to the ambient gas phase. In addition, the turbulent dispersion forces caused by the fluctuations in the continuous phase determine as well the momentum exchange. For details see section 4.4.4.

6.1.2.1 Boundary Conditions and Simulations Parameters

Numerical simulations of the spray processes have been based on the Eulerian multiphase model implemented in AVL's CFD code FIRE as described in a previous section. Five operating points of high pressure diesel sprays have been used for the simulation cases.

The simulation domain with relevant boundary conditions is shown in Figure 6.3. A two dimensional computational mesh with 1400 cells, extending from 0 to 120 mm in axial direction and from 0 to 25 mm in radial direction with applied axial symmetry in tangential direction, was used for the simulations. The mesh is refined towards the spray inlet and symmetry axis, as shown in Figure 6.3.
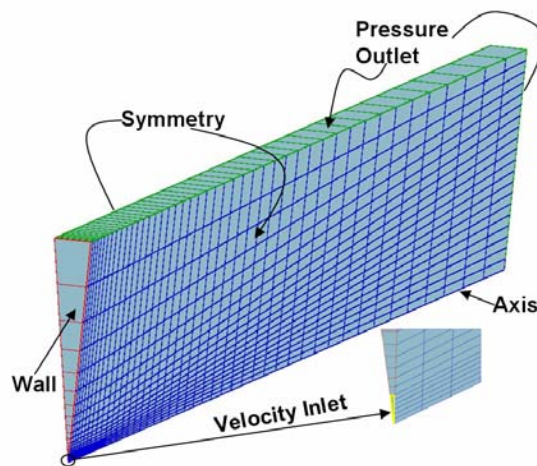
Figure 6.3: Computational mesh with boundary conditions

The inlet boundary condition was defined as inlet face selection with a diameter of liquid inlet orifice of 205 μm, as illustrated in Figure 6.3. The inlet velocities were imposed according to experimental data from injection rates, which were simplified into a normal velocity for each simulation case in order to eliminate the fluctuations of the measurements, as shown in Figures 6.4 - 6.6. A wall boundary condition was defined near the inlet, and symmetry boundary conditions were applied on either side of the faces. Static pressure outlet were imposed at downstream boundary faces. The chamber pressure and temperature were set according to the experimental data. The diesel fuel with 373 K was used for simulation cases.
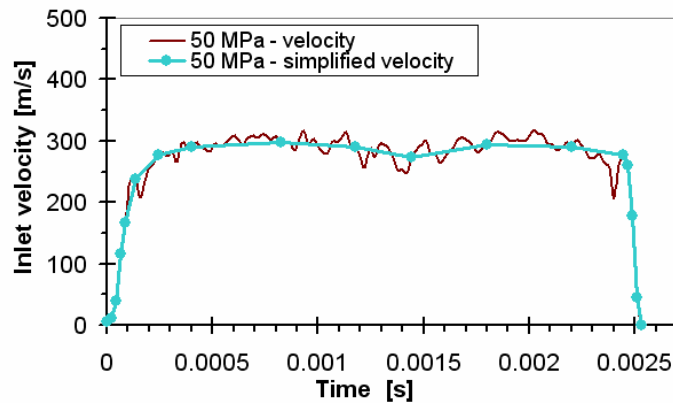
Figure 6.4: Inlet velocity profiles at 50 MPa rail pressure
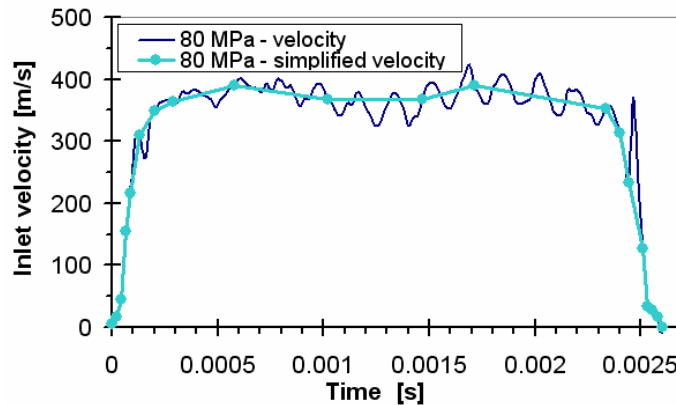
Figure 6.5: Inlet velocity profiles at 80 MPa rail pressure
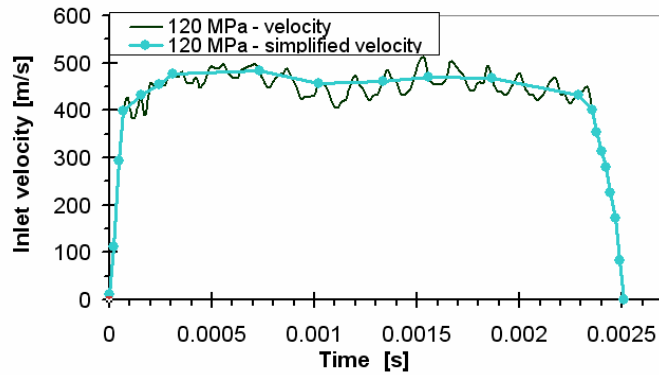
Figure 6.6: Inlet velocity profiles at 120 MPa rail pressure

Six phases in total were used, one gaseous phase, four droplet phases and one bulk liquid phase. The size class diameters for the droplet phases are 5, 10, 20 and 40 μm, and a nozzle diameter of 205 μm was assigned to the bulk liquid phase. Pressure velocity coupling of momentum and continuity equation was obtained using the SIMPLE algorithm. The central difference discretization scheme was used for the convective term in the continuity equation, while a hybrid between the central differences and the upwind scheme with a blending factor of 0.5 was used for the convective terms in the momentum equations. The time discretization used for simulation is given in Table 6.2. Different time-steps were used since the high-pressure injection of the fuel is highly transient and too large time-steps can cause an unstable calculation, owing to the fact that the gradients in mass exchange models can be very high. Therefore, at the beginning of the calculations the time-steps were very small, but they were continuously increased throughout the injection time, as shown in Table 2.

Table 6.2: Time discretization

Upto	Time [s]	Δt
upto	**1.0e-06**	**2.5e-08**
upto	**1.0e-04**	**2.5e-07**
upto	**0.0026**	**5.0e-07**

As part of the validation process of the Eulerian multiphase spray model, it has been considered important to asses the sensitivity of the predictions on different model coefficients. Therefore, variation of sub-model spray coefficients for primary break-up,

secondary break-up, droplet evaporation, turbulent dispersion forces and drag forces were performed and the impact on spray and vapor penetration was investigated. As a result of the comparison between the simulation predictions and experimental data, a final set of sub-model coefficients that is relatively more accurate for most simulation cases investigated was found. This final set of sub-model coefficients is referred to here as "standard" settings and was used in the results presented in the next section. It is possible that other values of sub-model coefficients may give better results for a specific case, but not for the all numerical simulations investigated here.

6.1.3 Results

One of the main liquid spray characteristics commonly used to describe spray dynamics is spray tip penetration. Characteristics such as liquid penetration and vapor penetration may be used to predict the rate at which the mixing proceeds. Therefore, the following numerical simulations, based on the Eulerian multiphase model, were validated against experimental data in terms of the fuel liquid and the fuel vapor tip penetration. The numerical simulations of high pressure diesel fuel injections were carried out for two chamber pressures, 5.4 MPa and 7.2 MPa, with varied injection pressure of diesel fuel.

Figure 6.7 shows the comparisons of calculated and measured penetration curves of fuel liquid and fuel vapor tip penetration at 50 MPa rail pressure and 7.2 MPa chamber pressure.
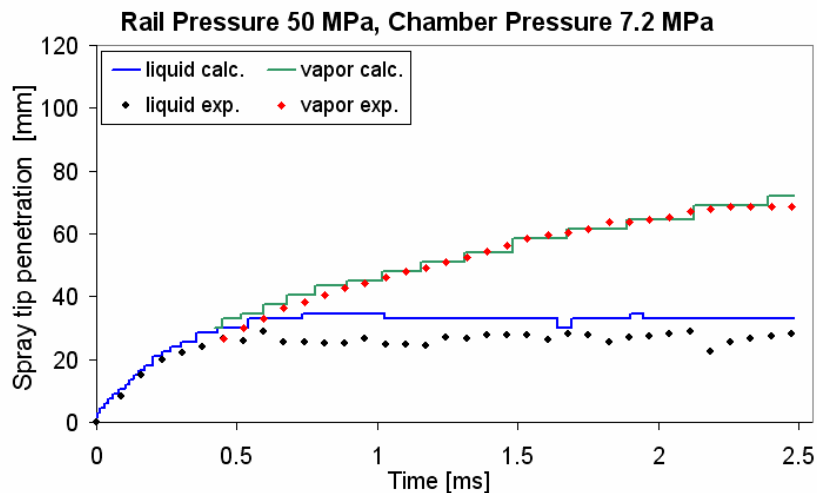
Figure 6.7: Comparison of the calculated and measured liquid and vapor penetration at 50 MPa rail pressure and 7.2 MPa chamber pressure

It can been seen that the predicted liquid penetration is in fairly good agreement with the measurements, indicating that the number of liquid phases and sub-models accounting for the appropriate physics of spray were chosen correctly. This is evidence of the model's ability to predict spray penetration with droplet size distribution discertised into only 5 size classes. However, higher numbers of liquid phases mean better spray resolution, but computational effort is significantly influenced. The penetration of the vapor over time is plotted in Figure 6.7 for an injection of diesel fuel into the high pressure-high temperature chamber. The fuel vapor penetration curve agrees very good with the measurement curve during the entire fuel injection process, indicating that the fuel evaporation of droplets was good predicted.

In this section the structure of the spray, the total liquid volume fraction, which is the sum over all liquid phase volume fractions, and the fuel vapor mass fraction are plotted for only one simulation case. The result analysis was obtained at the 2 ms, after the start of injection at 50 MPa rail pressure and 7.2 MPa chamber pressure, when the spray characteristic reached a developed state.
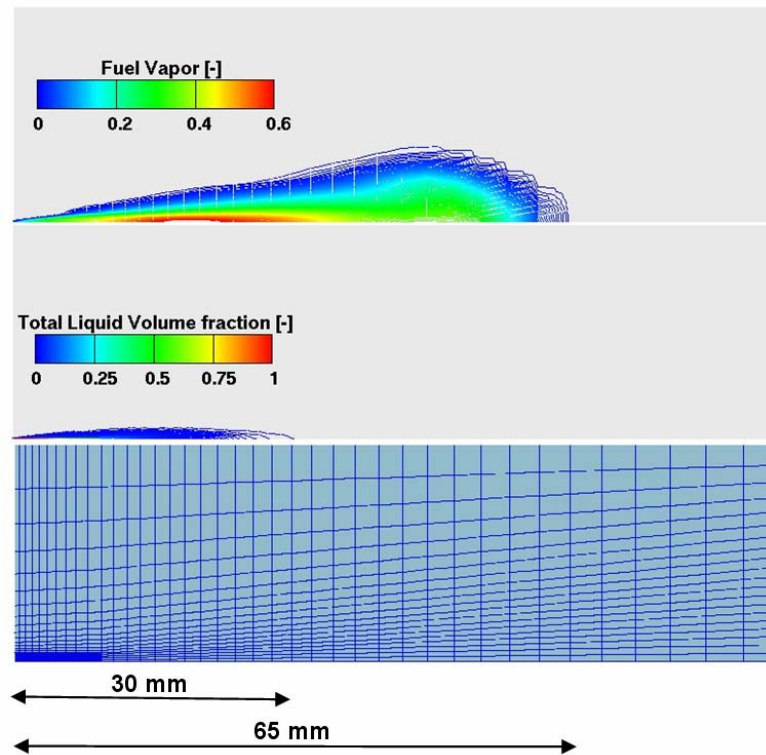
Figure 6.8: Total liquid volume fraction and vapor mass fraction 2 ms after start of injection

93

Figure 6.9 compares the experimental and computational penetration results for the simulation case with 80 MPa rail pressure and 7.2 MPa chamber pressure. The agreement is again reasonably favourable, with a small under-prediction of the fuel vapor penetration. This discrepancy, with respect to fuel vapor penetration, can be explained by the fact that all simulation cases were calculated with the same set of spray sub-model coefficients, as explained in a previous section. However, it is possible that some other values of sub-model coefficients may give more accurate fuel vapor penetration results for this specific case, but not for all the test cases investigated here. It should be reminded that the goal was to validate Eulerian multiphase spray simulations with one final set of spray sub-models coefficients for five sets of experimental data, covering a wide range of high pressure injection conditions.
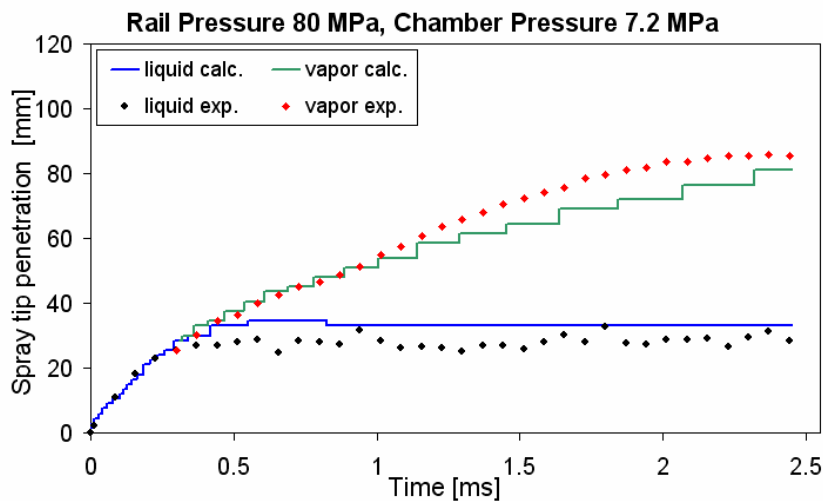
Figure 6.9: Comparison of the calculated and measured liquid and vapor penetration at 80 MPa rail pressure and 7.2 MPa chamber pressure

Figure 6.10 indicates that by increasing rail pressure, the Eulerian spray model was still able to predict liquid and fuel vapor penetration. Moreover, the fuel vapor penetration was more accurately predicted than in previous simulation case and agrees well with the penetration of vapor phase obtained by measurements for a rail pressure of 120 MPa.

94
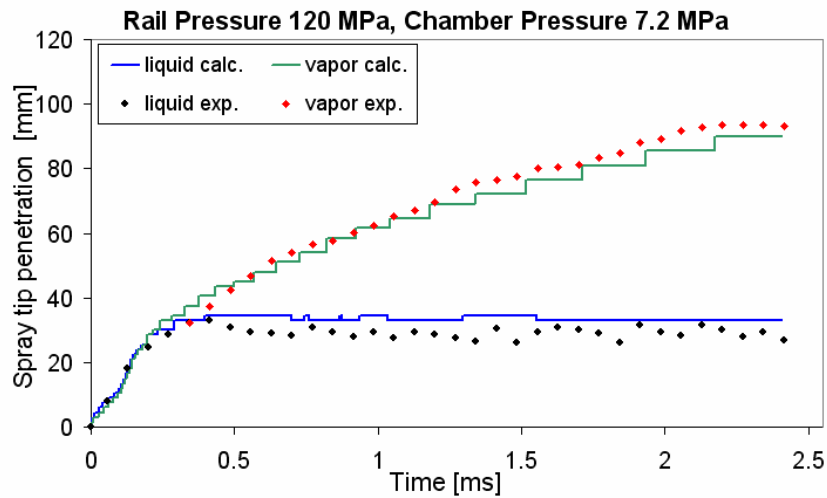
Figure 6.10: Comparison of the calculated and measured liquid and vapor penetration at 120 MPa rail pressure and 7.2 MPa chamber pressure

Figures 6.11 and 6.12 show the comparisons of calculated and measured penetration curves of the fuel liquid and the fuel vapor spray tip for diesel injection pressures of 50 MPa and 80 MPa combined with a chamber pressure of 5.4 MPa. The comparison presented in Figure 6.11 shows again demonstrates exceptional agreement of both penetration curves with experimental data. The penetration of the fuel vapor at 80 MPa rail pressure is under-predicted, while the penetration of fuel liquid matches well with the experimental data, as shown in Figure 6.12.
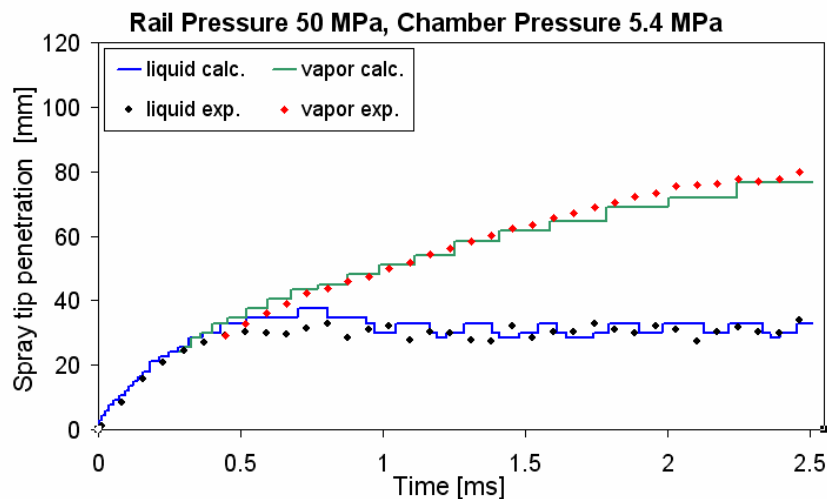
Figure 6.11: Comparison of the calculated and measured liquid and vapor penetration at 50 MPa rail pressure and 5.4 MPa chamber pressure

It should be noted that the turbulence model constant C_2 in the turbulence dissipation rate transport equation was adjusted from the standard value 1.92 to 1.8 in order to improve the predicted rate of spread. This adjustment was done for all simulation cases.
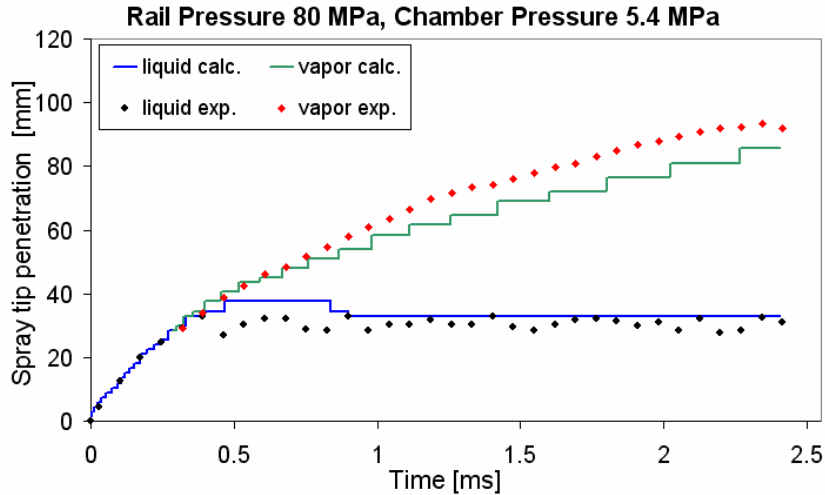
Figure 6.12: Comparison of the calculated and measured liquid and vapor penetration at 80 MPa rail pressure and 5.4 MPa chamber pressure

It should also be noted that the stepwise illustration of the spray tip penetration curves results from post-processing and depends on the mesh resolution in the corresponding region.

Overall, it can be said that the Eulerian multiphase spray model displays adequate liquid and fuel vapor penetration results in comparison with all 5 sets of experimental data, covering a wide range of high pressure injection conditions. The Eulerian multiphase spray model showed the capability to predict the strong impact of rail pressure on penetration of the fuel vapor and of the fuel liquid jet. Furthermore, it has been shown that with one set of the spray sub-model coefficients used in empirical closure relations (for primary break-up, secondary break-up, droplet evaporation, turbulent dispersion forces and drag forces), it is possible to obtain good results for variation of different injection pressures in combination with different chamber pressures. Hence it can be concluded that the Eulerian multiphase spray model with fixed droplet size classes can be applied with confidence for the accurate prediction of characteristics of complex multiphase droplet flows.

6.2 NO$_x$ Simulation

The nitrogen oxide (NO$_x$) model was tested, investigated and validated for the turbulent methane-air jet diffusion flame (Sandia flame D), experimentally investigated by Barlow & Frank [115]. Numerical simulation for the turbulent non-premixed flame was carried out where the formation of nitrogen pollutants was modelled by coupling reduced NO$_x$ chemical reaction mechanisms with the comprehensive combustion model. The model for nitrogen chemistry was integrated into the CFD code FIRE, using FIRE's user-defined functions capability [77]. User functions, written in FORTRAN programming language, were linked with the AVL's FIRE code, providing prediction of NO$_x$ emission in combustion systems on one hand and retaining all the usual FIRE features on the other.

NO$_x$ represents a family of seven compounds: nitric oxide (NO); nitrogen dioxide (NO$_2$); nitrous oxide (N$_2$O); dinitrogen dioxide (N$_2$O$_2$); dinitrogen trioxide (N$_2$O$_3$); dinitrogen tetroxide (N$_2$O$_4$); and dinitrogen pentoxide (N$_2$O$_5$). However, combustion sources emit NO$_x$ most commonly in the form of nitric oxide (NO), as addresses in section 5.2. Thus in this work, the formation of NO determines the total amount of NO$_x$, while the presence and effects of other nitrogen oxides formed during the combustion processes were neglected.

The reduced nitrogen scheme was based on two separate chemical mechanisms, thermal and prompt, respectively. As addressed in section 5.2.2 the thermal NO mechanism produces nitrogen emissions by oxidation of atmospheric nitrogen in the high-temperature post-flame region of the combustion system. Prompt NO is formed in a flame zone when hydrocarbon fragments and atmospheric nitrogen are present by reactions other than the direct oxidation of atmospheric nitrogen via the thermal reaction mechanism. As opposed to the slower thermal NO formation, prompt NO formation is rapid and occurs much earlier in the fuel-rich regions of hydrocarbon flames, as discussed in section 5.2.2.

The effects of turbulent fluctuations on the NO reaction rates were accounted for by integrating the kinetic rates with respect to fluctuating temperatures over the presumed probability density function (PDF), as detailed in section 5.2.3. For combustion prediction a Steady Laminar Flamelet Model (SLFM) was employed.

The prediction of NO_x emissions was decoupled from the generalized combustion model and executed after the flame structure was predicted because the total amount of nitrogen oxides formed in combustion is generally low and does not affect the flame structure. Moreover, the different time-scales of major species and NO_x pollutants allow the decoupling of the two processes. NO_x reactions occur at much slower rates than the main heat release, thus NO_x formation was analyzed separately.

The numerical predictions of the nitrogen pollutant formation obtained by the NO_x model are compared with the results obtained by the Steady Laminar Flamelet Model, and also with the experimental data.

6.2.1 Experimental Configuration

The NO_x model was validated by simulating the Sandia National Laboratories Flame D, a piloted, turbulent, non-premixed methane-air flame for which measurements of nitric oxides concentrations exist. The experimental measurements of Barlow and Frank were obtained for the axial and radial profiles at different locations, which are provided in [115]. The burner configuration is shown in Figure 6.13.
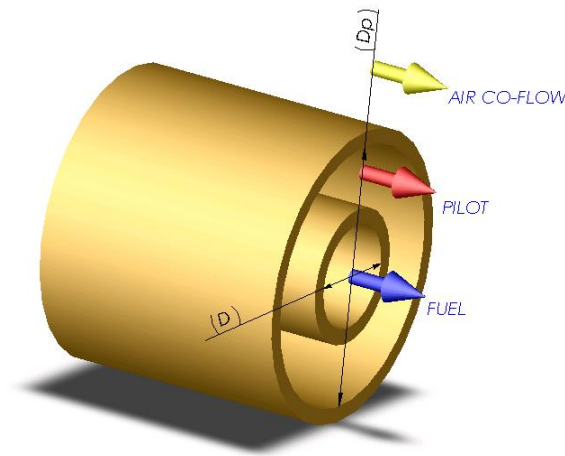
Figure 6.13: Burner configuration

The burner is placed in a co-flow of air and the flame is stabilized by a pilot jet. A stream of fuel is injected through the inner tube, while a pilot stream is injected through

the outer tube surrounding it. The co-flow of air is injected outside of the pilot, as illustrated in Figure 6.13. The burner dimensions are:

- Main jet inner diameter: D = 7.2 mm
- Pilot annulus inner diameter: 7.7 mm (wall thickness = 0.25 mm)
- Pilot annulus outer diameter: Dp = 18.2 mm
- Burner outer wall diameter: 18.9 mm (wall thickness = 0.35 mm)
- Wind tunnel exit: 30 cm by 30 cm

The fuel is a mixture of 25% methane (CH_4) and 75% air by volume. The bulk velocity of the fuel jet is 49.6 m/s and the temperature is 294 K. The annular pilot burns a mixture of C_2H_2, H_2, air, CO_2 and N_2 and has the same equilibrium state as the methane/air mixture at Z=0.27, with temperature 1880 K. The bulk velocity of the pilot is 11.4 m/s. The air co-flow temperature is 291 K, and the velocity is 0.9 m/s.

6.2.2 Numerical Simulation

The 3D steady-state simulations were performed using the AVL's CFD code FIRE, which uses conventional numerical methods, and differencing schemes for completely arbitrary mesh, and can solve large computational meshes which are required for simulating practical combustion devices. The simulation was performed using a computational mesh with 338 400 cells, extending from 0 to 1500 mm in the axial direction and from 0 to 400 mm in the radial direction. The computational mesh is refined towards the inlets and axis as shown in Figure 6.14.
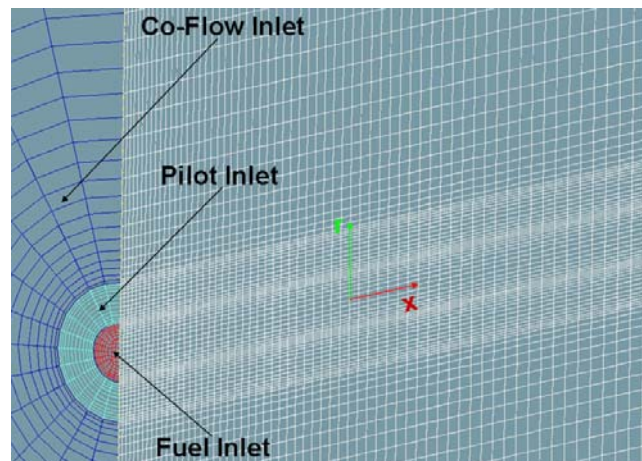
Figure 6.14: Computational mesh and inlet boundary conditions

Appropriate boundary conditions were defined using face selections to the computational mesh as the inlet, outlet and wall boundary conditions. The values of the velocity profiles were applied as the inlet boundary conditions according to the experimental data, as shown in Figure 6.15.

The outlet boundary conditions were assigned as constant ambient pressure conditions for all outlet boundary selections, while the fixed wall boundary conditions, specifying the temperature of the wall ,were assigned as the static wall. The values for other numerical parameters were the default FIRE solver values.
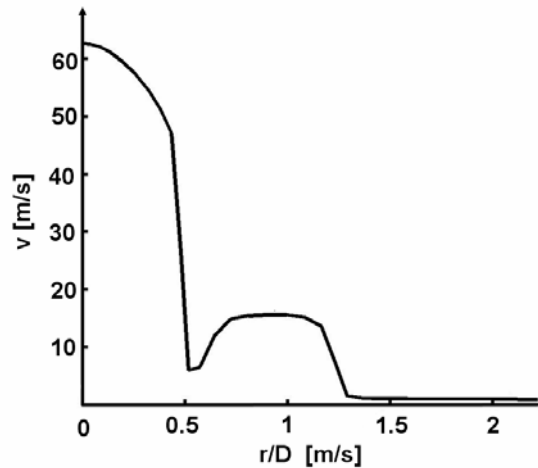
Figure 6.15: Inlet velocity profiles

The methane-air reaction mechanism was taken into account via the SLFM model [106][116]. Stationary flamelet profiles and appropriate Probability Density Function (PDF) tables were created in the pre-processor step by using the CSC solver [104]. A detailed chemical reaction mechanism GRI Mech 3.0 for methane [43], which consists of 53 species and 325 elemental reactions and contains nitrogen chemistry, was used for the calculation of flamelet profiles in the pre-processor step. The radiative heat transfer was calculated using the discrete transfer method, where the radiative properties are modelled as the weighted sum of grey gases.

Turbulent flows were modelled using the standard k-ε turbulence model, which quantifies turbulence in terms of its intensity k and its rate of dissipation ε. The model constant $C_{\varepsilon2}$ in the turbulent kinetic energy dissipation rate transport equation was adjusted to $C_{\varepsilon2}=1.8$ instead of the standard value in order to obtain an accurate spreading rate [117].

The formation of NO was attributed to two chemical kinetic processes, thermal and prompt NO, for the methane/air jet diffusion flame. Because methane does not contain chemically bound nitrogen, fuel NO was not considered in this simulation. Consequently, the NO_x model was used to predict thermal NO formation via the extended Zeldovich mechanism where O and OH concentrations were taken from the combustion code solution and the prompt NO mechanism.

Reduced reaction mechanisms were used in a post-processing mode to model nitrogen chemistry, which has little effect on the flow field and the flame structure. Hence, in the numerical simulation presented in this work, the CFD solver was used in a post-processing step to solve the NO transport equation where a converged combustion flow field solution was first obtained before performing the prediction of the NO formation. Consequently, the quality of the NO formation prediction is highly dependent on the quality of the flame structure prediction.

A 3D steady-state incompressible solution for governing the equation was performed by the iterative procedure to obtain the solution. The CFD simulation convergence was judged upon the residuals of all governing equations. The pressure velocity coupling of the momentum and the continuity equation was obtained by using the SIMPLE algorithm. The central difference discretization scheme was used for all of the diffusion terms and for the convective term in the continuity equation, while a hybrid between the central differences and the upwind scheme with a blending factor of 0.5 was used for the convective terms in the momentum equations. The convective term in the scalar equations was discretized using the first order upwind scheme.

6.2.3 Results

The numerical predictions of the nitrogen pollutant formation for the turbulent non-premixed jet diffusion flame obtained by the NO reduced mechanisms are compared with the results obtained by SLFM, as well as the experimental data.

Figure 6.16 shows the temperature distribution and the NO mass fraction distribution, calculated by the implemented NO_x model in a vertical plane crossing the burner. Higher concentration of the NO mass fraction occurs in the fuel-lean zone of the flame front in the region where the gas temperature is highest, as is expected from the

sensitivity of the nitrogen oxides reaction mechanisms to temperature. It is noticeable that in the furnace the greatest amount of NO is formed by thermal NO.
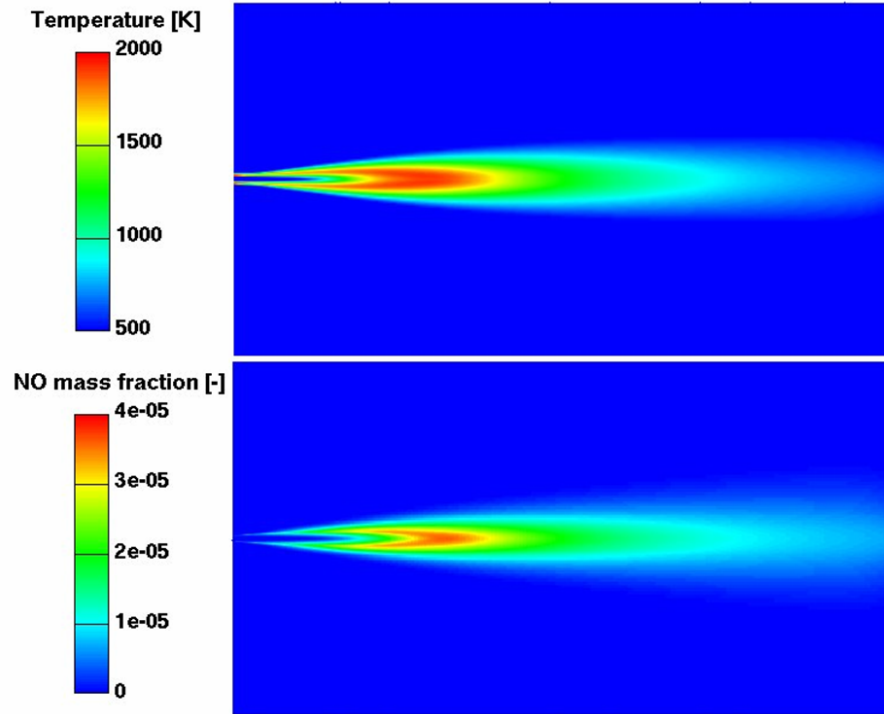
Figure 6.16: Temperature and NO distribution
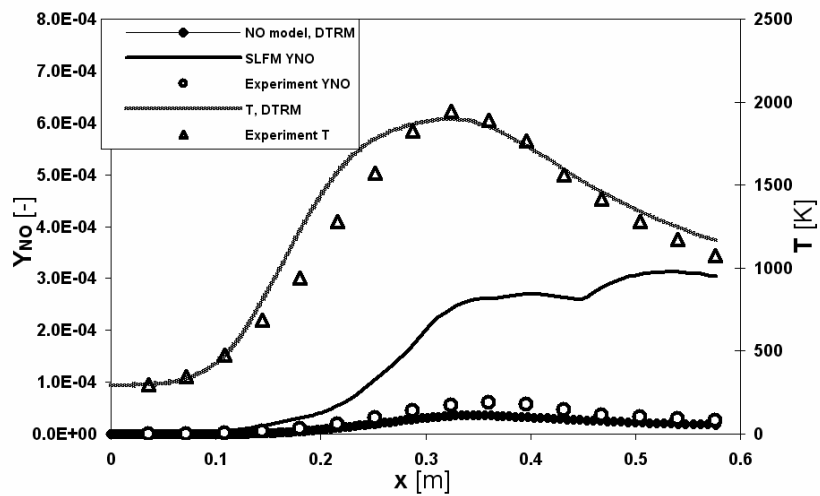
Figure 6.17: Axial profiles of mean temperature and NO mass fraction

Figure 6.17 shows a comparison of the temperature and the NO mass fraction profiles with experimental data along axis symmetry of the burner for the Sandia flame D. The predicted NO mass fraction profile obtained by the NO reduced reaction mechanism is in good agreement with the experimental data, while the NO mass fraction profile calculated by SLFM is over-predicted.
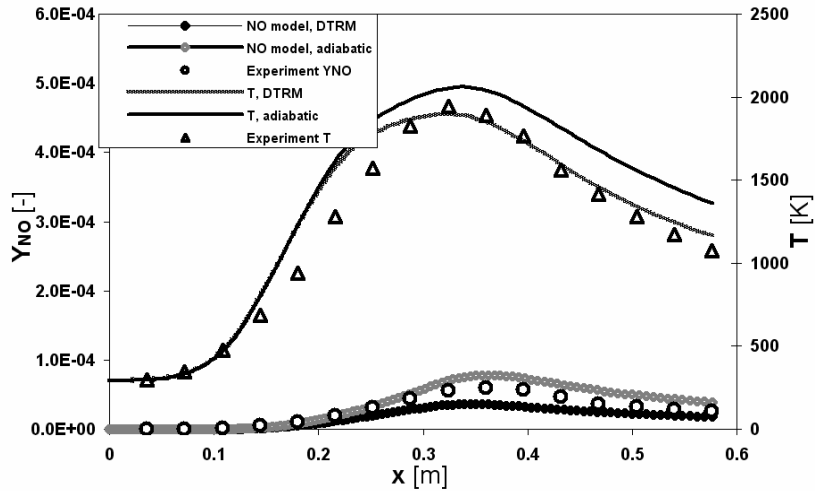
Figure 6.18: Axial profiles of mean temperature and mean NO mass fraction

The mean temperature and the NO mass fraction profiles along the flame axis obtained with and without radiation modelling are shown in Figure 6.18. The adiabatic calculation over-predicts the peak temperature values, while non-adiabatic values (with DTRM) are in better agreement with the experimental data, indicating the importance of radiation modelling for the present flame. A similar behaviour is observed with the NO mass fraction profile where radiation was not included, while in the non-adiabatic case the NO mass fraction profile is slightly under-predicted. The calculated NO mass fraction profiles show similar trends with the calculated temperature profile where the maximum temperature corresponds to the peak of the NO concentration.

The radial profiles of the NO mass fraction at axial location $x/d=15$ are given in Figure 6.19. The agreement between the NO mass fraction profile, predicted by the reduced NO reaction mechanisms, and the measurements, is fairly good, while the NO concentrations predicted by SLFM are more than several times over-predicted.
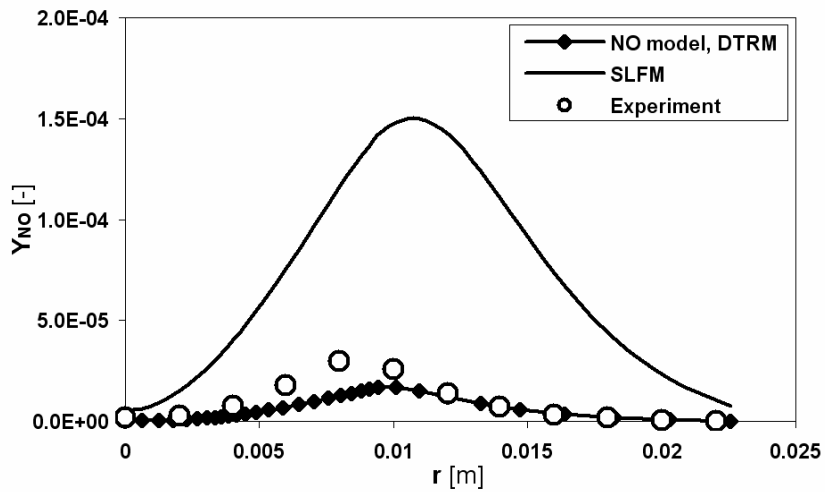
Figure 6.19: Radial profiles of mean NO mass fraction at axial distance x/d=15

The radial profiles of the mean NO mass fraction are shown in Figures 6.20 – 6.23. The predicted NO mass fraction profiles obtained by the NO reduced reaction mechanism again agree fairly well with the experimental data, including the magnitude and radial positions corresponding to peak value. The radial profiles of NO mass fraction obtained by SLFM, as in the axial profile case, are over-predicted.
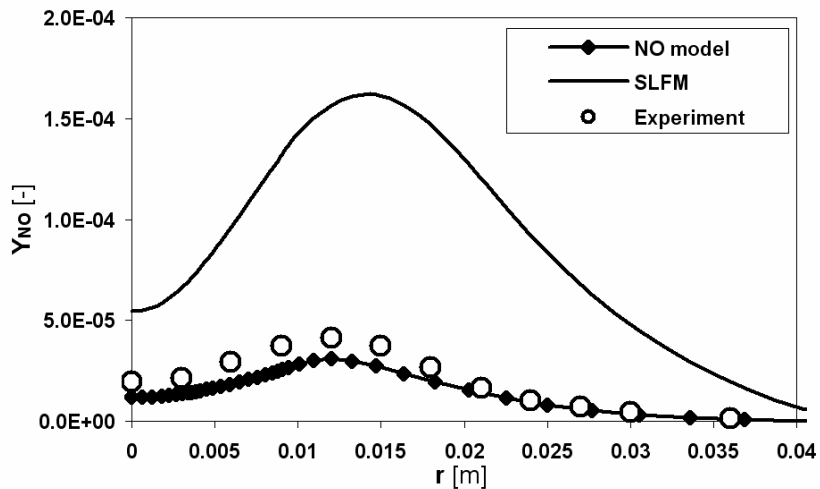
Figure 6.20: Radial profiles of mean NO mass fraction at axial distance x/d=30
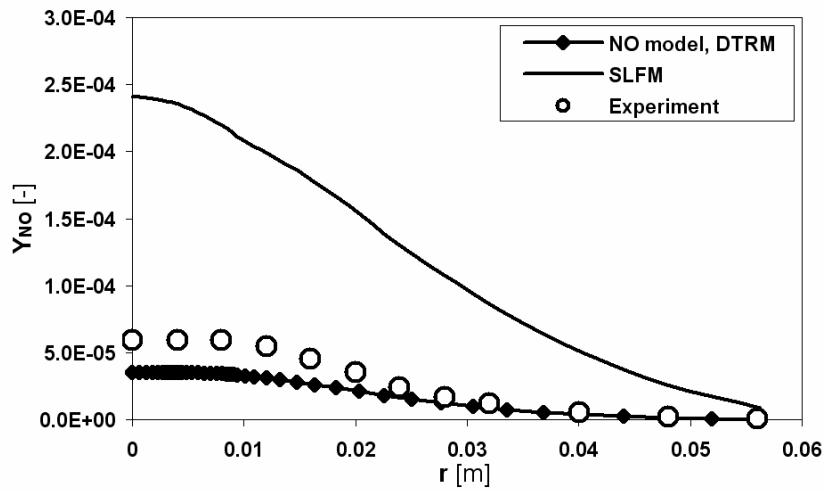
Figure 6.21: Radial profiles of mean NO mass fraction at axial distance x/d=45

It is noticeable that the NO formation calculated by SLFM is clearly over-predicted, making this model inadequate for predicting the important aspects of the flame as NO concentrations. Conversely, the NO predictions, when using the reduced chemical mechanisms for nitrogen chemistry, lead to a significant improvements, displaying nice agreement with the measurements.
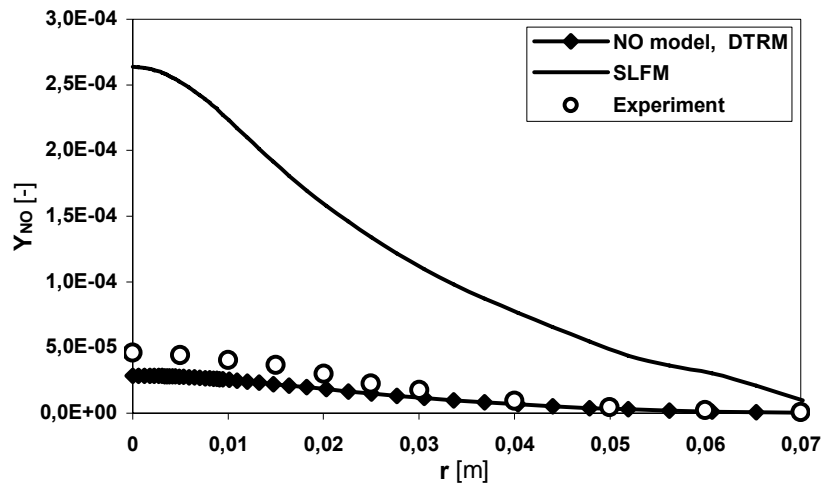
Figure 6.22: Radial profiles of mean NO mass fraction at axial distance x/d=60

The overall agreement between predictions of the NO formation obtained by the reduced mechanisms of nitrogen chemistry and measurements are satisfactory, while

the NO formation calculated with SLFM is quite severely over-predicted. It was also shown in other studies, for example [104], that SLFM over-predicts NO, since SLFM profiles for NO mass fraction exhibit stronger gradients near the equilibrium, while temperature and major species vary "regularly" over the stoichiometric scalar dissipation rate parameters. In this work is shown that the results obtained with implemented NO_x provide a significant improvement over the SLFM nitric oxide results.
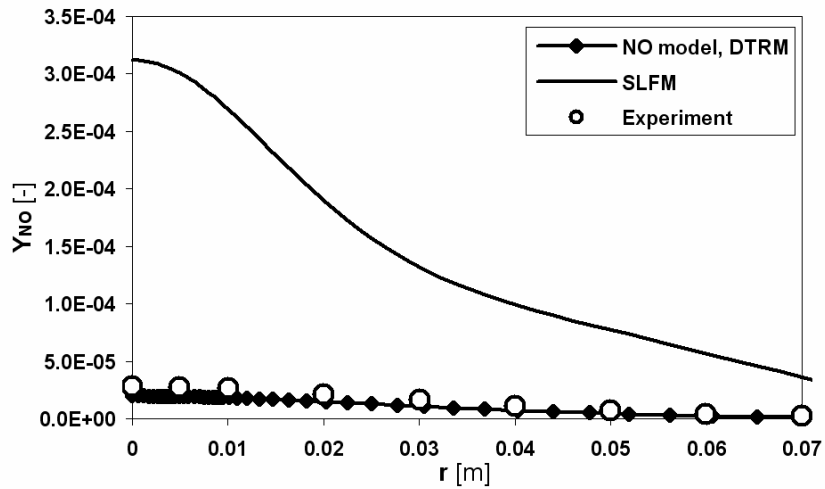
Figure 6.23: Radial profiles of mean NO mass fraction at axial distance x/d=75

The NO_x model presented in this thesis was also successfully applied and tested to a more complex configuration, an oil fired furnace equipped with four burners [118]. In addition, the NO model was also applied and validated for calculation of nitrogen pollutant formation in a high-speed DI diesel engine [119].

6.3 CFD Coupling of Eulerian Multiphase Spray Code with Engine Code

Numerous reliable methods must be used to simulate turbulent multiphase droplet flow in real internal engine configuration: calculation of dense spray flow; calculation of dispersed spray flow; calculation of combustion and emission formation. In this work, only some of these methods have been tested, investigated, and validated such as Eulerian multiphase model and nitrogen emission formation model, as stated in previous sections. All other models, such as the Lagrangian DDM model, combustion model etc., used in this section were selected from standard models within the FIRE code.

This section illustrates the capabilities for solving the more advanced problems in real engine configuration by the coupling concept of the Eulerian multiphase spray model with classic the Lagrangian DDM spray model, in conjunction with combustion and nitrogen emission formation. As stated in section 6.1, the validated Eulerian multiphase spray approach can be used with confidence for numerical simulation of high-pressure high-temperature spray in a dense spray region. This modelling approach provides a better description of the physics in the near nozzle region than the Lagrangian DDM spray approach.

The computational effort for DDM calculation increases drastically in flows near the nozzle region with a high concentration of droplets, leaving its main use for sufficiently diluted spray where the volume fraction of the dispersed phase is low enough to allow numerical simulation. In the region close to the nozzle where the volume fraction of dispersed phase is very high, the Eulerain multiphase spray approach is somewhat more efficient. However, in order to better capture droplet characteristics, the droplet-size distribution must be divided into a number of separate size classes, where each phase requires its own set of conservation equations that considerably increases computational effort. Therefore, the Eulerain multiphase spray approach is suitable for the dense spray region and not for the whole calculation domain. Overall, it can be said that the Eulerian multiphase spray approach and the Lagrangian DDM spray approach can result in a very long calculation time that to some extent these methods

are supplementary and that one method can contribute to the progress of the other through the coupling concept.

In this section, the coupling concept has been presented where the validated Eulerian multiphase spray approach was used together with the Lagrangian DDM spray approach to take advantage of the capabilities inherent in both methods. This concept was then applied for coupled simulation of real internal combustion engine, which is particularly challenging for such modelling.

Spray was calculated by the Eulerian multiphase spray method in a fine, non-moving mesh that covers only a small part of the engine downstream of the nozzle exit. The Eulerian multiphase spray simulation was coupled with single phase engine simulation performed in the coarser moving mesh that overlaps the spray mesh. The basic idea was to couple two different simulations, the Eulerian multiphase spray calculation in the dense spray region with the single-phase engine calculation applying DDM in the whole computational domain. This means that two different CFD codes, Eulerian multiphase spray code, referred here as spray code, and single-phase engine code, referred here as engine code, were performed simultaneously simulations.

Coupling of the Eulerian multiphase spray simulation with Lagrangian DDM engine simulation was done by AVL Code Coupling Interface (ACCI) [77]. Coupling of two simulations means that current field values of both simulations were used as either boundary condition values or source terms for other simulations. In this work, the flow field of the engine code calculations were used as boundary condition values for the Eulerian multiphase spray code calculation. In another direction, the source terms (mass, momentum and energy) between the liquid phases and the gaseous phase of the Eulerian multiphase spray code calculation were transferred to the gas phase calculation of the engine code in order to synchronise the flow field.

6.3.1 Code Coupling Interface

The AVL Code Coupling Interface (ACCI) was used in this work as a separate software module to enable coupling between two different CFD simulations, the Eulerian spray multiphase calculation and the Lagrangian DDM spray single-phase engine calculation. This module provides the required data exchange between two simulations, i.e., two

codes. Moreover, the ACCI module provides spatial mapping of data between different meshes, which was performed in a conservative manner based on a volume or area weighted interpolation. The coupling was implemented as a server-client system, where Eulerian multiphase spray simulation was calculated with the spray client and Lagrangian DDM single-phase engine simulation was calculated with the engine client. These clients send data to and receive data from the server as shown in Figure 6.24.
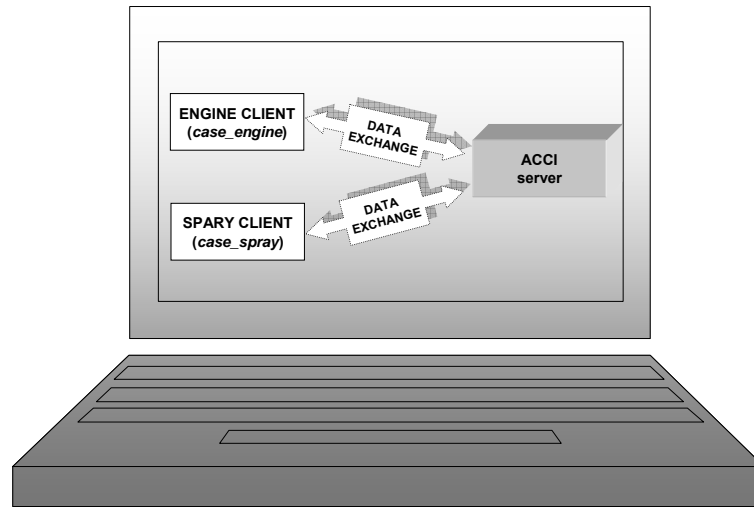
Figure 6.24: ACCI server-clients connection

The transferred data values between the clients are called attributes, while exchange spaces are called interfaces. An input file was used for coupled simulation to define the exchange process by specifying attributes to be exchanged, the exchange direction and the interface at which values need to be transferred. An example for an ACCI input file is as follows:

case_engine sets u at spray_boundary

case_engine sets t at spray_boundary

case_engine sets p at spray_boundary

case_spray gets u at spray_boundary

case_spray gets t at spray_boundary

case_spray gets p at spray_boundary

case_engine gets su_mom at spray_volume

case_engine gets su_ent at spray_volume

case_engine gets su_mas at spray_volume

case_spray sets su_mom at spray_volume

case_spray sets su_ent at spray_volume

case_spray sets su_mas at spray_volume

where *case_engine* is the engine client, *case_spray* is the spray client, *u, t, p, su_mom, su_ent and su_mas* are attributes and *spray_boundary* and *spray_voulume* are interfaces. This input file specifies which client sends or receives which attribute and at which interfaces. As can be noted there are two statements, *sets* and *gets*. The *sets* statement indicates that the client sends attribute values to the coupling server at the chosen interface and the *gets* statement indicates that the client requests attribute values from the coupling server at the chosen interface.

Since the spray client and engine client use 2 meshes with different topology and resolution, the data mapping is always performed in a conservative manner based on the intersection of volume of cells, or intersection of areas of faces in the different meshes [77]. In the ACCI input example above, engine client *case_engine* sends three-dimensional boundary conditions from the volume, and the spray client *case_spray* requests the boundary conditions mapped to the surface. The intersection of the surface of spray mesh and engine mesh cause that the attribute values in three-dimensional cells need to be transferred to two-dimensional boundary faces. The spatial mapping procedure is described in detail in [77].

6.3.2 Data flows between the Codes

As mentioned previously, the goal of coupled simulation is to use the benefits of both simulations, Eulerian multiphase spray simulation and single-phase engine simulation, when calculating the fuel injection, mixture preparation and combustion in real engine configuration. The fuel injection process was calculated at the spray client with a fine mesh only near the nozzle hole. Mixture preparation, combustion and nitrogen emission formation were calculated at the engine client in whole engine configuration with coarser moving mesh. Both meshes used for coupled simulation are shown in Figure 6.25.
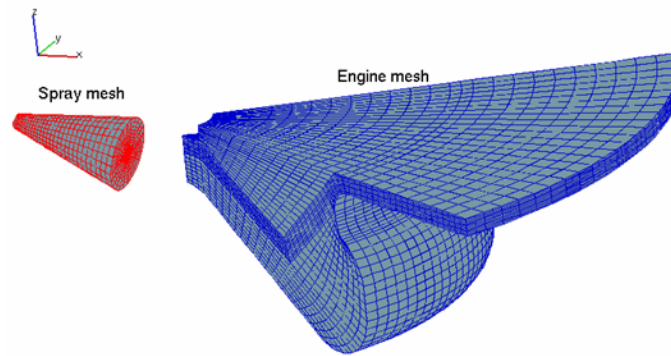
Figure 6.25: Spray and engine mesh

The 3D non-moving computational domain, used for Eulerian multiphase spray simulation, is only a small part of the 3D moving engine domain, as shown in Figure 6.25. The spray mesh is embedded in the engine mesh, as shown in Figure 6.26.
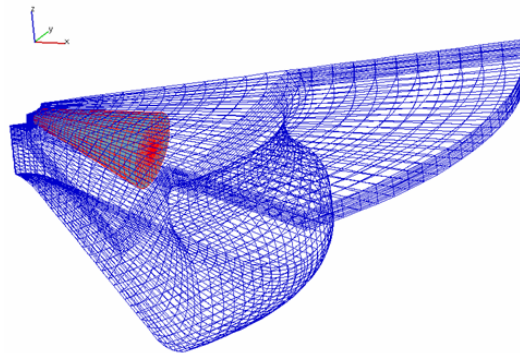
Figure 6.26: Spray mesh embedded in engine mesh

As addressed in previous sections, ACCI was used to couple two separate domains: spray domain calculated with spray client applying the Eulerian multiphase spray method, and engine domain calculated with engine client applying the Lagrangian DDM method. ACCI performs the spatial mapping between different meshes and transfers the attribute values between them. The main task of the ACCI is to exchange either the boundary condition values or source terms between two clients, as illustrated in Figure 6.27.

The data exchange was done at each coupling time step, which in this study was identical to the time step of the engine code. A smaller time step of the spray code was taken because the dynamic conditions and mesh resolution are different in engine and

spray code. The engine client time-step was determined as multiple of spray time-step client.

Initialization of coupled simulation must be performed as the first step where the engine client sends the initial conditions such as pressure, temperature, turbulence kinetic energy, etc., to the coupling server. The spray client gets the initialisation information from the coupling server.
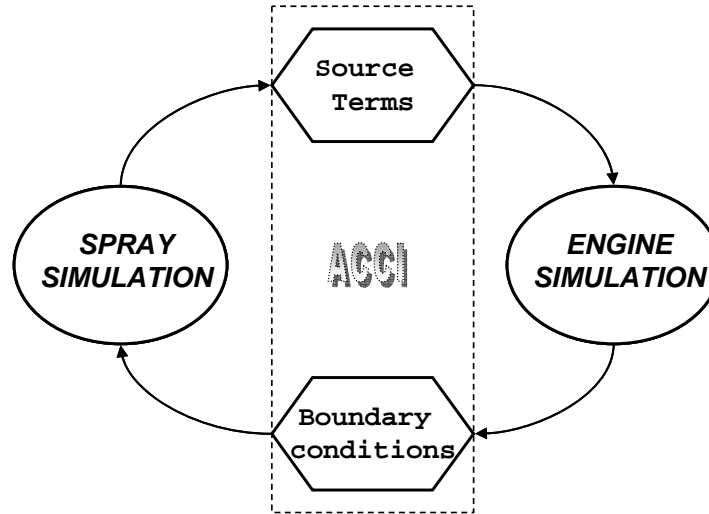
Figure 6.27: Data exchange in coupled simulations

In overlapping regions the gas phase was calculated at different spatial resolutions by both codes. Therefore, the source terms for mass, momentum, energy and scalar of the spray client were transferred to the engine client, providing a similar description of the phase interactions in both clients. Mass source term represents the interfacial mass exchange between dispersed liquid and gaseous phases due to droplet evaporation. Momentum source term represents the interfacial momentum exchange between the gaseous phase and liquid phases due to drag forces and turbulent dispersion forces. Energy sources were determined due to evaporation and heat exchange, and scalar sources represent the transport of vapor mass fraction.

The spray client transfers the source terms from the whole spray 3D volume mesh to the overlapping domain in the engine mesh. Since the spray client and engine client use different meshes, the source terms mapping was performed in a conservative manner using a weighting factor. This factor was calculated from the intersection volumes between spray and engine mesh as:

$$wf_{se} = \frac{CV_{se}}{CV_s} \qquad\qquad (166)$$

for extensive attributes such as mass or momentum sources. For example, mass source term S_e in the control volume of the engine mesh was calculated from all values in the control volumes in spray mesh as:

$$S_e = \sum_s wf_{se} S_s . \qquad\qquad (167)$$

Figure 6.28 illustrates the intersection of control volume of the source-interface spray mesh CV_s with control volume of the target-interface engine mesh CV_e. Source terms should be mapped from the spray mesh to the engine mesh.
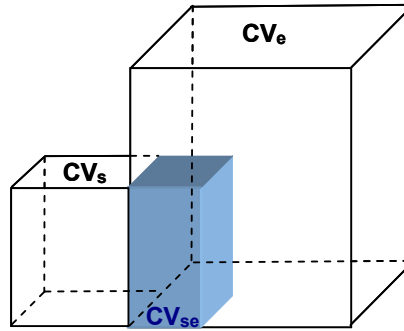
Figure 6.28: Intersection of control volumes between spray and engine mesh

In the case of non-extensive attributes such as mass fraction, velocity, pressure or temperature where these attributes do not depend on the size of control volumes the weighting factor is defined as:

$$wf_{se} = \frac{CV_{se}}{CV_e} . \qquad\qquad (168)$$

The boundary condition values (pressure, velocity, turbulence and temperature) in the 3D volume mesh of the engine client at the end of engine time-step were mapped to the 2D surface boundaries of the spray client. These values were used as boundary conditions in the spray calculation. For this purpose two different boundary conditions were defined for the spray mesh, static pressure and velocity at a face selection surface.

Liquid phases that cross the boundary of the spray mesh were treated in the engine code by classical DDM model, producing new parcels in the engine domain. The droplet phase conditions such as volume fractions of liquid, densities, droplet velocities and temperature were mapped to the engine client as initialisation of Lagrangian DDM spray as shown in Figure 6.29.
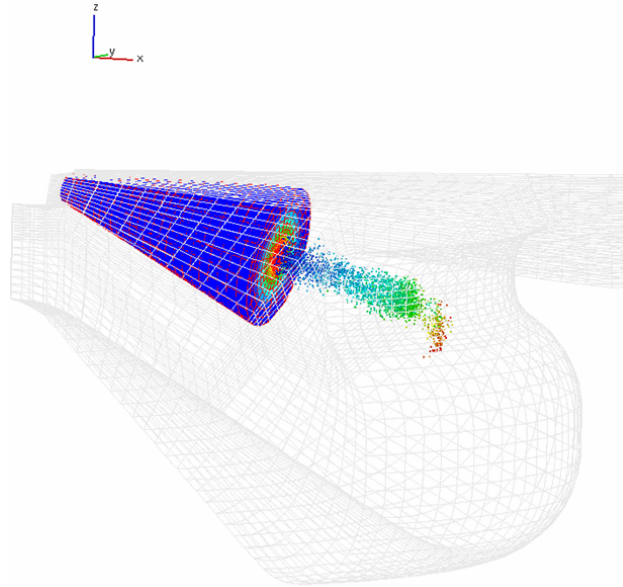
Figure 6.29: DDM parcels produced in the engine domain

6.3.3 Numerical Simulation

In this section, the numerical setup and simulation results obtained with the coupling approach using the various methodologies previously described are presented. The optimized and validated Eulerian multiphase spray approach was used together with the Lagrangiane DDM spray approach and applied for coupled simulation of the passenger diesel direct injection engine.

Since the combustion chamber geometry and the 6 hole injector configuration are symmetrical, the calculated engine domain is only 1/6 of the total chamber with one nozzle in order to save computational time, as shown in Figure 6.30. The Eulerian multiphase spray calculation was performed only close to the nozzle (full conical spray domain), while the Lagrangian spray calculation, combustion and formation of nitrogen

emission were performed in the remaining combustion chamber (60 degree sector of cylinder), as illustrated in Figure 6.30.
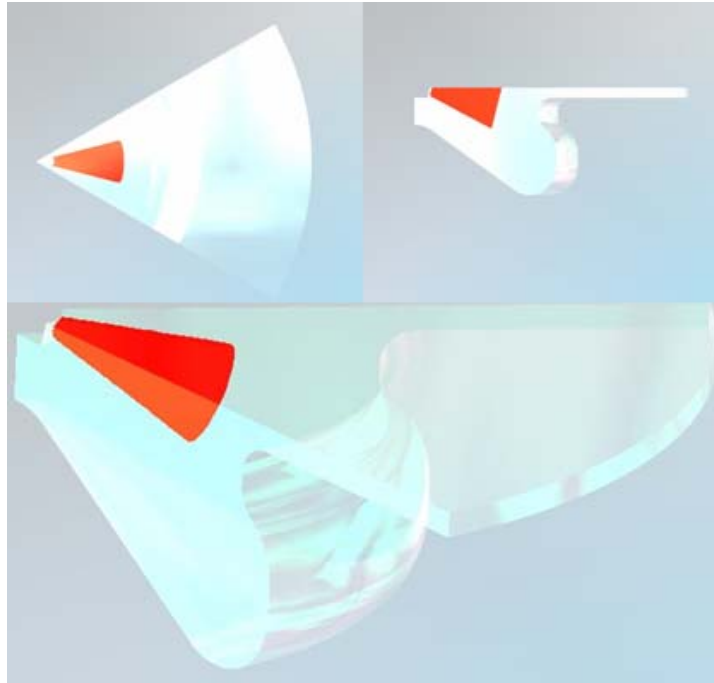
Figure 6.30: Engine and spray domain used for the simulation

The main engine specifications are summarized in Table 6.3.

Table 6.3: Engine specification

Stroke	0.0894 [m]
Bore	0.0815 [m]
Spray angle	76 [deg]
Compression ratio	17.5 [-]
Number of injection holes	6
Speed	4200 [rpm]

The in-cylinder region of the computational mesh consisted of 23664 control volumes at top dead centre (TDC) as shown in Figure 6.31.
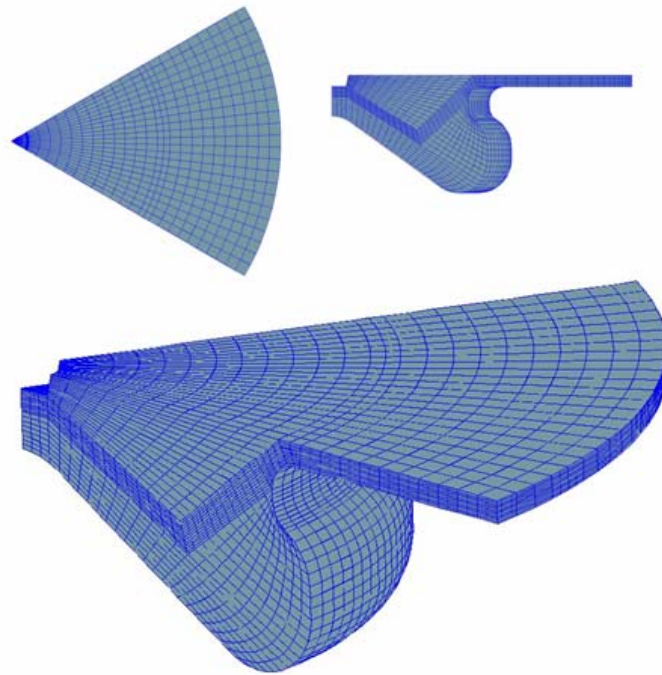
Figure 6.31: Engine mesh at TDC

The boundary conditions used for engine simulation are given in Figure 6.32. The cylinder geometry was assumed to be symmetric around the cylinder axis and cyclic boundary conditions were applied to the sides. A moving wall boundary condition was applied to the piston bowl, as shown in Figure 6.32.

The in-cylinder thermodynamic state and flow distribution prior to injection of diesel fuel were obtained through simulation of the compression stroke. Figure 6.32 shows the engine mesh at a 630 deg crank-angle (CA); at this point the engine client starts the calculation. The initial conditions used for engine calculation are summarized in Table 6.4.

The engine simulation was run from 630.0 to deg CA until 738.2, but in the first part of the simulation the engine client was run alone in the period of 630 to 703.4 deg CA. Injection of diesel fuel starts at 703.4 deg CA. At this point the coupling of engine and spray simulations were initiated. This means coupled simulations were run from the beginning of the injection of diesel fuel (703.4 deg CA) through the end of the injection (738.2 deg CA).

116
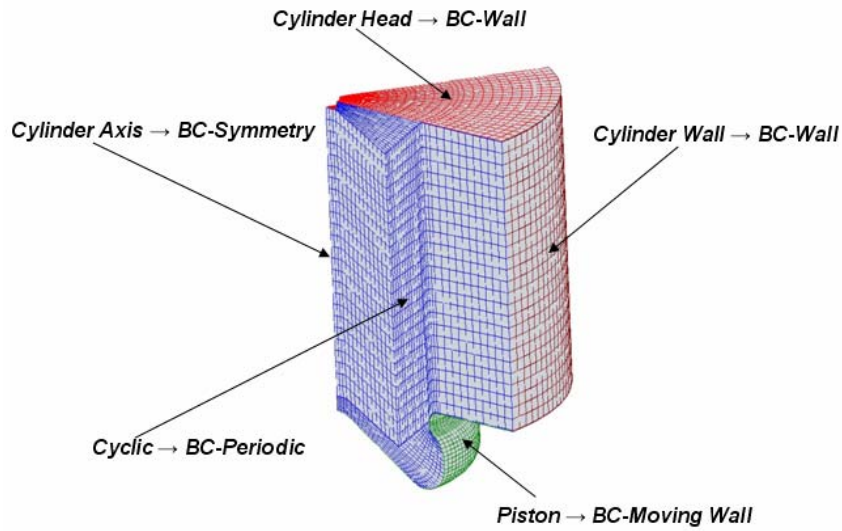
Figure 6.32: Engine boundary conditions

The engine simulations were performed as single-phase calculations based on the Lagrangian approach with standard species transport. Two types of simulations were conducted: swirl and non swirl. In the case of swirl simulation the swirl number used was 2.9. Turbulence was modelled by the standard k-epsilon model. The diesel combustion was represented by the Eddy Break-up Model, which is described in section 5. The NO_x model was integrated into FIRE code via user functions, and an additional NO transport equation was solved as active scalar. The central difference discretization scheme was used for the convective term in the continuity equation, while a hybrid between the central differences and the upwind scheme with a blending factor of 0.5 was used for the convective terms in the momentum equations. The upwind discretization scheme was used for the convective terms in the scalar equations.

Table 6.4: Initial conditions used for engine calculation

Pressure	0.45 [MPa]
Temperature	430 [K]
Gas composition	Air
Turbulent kinetic energy	50 [m^2/s^2]
Turbulent length scale	0.001 [m]
Number of injection holes	6

The particle tracking module based on the Lagrangian DDM method was applied for tracking the motion of fuel droplets. An important step in coupled simulation was to take the same sub-models for the description of spray for engine and spray simulation, but because there are different methods of Eulerian multi-phase and DDM approach, there were some minor differences. The diesel fuel with a temperature of 353 K was applied as model fuel. The effects of turbulent diffusion, evaporation and break-up of droplets were taken into account in engine simulations. The evaporation of droplets was modelled by the Abramzon/Sirignano model while for break-up the standard WAVE model was used [77].

An outline of the spray region of the computational mesh is given in Figure 6.34. The conical mesh consisted of 11760 control volumes. It was refined toward the spray inlet and the symmetry axis. The diesel fuel was injected by the nozzle with an orifice diameter of 137 μm into the cylinder. Injection starts near the end of the compression stroke at 703.4 deg CA and finishes at 738.2 deg CA. Figure 6.33 shows the injection velocity applied as inlet boundary conditions.
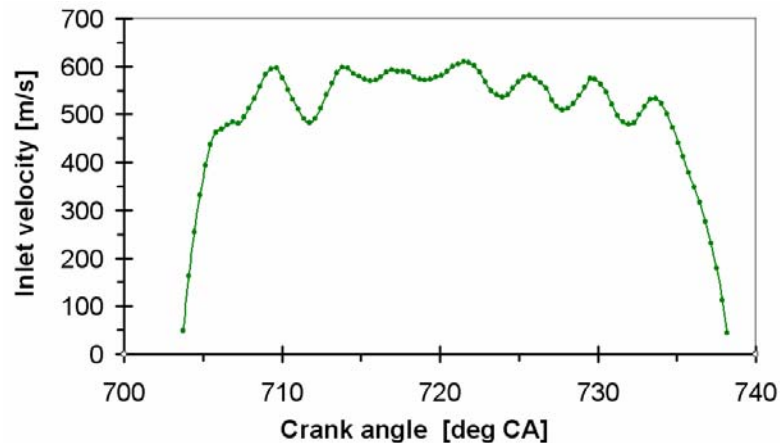
Figure 6.33: Injection velocity used for spray simulation

Figure 6.34 illustrates a velocity boundary condition applied at the conical surface of the mesh, and a pressure boundary condition applied at the bottom side of the spray mesh. The boundary condition values for these 2D surface boundaries come from the engine calculation. This transfer of boundary data was done by an ACCI server, as described in a previous section.
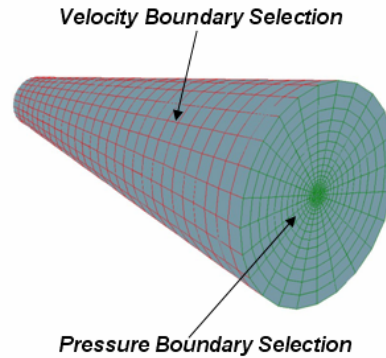
Figure 6.34: Spray mesh and boundary conditions used for calculation

Very small time-steps were required for simulation of the Eulerian multiphase spray because the injection of diesel fuel is a highly transient process and, as addressed in section 6.1, too big time-step can cause an unstable calculation. Therefore, at the beginning of the calculations the time-steps were very small and as the injection time progressed, were continuously increased, as listed in Table 6.5.

Table 6.5: Time discretization- spray simulation

Upto	Crank-angle [deg]	Δα
upto	**703.405**	**0.0005**
upto	**703.6**	**0.0025**
upto	**708**	**0.00625**
upto	**736**	**0.0125**
upto	**738.2**	**0.00625**
upto	**708**	**0.00625**

The 0.025 crank-angle step was used for engine simulation. As is seen, the engine time-step is approximately twice the size of the largest spray client time-step. However, this is not a problem because the data transferred from the spray client to the engine client were integrated over time. The engine time-step determines the coupling time-step, where the data exchanged was done between the engine and spray simulations, as addressed in a previous section.

The Eulerian multiphase results were generated using six phases total, one gaseous phase, four droplet phases, and one bulk liquid phase. All phases were treated as

interpenetrating multi-fluids represented by their volume fractions. The gas phase was treated as the primary phase, while the spray droplets were treated as the secondary phases. The droplets were classified into different size classes by volume fractions and diameters. The size class diameters are 5, 10, 20 and 40 μm for the droplet phases and the nozzle diameter of 137 μm was assigned to the bulk liquid phase.

A separate set of complete conservation equations, with some additional source terms accounting for droplet dynamics, was solved for each phase. For the purpose of consistency, the validated spray sub-models and their coefficients were kept identical to the simulations carried out in section 6.1. The same differencing schemes as for engine simulation were used. The interfacial mass exchange between the gaseous phase and the liquid phase includes droplet evaporation, primary break-up and secondary break-up, while the interfacial momentum exchange includes drag forces and turbulent dispersion force. For details about the exchange terms used in spray simulations see section 4.4.

6.3.4 Results

The work presented here was the first attempt to simulate a real internal combustion engine by the coupling concept of the Eulerian multiphase spray model with the classic Lagrangian DDM spray model and in conjunction with combustion and nitrogen emission formation. We emphasize that the coupled simulations in this thesis are the results of preliminary testing. The main goal of coupled simulations has been to investigate the capabilities of the coupling concept between validated 3D Eulerian multi-phase simulation and validated NO_x chemical reaction mechanisms for engine simulation. This means that the validated 3D Eulerian multi-phase model was used as a physical improvement of the spray process, while the combustion process was modelled on a single phase solver and furthermore was coupled with improved NO_x reaction mechanisms. In this work an improved NO_x model was investigated and implemented in FIRE code. For details see sections 5.2 and 6.2. It should be noted that the Eulerian multiphase model and the NO_x model are the only models investigated in this thesis. All other models such as the Lagrangian DDM model, the combustion model etc. used in this simulation were selected from standard models within the FIRE code.

Two types of coupled simulations were conducted in this work: swirl and non-swirl engine simulations. Two different cutting-planes are used to present the simulation results as shown in Figure 6.35.
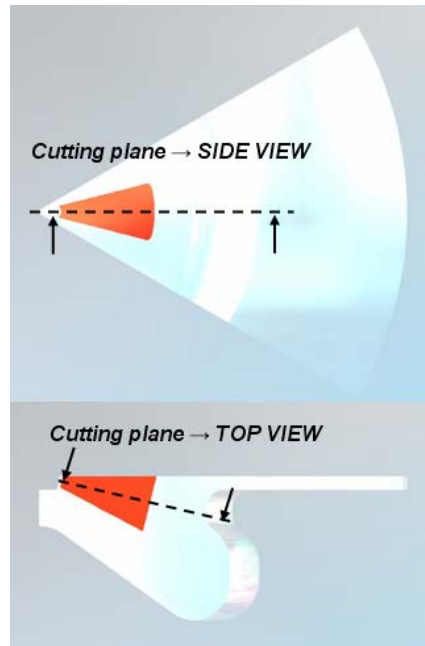
Figure 6.35: Cutting planes used for visualisation of simulation results

The gas phase velocity fields at 720 deg CA (16,6 deg CA after fuel injection) are shown in Figure 6.36. As can be seen in the plotted results, the maximum velocity is higher at the Eulerian spray domain than at the engine domain due to better mesh resolution. Furthermore, in the spray simulation a significant volume fraction of the liquid phases occupies the control volumes in a region near the nozzle, while in the engine simulations there is only the gas phase. The plots also show good agreement of the gas flow field between two codes, indicating that the gas flow field of the engine simulation was well mapped to the surface boundaries of the spray client. In another direction, source terms resulting from spray simulation were mapped to the engine client. This leads to the equivalent flow fields in the overlapping region in both simulations, as shown in the gas velocity plots in Figure 6.36. Overall, it can be said that velocity was resolved more accurately in the spray simulation due to much finer mesh resolution, and the momentum exchange between the liquid and gaseous phases calculated by spray code were well mapped to the engine simulation, providing a more accurate flow field.
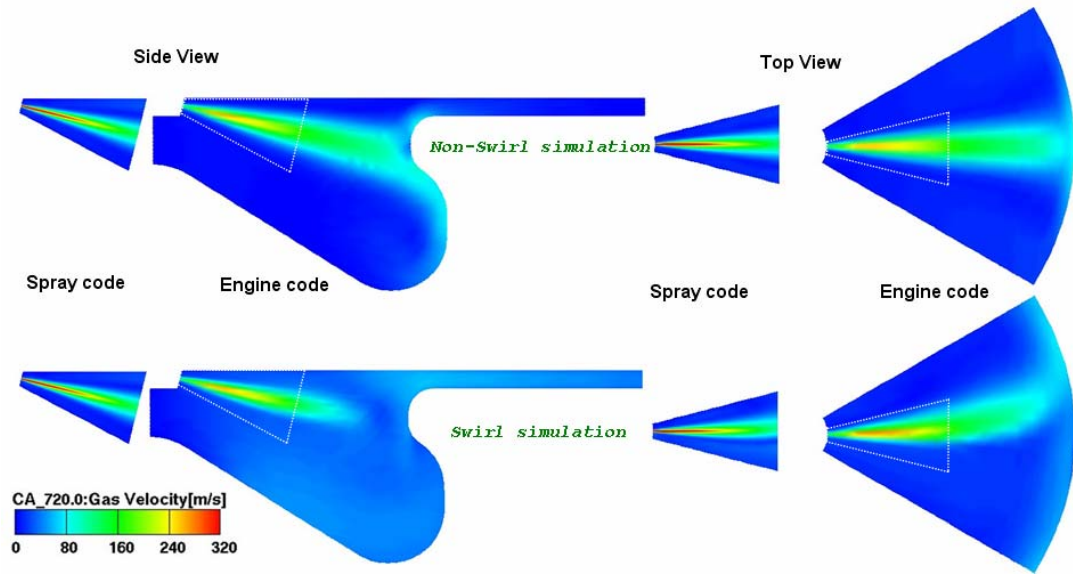
Figure 6.36: Gas velocity of the spray and engine code at 720 deg CA

Figure 6.37 shows the total liquid volume fraction of the spray simulation with and without engine swirl at 720 deg CA.
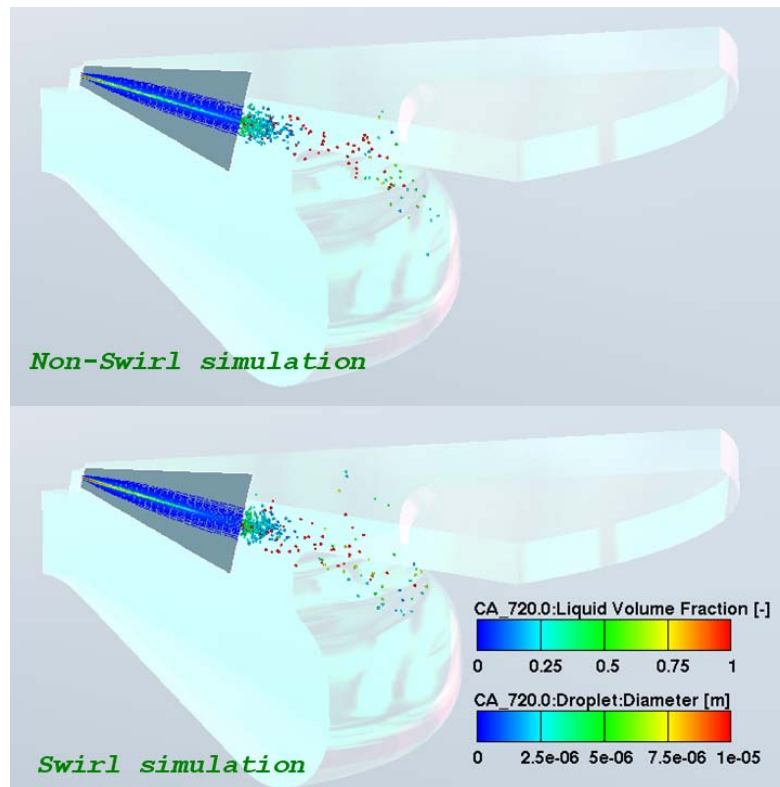
Figure 6.37: Total liquid volume fraction and DDM parcels at 720 deg CA

As can been seen in Figure 6.37, the maximum liquid volume fraction is near the nozzle exit. The liquid jet travels downstream from the nozzle exit and is disintegrated into droplets which then evaporate due to a rise in temperature caused by the absorption of heat from ambient gas. Finally, the vapor fuel is released. The left hand side of Figure 6.37 shows total liquid volume fraction in the Eulerian spray domain, while the right hand side of Figure 6.37 shows the DDM spray parcels in the engine domain. As can be seen, the liquid phases that cross the boundary of the spray domain, treated by Lagrangian DDM, produces new parcels in the engine domain. The circles denote spray parcels collared by droplet diameter.

Throughout the simulation the spray droplets disappear due to the evaporation process. The heat arrives at the droplets from the ambient gas by conduction and convection, producing the fuel vapor that leaves into the gas by convection and diffusion. Figure 6.38 shows a comparison of the fuel vapor mass fraction between spray and engine code.
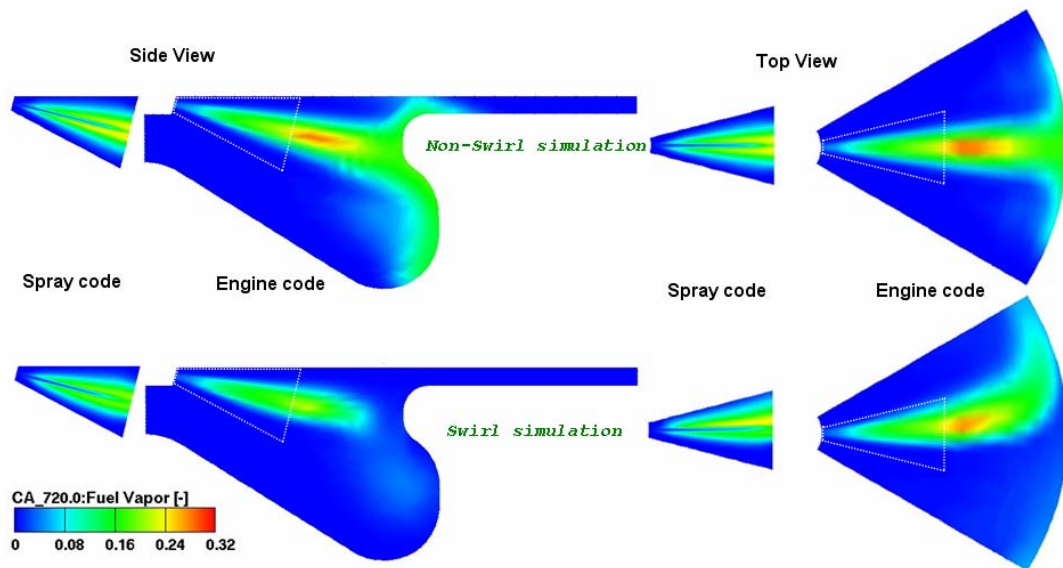
Figure 6.38: Fuel vapor of the spray and engine code at 720 deg CA

As can be seen, the spray and the engine fuel vapor results exhibit very similar trends and good agreement in the overlapping region. One can observe a difference between the swirl and non-swirl simulation. The swirl motion in the cylinder calculated by engine code impacts the spray simulation, and as can be seen, the fuel vapor is deviated.

123

This confirms that the gas flow field is well calculated and the transfer of boundary condition values and source terms between the two simulations is good.

Figures 6.39 and 6.40 show the gas temperature distribution and nitrogen oxide (NO) mass fraction distribution of the swirl and non-swirl engine simulations. The regions of NO can be examined by looking at contours of NO and temperature.
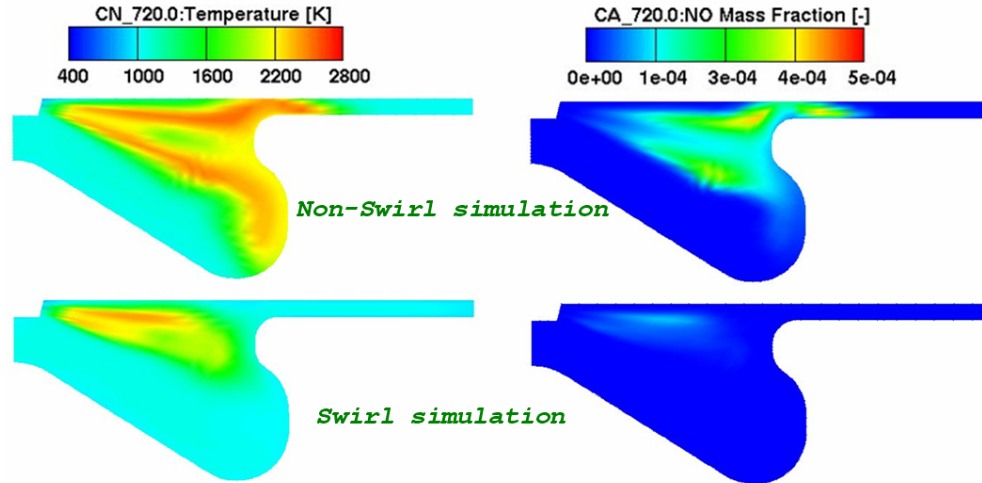
Figure 6.39: Temperature and NO distribution at 720 deg. CA - side view

The formation of NO in the combustion processes in engine simulations was predicted using reduced chemical reaction mechanisms described in section 5.2. The NO_x model was implemented through the user functions and coupled with combustion model in engine simulations. The nitrogen scheme was based only on thermal NO formed by oxidation of atmospheric nitrogen in a fuel-lean environment. Prompt NO was neglected since this mechanism contributes only a minor part of the total NO in diesel engine.

The thermal NO mechanism arises from the thermal dissociation and subsequent reaction of nitrogen and oxygen molecules in combustion air at relatively high temperatures. It is extremely sensitive to the temperature and it is produced only in very hot products regions. Figures 6.39 and 6.40 show a comparison of NO mass fraction distribution with the temperature distribution, indicating that NO occurs wherever there is high temperature. The plots also reveal the deviation of the temperature and NO distribution due to engine swirl effect.

Non-Swirl simulation

Swirl simulation

CN_720.0:Temperature [K]

400   1000   1600   2200   2800

CA_720.0:NO Mass Fraction [-]

0   0.0003 0.0006 0.0009 0.0012
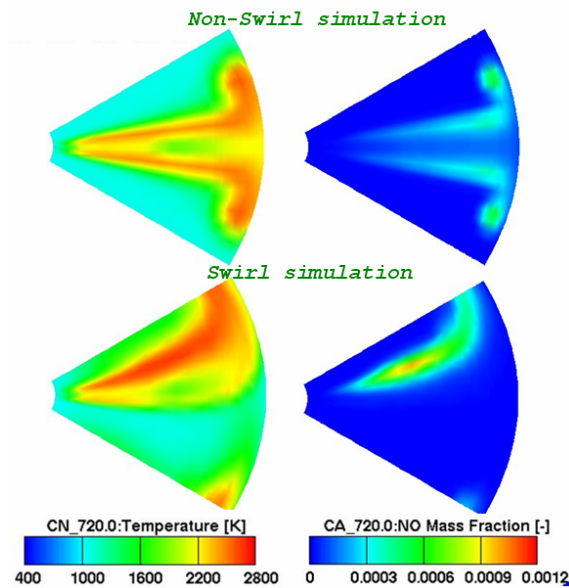
Figure 6.40: Temperature and NO distribution at 720 deg. CA - top view

In addition, the effects of the turbulent fluctuations on the NO reaction rates were accounted for by integrating the kinetic rates with respect to fluctuating temperatures over presumed probability density function (PDF), as described in section 5.2.3. It is also worth nothing also that the prediction of NO was calculated as a scalar variable and thus was not included in the mass balance as a chemical species. This was possible because the total amount of nitrogen oxides formed in combustion is generally low and does not affect the flame structure.

7 Conclusion

Numerous reliable and validated methods must be used to simulate turbulent reacting multiphase flow in real combustion configurations. In this work, an integrated simulation approach was applied in numerical simulation of turbulent multiphase droplet flow in the practical combustion system, adopting and optimizing methods for simulation of dense and dispersed liquid fuel spray in conjunction with combustion and nitrogen emission formation. An integrated simulation approach was based on methods that describe high pressure dense and dispersed spray behaviour in conjunction with the validated nitrogen pollutant formation model, resulting in a better description of the fuel-air mixing process and the pollutant formation process in the entire combustion chamber.

The first objective was to establish the validated Eulerian multiphase spray modelling approach, which can be applied with confidence in high pressure diesel spray simulations, particularly in dense spray regions. In this work optimization, verification and validation of the Eulerian multiphase spray method were performed and then applied for further coupling with the existing classic Discrete Droplet Method (DDM). Several simulations of high pressure diesel injections, combined with different chamber pressures, using an approach with fixed droplet size classes, were carried out and compared with experimental data. The results were in good agreement with the measured values for all simulation cases for different high pressure injections and pressure chamber conditions. The Eulerian multiphase spray model showed the capability to predict the strong impact of rail pressure on penetration of the fuel vapor and of the fuel liquid jet. Furthermore, it was shown that with one set of the spray sub-model coefficients used in empirical closure relations (for primary break-up, secondary break-up, droplet evaporation, turbulent dispersion forces and drag forces), it is possible to obtain good results for a variation of different injection pressures in combination with different chamber pressures. The Eulerian multiphase spray method can be improved by transporting additional number density transport equations to obtain variable droplet size classes, in order to improve prediction of evaporation dynamics.

The validated Eulerian multiphase spray method was then coupled with the classic Lagrangian DDM spray method, in conjunction with the classic combustion model and

126

the validated nitrogen oxides (NO_x) model. The NO_x chemical reaction mechanisms were investigated and implemented into the CFD code FIRE. The reduced reaction mechanisms for nitrogen chemistry were applied and validated for the Sandia National Laboratories Flame D, turbulent non-premixed methane-air flame. The NO_x formation was predicted in the post-processing mode, using the converged solution of the pre-calculated flame structure. Two chemical kinetic mechanisms, thermal and prompt, were implemented into the FIRE code to predict nitrogen pollutants. In addition, the effects of turbulent fluctuations on the NO_x reaction rates were accounted for by integrating the kinetic rates with respect to fluctuating temperatures over the presumed probability density function (PDF). The numerical results of nitrogen pollutant formation were presented in detail and compared with the results obtained by the Steady Laminar Flamelet Model (SLFM) and with the experimental data. The overall agreement between predictions of the nitrogen pollutant formation, obtained by the reduced mechanisms for nitrogen chemistry, and measurements was good, while the nitrogen pollutant formation calculated with SLFM was quite severely over-predicted. It was shown that the results obtained with the reduced mechanisms provide a significant improvement over the SLFM nitric oxide results.

Furthermore, to demonstrate the capability of the coupling concept, an integrated simulation approach was applied for calculation of the real internal combustion engine, which is particularly challenging for such modelling. An integrated simulation approach was based on the idea of coupling two different simulations, the Eulerian multiphase spray calculation performed only close to the nozzle in the dense spray region with the single-phase engine calculation applying DDM and the NO_x chemical reaction mechanisms in the whole computational domain. The Eulerian multiphase spray simulation was performed on a separate, fine mesh, while the single-phase engine simulation was performed on coarser mesh, presenting the whole domain and arbitrarily overlapping the spray mesh. These simulations were coupled and performed simultaneously to take advantage of the capabilities inherent in both simulations. The flow field of the engine code calculations were used as boundary condition values for the Eulerian multiphase spray code calculation, and the source terms of the Eulerian multiphase spray code calculation were transferred to the gas phase calculation of the engine code. The simulation results indicate that the coupling concept works well,

allowing an efficient data transfer between the Eulerian multiphase spray and single-phase engine simulation. It is important to note that further improvements can be made by implementation of the combustion process in the Eulerian multiphase domain, including the transfer of energy and vapor sources from the single-phase engine code to the Eulerian multiphase code. The continuation of this work would also entail the investigation and simulation of the flow inside of the injector nozzle in order to predict the fuel flow characteristics, which can then serve as input to the reliable predictions of all subsequent processes such as spray, mixture formation, combustion, and pollutant formation. Therefore, an integrated simulation method presented in this work can be improved by coupling with nozzle flow simulation, taking into account the influences from nozzle flow turbulence and cavitation dynamics on the primary break-up of the liquid fuel jet.

An integrated simulation methods presented herein can serve as an advanced tool to analyze and improve understanding of turbulent reacting multiphase flow in real combustion configurations. This approach can be used to describe the high pressure dense and dispersed liquid fuel spray behaviour and NO_x formation, resulting in a better description of the fuel-air mixing process and the pollutant formation process, which are crucial issues to ensure better combustion efficiency and to reduce emission pollutants in modern combustion systems.

Bibliography

[1]   S. C. Kong and R. D. Reitz, Application of detailed chemistry and CFD for predicting direct injection HCCI engine combustion and emissions, Proceedings of the Combustion Institute, Volume 29, Issue 1, 2002, pp. 663-66

[2]   C. Y. Choi and R. D. Reitz, An experimental study on the effects of oxygenated fuel blends and multiple injection strategies on DI diesel engine emissions, Fuel, Volume 78, Issue 11, 1999, pp. 1303-1317

[3]   R. D. Reitz and C. J. Rutland, Development and testing of diesel engine CFD models, Progress in Energy and Combustion Science, Volume 21, Issue 2, 1995, pp. 173-196

[4]   M. A. Patterson and R. D. Reitz, Modelling the effects of fuel spray characteristic on diesel engine combustion and emission" SAE paper NO. 970345, 1998

[5]   K. K. Kuo, Principles of combustion, New York, John Wiley & Sons, 1986

[6]   A. Saario, A. Rebola, P. J. Coelho, M. Costa, A. Oksanen, Heavy fuel oil combustion in a cylindrical laboratory furnace: measurements and modeling, Fuel, 84, 2005, p. 359

[7]   C. T. Bowman, Control of combustion-Generated Nitrogen Oxide Emissions: Technology Driven by Regulation, Twenty-Fourth Symposium (International) on Combustion, The Combustion Institute, Pittsburgh, PA, 1992, pp. 859-878

[8]   F. Tao, D. E. Foster, R. D. Reitz, Characterization of soot particle distribution in conventional, non-premixed di diesel flame using a multi-step phenomenological soot model, Proceedings of the Combustion Institute 31 II, 2007, pp. 2991-2998

[9]   G. M. Faeth, Mixing, transport and combustion in sprays, Progress in Energy and Combustion Science., 13, 1987, pp. 293–345

[10]   G. M. Faeth, Spray combustion phenomena, Symposium (International) on Combustion 1, 26, 1996, pp. 1593–1612

[11]   H. H. Chiu, Advances and challenges in droplet and spray combustion, I. Toward a unified theory of droplet aerothermochemistry, Progress in Energy and Combustion Science 26, 2000, pp. 381–416

[12]   C. K. Law, Heat and mass transfer in combustion, Fundamental concepts and

analytical techniques, Progress in Energy and Combustion Science, 10, 1984, pp. 295–318

[13]   W. A. Sirignano, Fluid dynamics of sprays , Journal of Fluids Engineering, 115, 3, 1993, pp. 345-378

[14]   C. T. Crowe, J. N. Chung, T. R. Trout, Particle mixing in free shear flows. Progress in Energy and Combustion Science, 14, 1988, pp. 171-194

[15]   C. T. Crowe, T. R. Trout, J. N. Chung, Annual Review of Fluid Mechanics 28, 1996, pp. 11-43

[16]   G. M. Faeth, Evaporation and combustion of spray, Progress in Energy and Combustion Science, 9, 1983, pp. 1-76

[17]   G. Gouesbet and A. Berlemont, Eulerian and Lagrangian approaches for predicting the behaviour of discrete particles in turbulent flows, Progress in Energy and Combustion Science, 25, 2, 1998, pp. 133-159

[18]   J. K. Dukowicz, A Particle-Fluid Numerical Model for Liquid Sprays, Journal of Computational Physics, 35, 1980, pp. 229-253

[19]   C. T. Crowe, M. P. Sharma and D. E. Stock, The particle-source-in-cell (PSI-CELL) method for gas-droplet flows, Trans. ASME J. Fluids Engrg., 99, 1997, pp.325-332

[20]   E. Loth, Numerical approaches for motion of dispersed particles, droplets and bubbles, Progress in Energy and Combustion Science, 26, 3, 2000, pp. 161-223

[21]   A. P. Watkins and H. Khaleghi, Modelling diesel spray evaporation using a noniterative implicit solution scheme, Applied Mathematical Modelling, 14, 9, 1990, pp. 468-474

[22]   X. Q. Chen and J. C. F Perreira, Stochastic-probabilistic efficiency enhanced dispersion modelling of turbulent polydispersed sprays, Journal of Propulsion and Power, 12. 1996, pp.760-769

[23]   J. Abraham, What is Adequate Resolution in the Numerical Computation of Transient Jets?, SAE Paper No. 970051, 1997, pp 141-145

[24]   V. A. Iyer and J. Abraham, Penetration and dispersion of transient gas jets and sprays, Combustion Science and Technology, 130, 1997, pp. 315-334

[25]   M. Hallmann, M. Scheurlen, and S. Wittig, Computation of turbulent evaporating sprays: Eulerian versus Lagrangian approach, Journal of Engineering for Gas

Turbines and Power, 117, 1995, pp. 112-119

[26] F. H. Harlow and A. A. Amsden, Numerical calculation of multiphase fluid flow, Journal of Computational Physics, 17, 1975, pp.19-52

[27] F. H. Harlow, Fluid dynamics in Group T-3 Los Alamos National Laboratory: (LAUR-03-3852), Journal of Computational Physics, 195, 2, 2004, pp. 414-433

[28] V. A. Iyer, J. Abraham and V. Magi, Exploring injected droplet size effects on steady liquid penetration in a Diesel spray with a two-fluid model, International Journal of Heat and Mass Transfer, 45, 2002, pp. 519-531

[29] R. I. Issa, P. J. Oliveira, Numerical prediction of phase separation in two-phase flows through T-junctions, Comput. Fluids, 23, 1994, pp. 347–372

[30] A. Behzadi, R. I. Issa, H. Rusche, Modelling of dispersed bubble and droplet flow at high phase fractions, Chemical Engineering Science, 59, 2004, pp. 759-770

[31] A. D. Gosman, C. Lekakou, S. Politis, R. I. Issa, M. K. Looney, Multidimensional modeling of turbulent two-phase flows in stirred vessels, Aiche Journal, 38, 1992, pp. 1946-1956

[32] E. Riber, M. Moreau, O. Simonin, B. Cuenot, Development of Euler-Euler les approach for gas-particle turbulent jet flow, Proceedings of ASME Fluids Engineering Division Summer Meeting, 2006, pp. 1663-1672

[33] D. A. Drew, Mathematical modeling of two-phase flow, Annual Review of Fluid Mechanics 15, 1983, pp. 261-291

[34] J. C. Beck, Computational Modelling of Polydisperse Sprays without Segregation into Droplet Size Classes", Ph.D. Thesis at UMIST, Manchester, United Kingdom, 2000

[35] J. C. Beck and A. P. Watkins, Simulation of Water and other Non Fuel Sprays Using a New Model, Atomization and Sprays, 13, 2003, pp. 1 26

[36] J. C. Beck and A. P. Watkins, The droplet number moments approach to spray modelling: The development of heat and mass transfer sub-models, International Journal of Heat and Fluid Flow, 24, 2003, pp. 242–259

[37] W. Edelbauer, H. Kratochwill, G. Brenn, R. Tatschl, Basics of the Numerical Simulation of Oil Droplet Formation in the Crankcase of an IC Engine, Proceeding of 13th International Conference on Modelling Fluid Flow CMFF'06,

2006, pp. 692 699

[38] C. W. Hirt and B. D. Nicholls, Volume of Fluid (VOF) method for the dynamics of free boundaries, Journal of Computational Physics, 39, 1981, pp. 201-225

[39] R. Scardovelli and S. Zaleski, Direct numerical simulation of free-surface and interfacial flow, Annu. Rev. Fluid Mech. 31, 1999, pp. 567-603

[40] D. A. Drew, S. L. Passman, Theory of Multi component Fluids, Springer, New York, 1998

[41] J. A. Miller and C. T. Bowman, Mechanism and modeling of nitrogen chemistry in combustion, Progress in Energy and Combustion Science, 15, 1989, pp. 287-338

[42] P. Glarborg, A. B. Bendtsen, J. A. Miller, Nitromethane dissociation: Implications for the CH3 + NO2 Reaction , International Journal of Chemical Kinetics, 31, 1999, pp. 591-602

[43] http://www.me.berkeley.edu/gri_mech/releases.html

[44] D. L. Baulch, C. J. Cobos, R. A. Cox, P. Frank, G. Hayman, T. Just, J. A. Kerr, T. Murrells, M. J. Pilling, J. Troe, R. W. Walker, J. Warnatz, Summary table of evaluated kinetic data for combustion modeling: Supplement 1, Combustion and Flame, 98, 1994, pp. 59-79

[45] P. Dagaut, J. Luche, M. Cathonnet, Reduction of NO by n-butane in a JSR: Experiments and kinetic modeling, Energy Fuels, 14, 2000, pp. 712-719

[46] I. Glassman, Combustion, Third Edition, Academic Press, 1996

[47] P. Kilpinen, M. Hupa, M. Aho, M. J. Hämäläinen,, Proceedings of the 7th International Workshop on Nitrous Oxide Emissions, Bergische Universität Gesamthochschule Wuppertal, Germany, 1997

[48] C. Hill and L. D. Smoot, Modeling of nitrogen oxides formation and destruction in combustion systems, Progress in Energy and Combustion Science, 26, 2000, pp. 417–458

[49] E. C. Zabetta, P. Kilpinen, Improved NO_x Submodel for In-Cylinder CFD Simulation of Low- and Medium-Speed Compression Ignition Engines, Energy & Fuels, 15, 2001, pp. 1425-1433

[50] Z. Wang, S. Shuai, J. Wang, G Tian, A computational study of direct injection gasoline HCCI engine with secondary injection, Fuel, 85, 2006, pp. 1831-1841

[51] G. Loffler, R. Sieber, M. Harasek, H. Hofbauer, R. Haussb, J. Landaufb, NO_x formation in natural gas combustion a new simplified reaction scheme for CFD calculations, Fuel, 85, 2005, pp. 513-523

[52] M. Falcitelli, S. Pasini, L. Tognotti, Modelling practical combustion systems and predicting NO_x emissions with an integrated CFD based approach, Computers & Chemical Engineering, 26, 2002, pp. 1171-1183

[53] A. Frassoldati, S. Frigerio, E. Colombo, F. Inzoli, and T. Faravelli, Determination of NO_x emissions from strong swirling confined flames with an integrated CFD-based procedure, Chemical Engineering Science, 60, 2006, pp 2851-2869

[54] A. Vallet, A. Burluka, R. Borghi, Development of a Eulerian Model for the Atomization" of a Liquid Jet, Atomization and Sprays, 11, 2001, pp. 619-642

[55] G. Blokkeel, B. Barbeau, R. Borghi, A 3D Eulerian Model to Improve The Primary Breakup of Atomizing Jet, SAE 2003-01-0005, 2003

[56] R. Lebas, P. A. Beau, G. Blokkeel, F. X. Demoulin, Elsa model for atomization: To benefit of the eulerian and lagrangian descriptions of the liquid phase, Proceedings of ASME Fluids Engineering Division Summer Meeting 2006, 2006

[57] W. Edelbauer, D. Suzzi, P. Sampl, R. Tatschl, C. Krueger, B. Weigand, New Concept for On-line Coupling of 3D Eulerian and Lagrangian Spray Approaches in Engine Simulations, Proc. 10th International Conference on Liquid Atomization and Spray Systems, 2006

[58] R. D. Reitz, Modeling Atomization Processes in High-Pressure Vaporizing Sprays, Atomization and Spray Technology, 1987, Vol. 3, pp. 309-337

[59] M. Pilch, C. A. Erdman, Use of break-up time data and velocity history data to predict the maximum size of stable fragments for acceleration-induced break-up of liquid drop, Int. J. Multiphase flow 13, 1987. pp. 741-757

[60] A. Wierzba, Deformation and Break-up of Liquid Drops in a Gas Stream at Nearly Critical Weber Numbers, Experiments in Fluids, 1993, vol 9, pp 59–64

[61] J. Xin, L. Ricart, and R. D. Reitz, Computer modelling of spray atomization and combustion. Combustion Science and Technology, 1998. 137(1-6), pp. 171-194

[62] T. Cebeci, J. P. Shao, F. Kafyeke, E. Laurendeau, Computational Fluid Dynamics for Engineers, Springer, 2005

[63]   J. Blazek, Computational Fluid Dynamics: Principles and Applications, Elsevier, 2001

[64]   H. K. Versteeg and W. Malalasekera, An introduction to computational fluid dynamics:The finite volume method, Longman Scientific & Technical, 1995

[65]   I. Alfirevic, Uvod u tenzore i mehaniku kontinuuma, Golden marketing, 2003

[66]   D. C. Wilcox, Turbulence modelling for CFD, DCW Industries, Inc, California, 1993

[67]   T. Poinsot and D. Veynante, Theoretical and Numerical Combustion, R.T. Edwards, Inc., Philadelphia, 2001

[68]   A. W. Cook and J. J .Riley, Direct Numerical Simulation of a Turbulent Reactive Plume on a Parallel Computer. J. Computational Physics, 1996, 129, pp. 263-283

[69]   M. P. Martin, U. Piomelli, and G. V. Candler. Subgrid-scale models for compressible large-eddy simulations. Theoretical and Computational Fluid Dynamics, 2000, 13, pp. 361-376

[70]   W. W. Kim, S. Menon and H. Mongia, Numerical Simulations of Reacting Flows in a Gas Turbine Combustor,Combustion Science and Technology, 1999, Vol. 143, pp. 25-62

[71]   S. Menon, S. and W. H. Jou, Large-eddy Simulations of Combustion Instability in an Axisymmetric Ramjet Combustor, Combustion Science and Technology, 1991, Vol. 75, pp. 53-72

[72]   F. Ducros, V. Ferrand, F. Nicoud, C. Weber, D. Darracq, C. Gacherieu, T. Poinsot, Large-Eddy Simulation of the Shock,/Turbulence Interaction, J. Computational Physics, 1999, 152, pp. 517-549

[73]   A. W. Cook, J. J. Riley, G. Kosaly, A Laminar Flamelet Approach to Subyrid-Scale Chemistry in Turbulent Flows. Combustion and Flame, 1997, 109, pp. 332-341

[74]   Q. Wang nad K. D. Squires, Large Eddy Simulation of Particle Laden Turbulent Channel Flow, Phys. Fluids, 1996, 8(5), pp. 1207-1223

[75]   W. Frost and T. H. Moulden, Handbook of Turbulence, Plenum Press, New York, 1977

[76]   W. P. Jones and B. E. Launder, The prediction of laminarization with a two-equation model of turbulence, Int. J. Heat Mass Transfer, 1972, 15 pp. 301-314

[77] AVL AST, FIRE manual version 2008, AVL List GmbH, 2008

[78] J. C. Oefelein, and V. Yang, Analysis of Transcritical Spray Phenomena in Turbulent Mixing Layers, AIAA 96-0085, 34th AIAA Aerospace Sciences Meeting, Reno, NV, 1996

[79] Q. Wang, and K. D. Squires, Large Eddy Simulation of Particle Laden Turbulent Channel Flow, hys. Fluids, 8(5), 1996, pp. 1207-1223

[80] D. Drew, Mathematical modelling of two-phase flow, Annu. Rev. Fluid Mech., 15, 1983, pp. 261-291.

[81] D. Drew and S. L. Passman, Theory of Multi component Fluids, Springer, New York, 1998

[82] C. T. Crowe, T. R. Troutt and J. N. Chung, Numerical models for two-phase turbulent flows, Annu. Rev. Fluid Mech. 28, 1996, pp. 11-43

[83] R. T. Lee Lahey and O. C. Jones, The Prediction of Two Phase Turbulence and Phase Distribution Phenomena Using a k Epsilon Model, Japanese Journal Multiphase Flow 3 (4), 1989, pp. 335 368

[84] G. M. Bianchi and P. Pelloni, Modeling the Diesel Fuel Spray Break-up by Using a Hybrid Model, SAE Paper 1999-01-0226, 1999

[85] R. D, Reitz, Modeling Atomization Processes in High-Pressure Vaporizing Sprays, Atomization and Spray Technology, 3, 1987, pp. 309-337

[86] M. A. Patterson and R. D. Reitz, Modelling the Effect of Fuel Spray Characteristics on Diesel Engine Combustion and Emission, SAE-Paper 980131, 1998

[87] B. Abramzon, and W. A. Sirignano, Droplet Vaporization Model for Spray Combustion Calculations, Int. J. Heat Mass Transfer, 1989, pp. 1605 1618

[88] R. Clift, J. R. Grace and M. E. Weber, Bubbles, drops and Particles, Academic Press, New York, 1978

[89] M. C. Yuen and L.W. Chen, On drag of evaporating liquid droplets, Combust. Sci. Technol. 14, 1976, pp. 147-154

[90] P. J. O'Rourke and F. V. Bracco, Modeling Drop Interactions in Thick Sprays and a Comparison with Experiments, Stratified Charge Automotive Engines, I. Mech. E. Conference Publications 1980-9, 1980, pp. 101-116

[91] P. J. O'Rourke, Collective Drop Effects on Vaporizing Liquid Sprays, Ph. D.

Thesis, Los Alamos Lab. Report LA 9069 T, 1981

[92] A. B. Liu, D. Mather and R. D. Reitz, Modeling the Effects of Drop Drag and Break-up on Fuel Sprays, SAE Paper 930072, 1993

[93] P. J. O'Rourke and A. A.Amsden, The TAB Method for Numerical Calculation of Spray Droplet Break-up, SAE 872089, 1987

[94] M. A. Lopez Bertodano, Two fluid model for two phase turbulent jets, Nuclear Engineering and Design 179, 1998, pp. 65 74

[95] J. Warnatz, U. Mass and R. W. Dibble, Combustion, Springer, 1995.

[96] A. M. Eaton, L. D. Smoot, S. C. Hill,. C. N. Eatough, Components, formulations, solutions, evaluation, and application of comprehensive combustion models, Prog. Energy Combust. Sci., 33, 1999. p. 387

[97] N. Duić, Contribution to the Mathematical Modelling of Gaseous Fuel Combustion in a Steam Generator Furnace, PhD thesis (in Croatian), Department of Energy, Power Engineering and Environment, University of Zagreb, Zagreb, 1998

[98] Ž. Bogdan, N. Duić and D. R. Schneider, Three-dimensional simulation of the performance of an oil-fired combustion chamber, Proc. 2nd European Thermal Sciences & 14th UIT National Heat Transfer Conference, Rome, 1996

[99] D. R. Schneider, Investigation of the possibility of the SO_3 reduction during heavy-oil fuel combustion, PhD thesis (in Croatian), Department of Energy, Power Engineering and Environment, University of Zagreb, Zagreb, 2002

[100] B. S. Brewster, S. M. Cannon, J. R. Farmer, F. Meng, Modeling of lean premixed combustion in stationary gas turbines, Prog. Energy Combust. Sci., 25, 1999, p. 353

[101] R. W. Bilger, S. B. Pope, K. N. C. Bray, J. F. Driscoll, Paradigms in turbulent combustion research, Proc. of the Comb. Institute, 30, 2005, p. 21

[102] B. F. Magnussen and B. H. Hjertager, On mathematical models of turbulent combustion with special emphasis on soot formation and combustion, In 16th Symp. (Int'l.) on Combustion, The Combustion Institute, Pittsburgh, PA, 1976, pp. 719-729

[103] D. B. Spalding, 13th symposium on Combustion, The combustion Instituite, 1970, p. 649

[104] M. Baburić, Numerically efficient modelling of turbulent non-premixed flames, PhD thesis, Department of Energy, Power Engineering and Environment, University of Zagreb, Zagreb, 2005

[105] S. Pope, Pdf method for turbulent reactive flows, Prog. Energy Combust. Sci., 11, 1985, pp. 119-195

[106] N. Peters, Turbulent Combustion, Cambridge University Press, Cambridge, 2000

[107] http://powerlab.fsb.hr/mbaburic/CSC.htm

[108] M. Baburić, R. Tatschl and N. Duić, Numerical simulation of jet diffusion flames with radiative heat transfer modeling, Proceedings of ASME Heat Transfer Conference, USA, 2005

[109] S. M. Cannon, B. S. Brewster, and L. D.Smoot, Stochastic Modeling of CO and NO in Premixed Methane Combustion, Combustion and Flame, 1998, 113, pp 135-146

[110] C. S. Correa and M. D. Smooke, NO_x in Parametrically Varied Methane Flames, Twenty-Third Symposium (International) on Combustion, The Combustion Institute, Pittsburgh, PA, 1990, pp 289-295

[111] R. K. Hanson, and S. Salimian, Survey of Rate Constants in H/N/O System, Combustion Chemistry, W.C. Gardiner, Jr (Ed.), Springer, New York,1984, p. 361

[112] G. G. De Soete, Overall reaction rates of NO and N2 formation from fuel nitrogen, 15th Symposium (International) on Combustion, The Combustion Institute, Pittsburgh, 1975, p. 1093

[113] V. Dupont, M. Porkashanian, A. Williams, R. Woolley, The reduction of NO_x formation in natural gas burner flames, Fuel, 1993, 72(4), pp 497-503

[114] F. Bachmaier, K. H. Eberius, T. Just, The formation of nitric oxide and detection of HCN in premixed hydrocarbon-air flames at 1 atmosphere, Combust. Sci. and Tech 7, 1973, pp. 77-84

[115] R. S. Barlow and J. H. Frank, Piloted CH4/Air Flames C, D, E, and F - Release 2.0,www.sandia.gov/TNF/DataArch/FlameD.html, Sandia National Laboratories, 2003

[116] M. Baburić, B. Basara, P. Priesching, R. Tatschl, D. R. Schneider,and N. Duić, Steady laminar flamelet concept and hybrid turbulence modelling strategy

applied on numerical simulation of a turbulent piloted jet diffusion flame, roceedings 2nd International Workshop on trends in numerical and physical modelling of turbulent processes in gas turbine combustors Germany, 2004, pp. 45-51

[117] R. P. Lindstedt, S. A. Louloudi, E. M. Vaos, Joint scalar probability density function modeling of pollutant formation in piloted turbulent jet diffusion flames with comprehensive chemistry, In: Proceedings of the Combustion Institute. The Combustion Institute, Pittsburgh, PA, 28, 2000, pp. 149–156

[118] M. Vujanović, D. R. Schneider, M. Baburić and N. Duić, A comprehensive modelling of NO_x formation in combustion systems based on reduced chemical reaction mechanisms, CD Proceedings of the 3rd Dubrovnik Conference on Sustainable Development of Energy, Water and Environment Systems, 2005

[119] R. Tatschl, P. Priesching, J. Ruetz, Recent Advances in DI-Diesel Combustion Modeling in AVL FIRE-A Validation Study, International Multidimensional Engine Modeling User's Group Meeting at the SAE Congress, Detroit, 2007

Curriculum vitae

Name and family name:	Milan Vujanović
E-mail:	milan.vujanovic@fsb.hr
Web:	http://powerlab.fsb.hr/mvujanovic
Date of birth:	11. August 1977.
Place of birth:	Karlovac, Croatia
Primary school:	<u>1983. - 1991.</u> Primary School 'Švarča', Karlovac
High school:	<u>1991. - 1995.</u> Technical High School, Karlovac
Study:	<u>1996. - 2003.</u> University of Zagreb, Faculty of Mechanical Engineering and Naval Architecture
Post-graduate study:	<u>2003. - 2010.</u> University of Zagreb, Faculty of Mechanical Engineering and Naval Architecture, Department of Energy, Power Engineering and Environment
Training:	<u>November 2001. – November 2002.</u> Assistant Project Manager for Termobahia Power Plant Project, Turbo Machinery Project Management, Baden, Switzerland <u>February 2003. – April 2003.</u> Researcher at AVL List GmbH, Advanced Simulation Technologies, Graz, Austria <u>March 2006.</u> Course: Modelling and Computation of Multiphase Flows, Swiss Federal Institute of Technology, ETH, Zurich, Switzerland
Occupation or position held:	<u>October 2003.</u> Researcher at Faculty of Mechanical Engineering and Naval Architecture, Department of Energy, Power Engineering and Environment
Membership:	European Research Community On Flow, Turbulence And Combustion; Croatian Section of The Combustion Institute

Životopis

Ime i prezime:	Milan Vujanović
E-mail:	milan.vujanovic@fsb.hr
Web:	http://powerlab.fsb.hr/mvujanovic
Datum rođenja:	11. kolovoza 1977.
Mjesto rođenja:	Karlovac, Hrvatska

Osnovna škola:
1983. - 1991.
Osnovna škola 'Švarča', Karlovac

Srednja škola:
1991. - 1995.
Tehnička škola, Karlovac

Studij:
1996. - 2003.
Sveučilište u Zagrebu, Fakultet strojarstva i brodogradnje, studij strojarstva, procesno-enrgetski smjer

Poslijediplomski studij:
2003. – 2010.
Sveučilište u Zagrebu, Fakultet strojarstva i brodogradnje, poslijediplomski studij strojarstva, procesno-energetski smjer

Usavršavanje:
studeni 2001. – studeni 2002.
boravak u Alstomu, Turbo Machinery Project Management, Baden, Švicarska

veljača 2003. – travanj 2003.
boravak u AVL List GmbH, Advanced Simulation Technologies, Graz, Austria

ožujak 2006.
Course: Modelling and Computation of Multiphase Flows, Swiss Federal Institute of Technology, ETH, Zurich, Švicarska

Namještenja:
Listopad 2003.
Asistent na Fakultetu strojarstva i brodogradnje, Zavod za energetska postrojenja, energetiku i ekologiju

Članstva:
European Research Community On Flow, Turbulence And Combustion; Croatian Section of The Combustion Institute